The role of alternative splicing of Ca_V2 channels for synaptic transmission and behavior in *Drosophila melanogaster*

Dissertation zur Erlangung des Grades

Doktor der Naturwissenschaften (Dr. rer. nat.)

Am Fachbereich Biologie

Der Johannes Gutenberg-Universität Mainz

Christopher Bell,

geb. am 16.10.1992 in Mainz

Mainz, 2024

Dekan: Prof. Dr. Eckard Thines

1. Berichterstatter: Dr. Stefanie Ryglewski

2. Berichterstatter: Prof Dr. Martin Heine

Tag der mündlichen Prüfung: 13.12.2024

Abstract

Alternative splicing is known to increase functional diversity of proteins beyond the possibilities of expressing one protein per gene alone. In this thesis, I explored the role of alternative splicing of the voltage-gated calcium channel *cacophony* in *Drosophila melanogaster* with special focus on its role in synaptic transmission. I could show that the functional diversity of *cacophony*, which is homologous to the Ca_V2 channel family in vertebrates, relies heavily on alternative splicing of two splicing sites, one in the voltage sensor and one with a binding site for accessory subunits. I used CRISPR/Cas9 mediated exon excision for both mutually exclusive exon pairs to force sole expression of certain isoforms and subsequently analyze the functions of different Ca_V2 exons.

This analysis was conducted using electrophysiological methods, confocal laser scanning microscopy, single particle tracking with total internal reflection fluorescence microscopy and behavioral assays. Ca_V2 channels are essential in most presynaptic terminals for evoked synaptic vesicle release. My acquired data demonstrate that evoked synaptic vesicle release is possible only with one of the two alternative exons in the voltage sensor of the first homologous repeat, namely IS4B. Thus, homozygous exon excision of said exon results in lethality likely due to loss of synaptic transmission, which is caused by the lack of sufficient cacophony channels containing IS4B. My data provide evidence that isoforms with the other alternative exon, IS4A, comprise only a fraction of presynaptic calcium channels in the active zone and are not required and not sufficient for normal synaptic transmission. Still, animals lacking exon IS4A show a severely impaired behavior and life expectancy is extremely reduced. As for the other investigated splice site, the binding site for accessory subunits in the intracellular loop between homologous repeats I and II, animals with a homozygous loss of either exon are still viable. Although loss of the exon I-IIB results in a reduced synaptic transmission amplitude, this does not result in an effect on motor behavior or life expectancy.

Additionally, I provide evidence that while the B variants of both exon pairs are required for normal synaptic transmission in presynaptic terminals in the neuromuscular junction, the A variants are required in the visual system. Loss of IS4A and I-IIA results in impairments in both parameters analyzed via electroretinograms: presynaptic sustained photoreceptor potential amplitude and postsynaptic transient lamina response amplitude. To summarize, my results provide evidence for some isoforms being essential to synaptic function and vitality, while others have more subtle effects, whereas yet others display redundant or degenerate functions.

Table of contents

1 Introduction

The electrochemical properties of neurons are predominantly shaped by ion channels, which are therefore of utmost importance to neuronal function. Ion channels are transmembrane proteins, which enable ions to pass through the channel's pore-forming subunit along the electrochemical gradient (Simms and Zamponi, 2014; Fernández-Quintero *et al.*, 2021). A common classification for ion channels is determined by which ions it is selectively permeable for – calcium channels for example are selective for Ca^{2+}.

Neurons only work properly if the right set of ion channels is present in the cells' different compartments. The set with which neurons operate varies greatly between different neuron types, depending on their localization in the nervous system, their morphology and connection to other neurons or muscles as well as their specific functions. The four main compartments of neurons are the dendrites, the soma, the axon and the axon terminals. Each compartment has a different structure with various ion channel compositions for their purposes. For example, presynaptic axon terminals need a different composition of ion channels to serve their purpose (e.g., calcium induced vesicle release) (Tsien *et al.*, 1988a; Dunlap, Luebke and Turner, 1995; Kawasaki *et al.*, 2004) than dendrites, which are on the receiving side of the synapse and integrate postsynaptic information (Takagi, 2000; Stuart and Spruston, 2015), including postsynaptic computations that require voltage gated calcium channels (VGCCs), such as synaptic boosting (Heckman, Lee and Brownstone, 2003), dendritic amplification (Kadas *et al.*, 2017), and more. By contrast, at axon terminals VGCCs are required for evoked synaptic vesicle (SV) release (Tsien *et al.*, 1988b; Kawasaki *et al.*, 2004). This thesis will focus on VGCCs with special regard to their function in presynaptic terminals of fast glutamatergic synapses.

Considering the diverse ion channel composition stated above, impairment of ion channel function can result in a broad variety of neurological diseases. Especially channelopathies of VGCCs can result in ataxia, cardiac disorders, autism spectrum disorders, epilepsy, migraines, bipolar disorder, schizophrenia, retinal disorders and others (Splawski *et al.*, 2005, 2006; Jalkanen *et al.*, 2006; Singh *et al.*, 2007; Ferreira *et al.*, 2008; Saito *et al.*, 2009; Strom *et al.*, 2010; Cain and Snutch, 2011; Curtis *et al.*, 2011). Among some of these, for example migraines (Adams *et al.*, 2009), cone-rod dystrophy (Jalkanen *et al.*, 2006), congenital deafness and sinoatrial node dysfunction (Platzer *et al.*, 2000), impairment of splice isoforms or misregulation of splicing is the cause of these diseases. It has even been reported that familial hemiplegic migraine is associated with mutations regarding the voltage sensing unit of $Ca_V2.1$ calcium channels (Müllner *et al.*, 2004; Hering *et al.*, 2008).

Considering that alternative splicing has a profound effect on protein function and diversity and that VGCCs are spliced quite extensively (Dolphin, 2016), it is worth characterizing certain splice isoforms and the resulting impairments of reduced isoform variability.

1.1 Calcium ions in neurons

Ca^{2+} serves as both a charge carrier as well as second messenger and fulfills numerous roles in neurons (Simons, 1988; Clapham, 1995, 2007): it triggers synaptic vesicle release in presynaptic axon terminals (Katz and Miledi, 1967; Südhof, 2012a), its influx into dendrites depolarizes the cell membrane (Higley and Sabatini, 2012) and Ca^{2+} regulates gene (West *et al.*, 2001) and ion channel activity (Shah, Chagot and Chazin, 2006). The manifold of these functions and the fact that high intracellular Ca^{2+} concentrations are toxic require a precise regulation of intracellular Ca^{2+}, which is achieved via Ca^{2+} pumps (Brini and Carafoli, 2009; Krebs, 2022). Since the extracellular Ca^{2+} concentration of multiple mM is ~10^5 – 10^7 fold higher than the intracellular Ca^{2+} concentration of ~1-100 nM, the opening of Ca^{2+} channels in the cell membrane will force Ca^{2+} influx along the electrochemical gradient (Clapham, 1995). Furthermore, Ca^{2+} can also be released from and taken up into internal Ca^{2+} stores like the endoplasmic/sarcoplasmic reticulum (ER/SR) (Wu *et al.*, 1995; Verkhratsky and Petersen, 1998).

On the other hand, ATPase pumps are responsible for transportation of Ca^{2+} against the electrochemical gradient into internal stores like the ER/SR or outside the cell (Strehler *et al.*, 2008). The reduction of free Ca^{2+} is also assisted by buffering proteins to prevent Ca^{2+} toxicity (Berridge, Lipp and Bootman, 2000; Bagur and Hajnóczky, 2017). In fact, it has been shown in *Xenopus* oocytes that Ca^{2+} ions remain unbuffered for around 30ms before binding to a protein (Allbritton, Meyer and Stryer, 1992). All of these mechanisms show that Ca^{2+} levels inside the cell are highly regulated.

1.2 Voltage-gated calcium channels

VGCCs open, as the name suggests, upon the plasma membrane voltage exceeding certain membrane voltage thresholds. Typically, the resting membrane potential of neurons is around -70 mV (Clapham, 1995). VGCCs serve many functions in neurons: triggering of synaptic vesicle release in chemical synapses, boosting of synaptic drive in dendrites, increase of action potential firing frequency by co-localization to Ca^{2+} dependent K^+ channels (BK channels) in *Drosophila* (Kadas *et al.*, 2017) as well as the creation of persistent inward currents (PIC) in

spinal motoneurons of vertebrates (Heckman, Lee and Brownstone, 2003). This manifold of functions requires channels with different properties and localizations.

These channels are comprised of several subunits, whose different combinations offer a large variability in channel kinetics and localization. There are five known subunits to form a functional VGCC: the pore forming α_1-subunit and the auxiliary subunits α_2, β, γ and δ (Dolphin and Lee, 2020).

The $\alpha_2\delta$-subunit binds extracellularly to the α_1-subunit and influences channel kinetics as well as trafficking, localization and surfacing of channels in the membrane (Dolphin, 2013; Heinrich and Ryglewski, 2020). The β-subunit can bind intracellularly and can influence channel kinetics via binding of other proteins and their subunits, such as calmodulins and G-protein subunits. Additionally, it is required for transport of the VGCC out of the endoplasmic reticulum (ER) and surfacing of the channel (Buraei and Yang, 2010a). The γ-subunit is involved in channel trafficking as well as localization and is known to bind to VGCCs in skeletal muscles (Takahashi *et al.*, 1987). While Ca_V1 and Ca_V2 require auxiliary subunits $\alpha_2\delta$ and β for proper surfacing and function, Ca_V3 does not need other subunits than α_1 (Dolphin, 2016).

The α_1-subunit of VGCCs typically consists of four homologous repeats I – IV (Figure 1), which in turn, consist of six transmembrane segments (S1-S6) each. The repeats are connected to neighboring repeats via intracellular linker loops. Multiple descriptions of which segments actually comprise the voltage sensor exist: publications either solely mention S4 as the voltage sensor (Hering *et al.*, 2008), S1-S4 as the voltage sensing unit (Fernández-Quintero *et al.*, 2021) or use both descriptions without further differentiating (Hering *et al.*, 2018; Jurkovicova-Tarabova *et al.*, 2018). A common denominator is that S4 of each repeat contains a larger number of positively charged amino acid residues and since in either case S4 is thought to play a role in voltage sensing, its alternative splicing in *Drosophila* might contribute to functional diversity.

The loop connecting repeats I and II contains the α_1-interaction domain (AID), which is the binding site of the β-subunit, and in adjacent proximity G-protein subunits β & γ bind to the I-II loop (Pragnell *et al.*, 1994). It has also been shown in vertebrates that some VGCCs physically interact with G-protein coupled receptors, thus providing further possibilities for maintaining regulation of VGCC density in the membrane (Kisilevsky *et al.*, 2008). The N- and C-termini of the α_1-subunit are both located intracellularly and are also known to interact with the I-II-loop. The C-terminus contains an IQ-motif, which impacts Ca^{2+} binding and promotes Ca^{2+}-dependent channel inactivation via interaction with the Ca^{2+} binding regulatory protein calmodulin (CaM) (Peterson, DeMaria and Yue, 1999; Catterall, 2011). Closely located nearby is an EF-hand, which has also been shown to promote Ca^{2+}-dependent inactivation via binding of CaM (De Leon *et al.*, 1995; Peterson *et al.*, 2000).

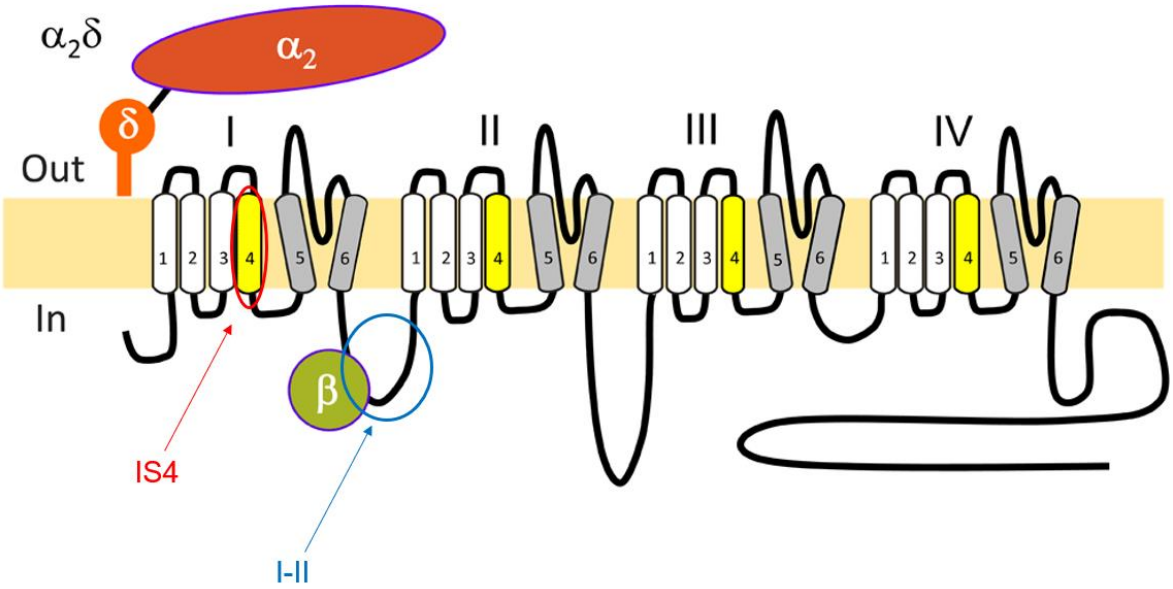

Figure 1: Schematic depiction of an α_1-subunit of a VGCC. Depicted are several subunits: the pore-forming α_1-subunit, composed of four homologous repeats, which are indicated by roman numerals I-IV and itself are made up of six subunits each (S1-S6), the extracellularly located $\alpha_2\delta$-subunit and the β-subunit, which is able to bind to the intracellular linker-loop I-II. Encircled in red is the fourth transmembrane segment of homologous repeat I (IS4), which acts as part of the voltage sensor. The intracellular loop between repeats I & II is encircled in blue (I-II) and serves as a binding site for β-subunits and βγ-subunits of G-proteins. The yellow segments are the voltage sensors of each homologous repeat. Figure modified after Dolphin, 2018.

This common composition of α_1-subunit and the auxiliary subunits is highly conserved throughout invertebrates as well as vertebrates. While in vertebrates the α_1-subunit is encoded by ten different genes, differentiated into three families, in invertebrates only three genes exist – one homolog per vertebrate family (table 1). These three genes in *Drosophila* are named DmCa1D (Ca_V1 homolog), DmCa1A (Ca_V2) and DmCa1G (Ca_V3). Each of these families has been categorized based on the channel kinetics and pharmacological blockers (Catterall, 2000).

Table 1: Gene families of VGCC α_1-subunits in vertebrates with differing current types, activation voltages and their respective homologs in Drosophila. While vertebrates express several genes per VGCC family, Drosophila only offers one gene homolog per family. Ca_V1 mediates high voltage activated (HVA) L-type currents, Ca_V2 HVA and low voltage activated (LVA) P/Q, N- & R-type currents and Ca_V3 LVA T-type currents. Table modified after Ryglewski *et al.*, 2012.

Vertebrate nomenclature	Current type	Activation voltage	Drosophila homolog (CG number)
$Ca_V1.1$ $Ca_V1.2$ $Ca_V1.3$ $Ca_V1.4$	L-type	HVA	DmCa1D (CG4894)
$Ca_V2.1$ $Ca_V2.2$ $Ca_V2.3$	P/Q-type N-type R-type	HVA/LVA	DmCa1A (CG43368) [cacophony/nightblind-A]
$Ca_V3.1$ $Ca_V3.2$ $Ca_V3.3$	T-type	LVA	DmCa1G (CG15899)

1.3 Cacophony and alternative splicing

The focus of this thesis will be on investigating the Ca_V2 homolog of α_1-subunits in *Drosophila*, DmCa1A, which is also called *cacophony* (*cac*) or *nightblind-A*. Both alternative names root from results of impairments of *Drosophila* courtship song and defects in the visual system, respectively (Von Schilcher, 1976; Smith *et al.*, 1996). Courtship success in flies with a *cacophony* mutation was reduced due to impairment of courtship song (Von Schilcher, 1976). In the *nightblind-A* mutant, which carries a point mutation in a coding region, photoreceptor and transient lamina responses to light stimuli were reduced (Smith *et al.*, 1996, 1998a).

It has been shown that *cacophony* does not solely conduct high voltage activated currents (HVA) as previously believed but also low voltage activated currents (LVA) (Ryglewski *et al.*, 2012). As mentioned previously, there is only one gene for this Ca_V2 channel homolog, so three possible explanations were of interest: pre-mRNA editing, differential pairing of the α_1-subunit with various accessory subunits and alternative splicing of the α_1-subunit, with the latter being the focus of this study. The effects of pairing different accessory subunits with cacophony have been studied previously (Heinrich and Ryglewski, 2020) while pre-mRNA editing of cacophony has been investigated and yielded no sufficient results in that matter. Although activation voltage shifts by 10 mV towards more depolarized potentials upon knockdown of the protein dAdar, which is responsible for A-I pre-mRNA editing, neurons were still able to

mediate HVA as well as LVA currents (Stefanie Ryglewski, personal communication). This indicates that additional mechanisms are needed to diversify cacophony function.

Alternative splicing with different exons is a mechanism to profoundly expand protein diversity and function beyond the rather limited possibilities of expressing a single protein per gene. While it is known that at least 50% of human genes are alternatively spliced, it is estimated that this number could be as high as 95% (Lander *et al.*, 2001; Pan *et al.*, 2008; Wang *et al.*, 2008). Two particular splice sites are of interest to us in this thesis, based on their probable contribution to the diversification on activation voltages and channel kinetics:

There are two mutually exclusive alternative exons in the fourth transmembrane segment of repeat I (IS4): A and B (IS4A & IS4B). The same applies for parts of the intracellular loop between repeats I and II (I-IIA & I-IIB). Previous studies have also shown that the replacement of voltage sensors in the second repeat (IIS4) of human $Ca_V3.3$ with a IIS4 of $Ca_V1.2$ channels shifts the activation voltage towards more depolarized potentials by roughly 30 mV (Sanchez-Sandoval *et al.*, 2018). These findings further support the idea that alternative splicing of IS4 might produce channels with different activation voltages. My collaborator on this project, Lukas Kilo, has already shown that the homozygous removal of IS4A leads to a reduction in fitness and lifespan (Ph.D. thesis Lukas Kilo, 2021). Additionally, the removal of IS4A results in a shift of activation voltage of HVA current of 10 to 20 mV towards more hyperpolarized potentials in the adult flight motoneuron MN5 (Ph.D. thesis Lukas Kilo, 2021). The main difference between I-IIA and I-IIB is that I-IIB can bind both subunits, Ca_β & $G_{\beta\gamma}$, while I-IIA can only bind β-subunits. However, the Ca_β binding motive is relatively poorly conserved in I-IIA (Smith *et al.*, 1998). This difference is also subject to investigation in this thesis since differential binding of subunits suggests different function of both exons.

Flybase.org and the National Center for Biotechnology Information (NCBI) report differently on the number of annotated exons for *cacophony*. While flybase.org lists 46 exons, NCBI lists 40 exons (December 2023). This discrepancy might be a result of exons on flybase.org, which have been described multiple times, but actually report on the same exon. While 40 or 46 total exons could in theory give rise to a large variety of possible protein isoforms, only 18 of those have been annotated on flybase.org (December 2023) so far. While the excision of these exons via CRISPR/Cas9 results in homozygous viable animals for IS4A, I-IIA & I-IIB, animals are embryonic lethal without any isoforms expressing IS4B. For the remainder of this thesis, I will call specific cacophony variants depending on their exon excision, for example ΔIS4B, meaning IS4B is not present and only isoforms containing IS4A are available to be expressed.

1.4 Cacophony in presynaptic terminals of neuromuscular junctions (NMJs)

As stated previously, VGCCs are responsible for triggering vesicle (SV) release in presynaptic terminals, thereby enabling synaptic transmission (Borst and Sakmann, 1996). In vertebrates mainly $Ca_V2.1$ and $Ca_V2.2$ channels are responsible for this mechanism while in *Drosophila*, cacophony triggers SV release (Kawasaki, Felling and Ordway, 2000; Kawasaki, Collins and Ordway, 2002; Kawasaki *et al.*, 2004; Dolphin and Lee, 2020). More precisely, cacophony channels are localized in so called active zones (AZ), which make up the release sites at which SVs are docked to and can fuse with the plasma membrane, thus releasing neurotransmitters into the synaptic cleft (depicted in Figure 2). This docking and fusing require a certain protein complex (SNARE complex), which is highly conserved throughout the animal kingdom (Südhof, 2012b). In *Drosophila*, Bruchpilot (brp), which is homologous to the mammalian ELKS/CAST protein family, is responsible for providing the proximity between cacophony and primed SVs to ensure efficient neurotransmission (Fouquet *et al.*, 2009). Previous studies have shown that *brp* deficiency mutants accumulate less VGCCs in AZs, and thus, evoked release of SVs is reduced (Robert J Kittel *et al.*, 2006; Wagh *et al.*, 2006).

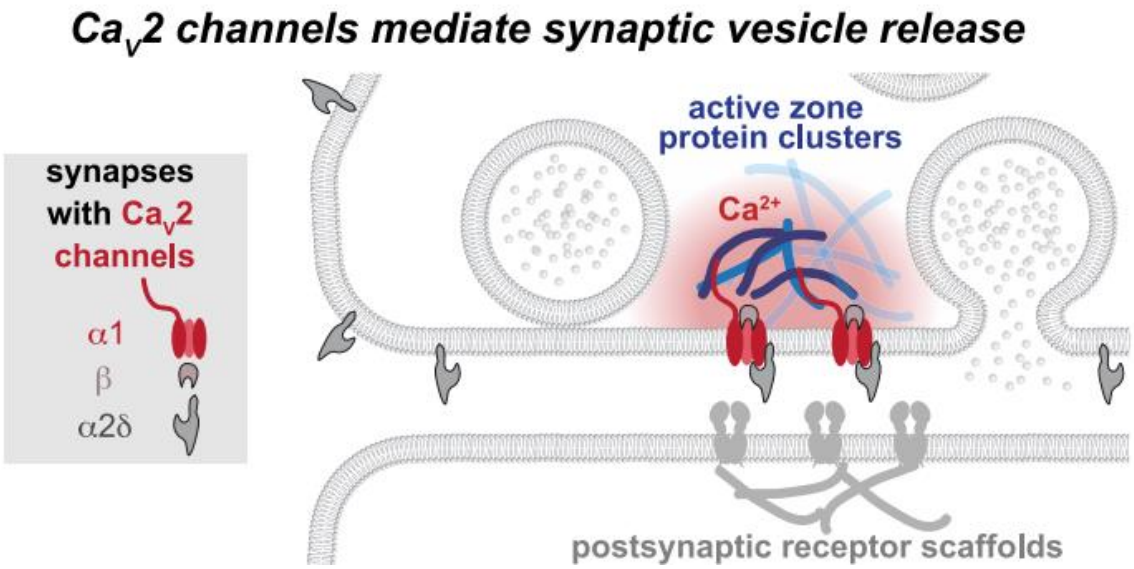

Figure 2: Simplified schematic of the role of presynaptic Ca_V2 channels in active zones of presynaptic terminals. The pore forming α_1-subunit of Ca_V2 channels is highlighted in red, while the intracellular β-subunit and the extracellular $\alpha_2\delta$-subunit are indicated in gray shapes. The calcium channels are located in the active zones of presynaptic terminals with close proximity to primed and docked synaptic vesicles (left). A depiction of a synaptic vesicle fused with the presynaptic membrane is located to the right of the highlighted calcium channels with neurotransmitters being released into the synaptic cleft. A very simplified version of protein clusters located in the active zone, including the SNARE complex, is indicated with elongated dark and light blue structures in the red shaded area (active zone). Postsynaptically located receptors, which transduce the chemical signal of neurotransmitters into an electrical signal in the postsynaptic neuron or myocyte, are depicted to the bottom of the figure with gray shapes. Figure altered after Held *et al.*, 2020.

Consequently, the homozygous loss of *cac* leads to lethality due to abolishment of synaptic transmission (Perrimon, Engstrom and Mahowald, 1989; Kawasaki, Collins and Ordway, 2002). Interestingly, rescue of this phenotype can be achieved by pan-neuronal expression of

one single *cac* isoform called *cac1*, which contains exons IS4B and I-IIB (Kawasaki, Collins and Ordway, 2002). It is not known however, which exons are needed in presynaptic terminals and how isoform diversity affects synaptic function. This is one of the main points that I will elucidate during this thesis.

1.5 Cacophony in the visual system

As previously mentioned, *cacophony* has also been called *nightblind-A* due to defects in ERGs conducted in *cacophony* mutants (Smith *et al.*, 1996, 1998a). These findings suggest a role of alternatively spliced cacophony in the visual system since *nightblind-A* contains a point mutation in the exon I-IIA, resulting in a premature stop of all protein isoforms containing exon I-IIA.

In *Drosophila*, the visual system is comprised of the retina and the four subsequent neuronal layers: lamina, medulla, lobula and lobula plate (Figure 3). Retinal photoreceptor cells (PR) are stimulated by photons and transduce this optical stimulus via a signal cascade initiated by G-protein coupled receptors called rhodopsins into an electrical signal via TRP & TRP-like receptors, which are cation channels (Ranganathan, Harris and Zuker, 1991; Niemeyer *et al.*, 1996; Astorga *et al.*, 2012). In contrast to synapses at the NMJ, the ion channels of presynaptic terminals from PRs onto lamina cells mediate graded potentials, meaning they increase the amount of SV released in proportion to the input they receive via photons (Juusola *et al.*, 1996; Kurt, Warzecha and Egelhaaf, 2001; Astorga *et al.*, 2012).

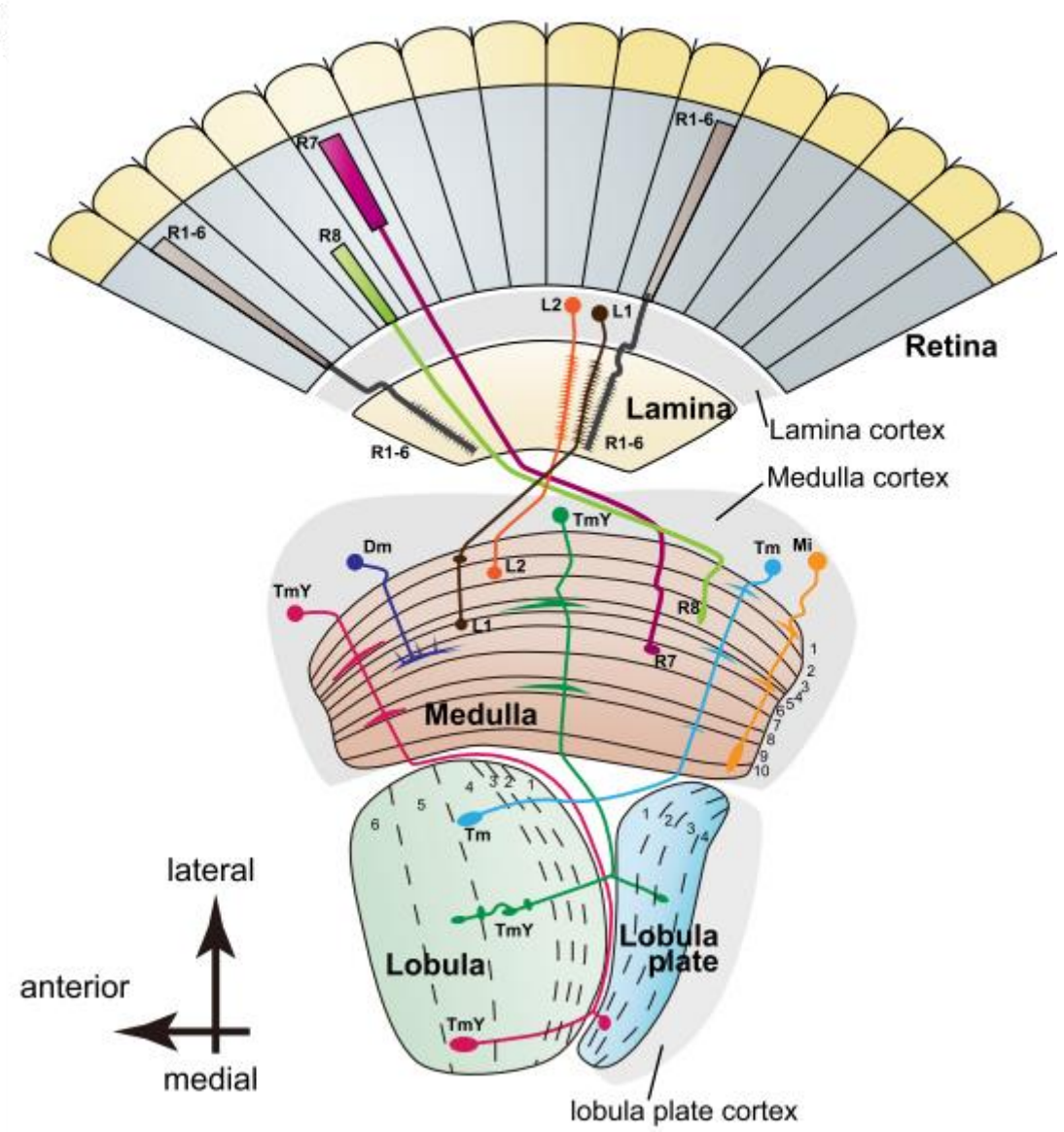

Figure 3: Schematic of the Drosophila visual system. Photoreceptor cells are organized in ommatidia in the retina. They are the primary cells transducing optical stimuli into electrical signals and transmitting this information onto the large monopolar cells (LMC) in the lamina. The lamina is the most apical of four neuronal layers forming the optical lobes. While PR cells R1-R6 project into the lamina and detect motion, R7 & R8 project directly into the medulla and are involved in color vision. Downstream of the lamina are the optical layers medulla, lobula and lobula plate. Figure altered after Sato, Suzuki and Nakai, 2013.

Cacophony has been shown to contribute to Ca^{2+} release in PR axons as well as to exocytosis in synaptic terminals onto postsynaptic lamina cells (Astorga *et al.*, 2012). How alternative splicing might affect synaptic transmission in PR cells and how this differs to possible effects at the NMJ is an exploratory objective of this thesis.

1.6 Aims of this study

This study primarily aims on resolving the question why synaptic transmission relies on and is altered by differential expression of certain cacophony isoforms. Secondly, we want to determine whether differences in synaptic transmission are caused by altered numbers of cacophony channels at the presynaptic terminals of NMJs, by altered channel kinetics, different morphology, or a combination of the above.

Hypotheses:

1. Cacophony isoform expression in the synaptic terminals of the NMJ is different compared to the expression in synaptic terminals in the visual system.
2. Some specific exons are essential for normal fast synaptic transmission at the NMJ, and their absence affects motor behavior and fitness.
3. Other specific axons (as compared to the NMJ) are required for neuronal responses in the visual system to light.
4. Loss of some exons can be compensated for by other exons.

Specific predictions:

1. Since removal of IS4B is homozygous lethal and deletion of cacophony can be rescued by a UAS-cac1 overexpression (one single isoform with IS4B), I predict the abolishment of synaptic transmission at the larval and adult NMJ in ΔIS4B animals.
2. I predict that while certain exon removals will not affect larval NMJ morphology, it will impact synaptic transmission by increased and decreased channel numbers.
3. Due to the observed reduction of light responsiveness in the *nightblind-A* (=cacophony) mutation H^{18}, which is located in exon I-IIA, I expect ΔI-IIA animals to phenocopy these effects.
4. ΔIS4A adults show a severely reduced lifespan and seizure-like behavior. I predict that these observations are consequential to impairments in synaptic transmission at the NMJ.
5. Since I-IIB contains a binding site for $G_{\beta\gamma}$-subunits and I-IIA does not, the knockdown of neuronal $G_{\beta\gamma}$-subunits in controls and ΔI-IIA animals will phenocopy possible effects of ΔI-IIB on synaptic transmission amplitude.

2 Material & Methods

2.1 Fly keeping:

Flies were reared and kept in plastic vials (diameter: 2 cm) on standard cornmeal-agarose food (see appendix). Flies ready for experiments were kept at 25°C in incubators with a 12 h day/night cycle. Fly strains that were kept for long-term storage were kept at 17°C in incubator rooms with a 12h day/night cycle.

2.2 Fly stocks

Most of the cacophony exon-out variants in this thesis were tagged with a superfolder-GFP (sfGFP) N-terminally, originally designed and published by (Gratz *et al.*, 2019). Information about tagged cacophony variants are included in the legend below the respective figures and their introducing texts, but for reasons of readability, the tags will not be included in the texts of the results and discussion. Additionally, I will abbreviate $cac^{\Delta exon}$ with Δexon for the remainder of this thesis for readability. For detailed information on which fly line was used for each experiment, please see 5.5.

Table 2: General fly stocks used for experiments and/or crosses. Exon excisions are indicated by a Δ symbol and were mediated via CRISPR/Cas9 (see 2.3 for more detailed description).

Abbreviated term	Genotype	Origin	Notes
CS	Canton Spezial (+ ; + ; +)		General laboratory wild-type strain
$Cac^{sfGFP\text{-}N\text{-}term}$	$\frac{CacsfGFP}{CacsfGFP}$; + ; + ; +	Lukas Kilo/(Gratz *et al.*, 2019)	
$Cac^{sfGFP\Delta IS4A}$	$\frac{CacsfGFP\Delta IS4A}{CacsfGFP\Delta IS4A}$; + ; + ; +	Lukas Kilo	
$Cac^{sfGFP\Delta IS4B}$	$\frac{CacsfGFP\Delta IS4B}{Fm7a}$; + ; + ; +	Lukas Kilo	
$Cac^{sfGFP\Delta I\text{-}IIA}$	$\frac{CacsfGFP\Delta I-IIA}{CacsfGFP\Delta I-IIA}$; + ; + ; +	Lukas Kilo	
$Cac^{sfGFP\Delta I\text{-}IIB}$	$\frac{CacsfGFP\Delta I-IIB}{CacsfGFP\Delta I-IIB}$; + ; + ; +	Lukas Kilo	
$Cac^{tagRFP\Delta IS4A}$	$\frac{Cactag RFP}{CactagRFP}$; + ; + ; +	Lukas Kilo/Gratz *et al.*, 2019	
Cac^{mEOS4b}	$\frac{\text{w CacmEOS4b}}{\text{w CacmEOS4b}}$; + ; + ; +	Martin Heine	

Abbreviated term	Genotype	Origin	Notes
$Cac^{mEOS4b\Delta IS4A}$	$\frac{\text{w CacmEOS4b } \Delta IS4A}{\text{w CacmEOS4b } \Delta IS4A}$; + ; + ; +	this thesis	
$Cac^{mEOS4b\Delta IS4B}$	$\frac{\text{w CacmEOS4b } \Delta IS4B}{\text{Fm7c P\{2xTbRFP\}}}$; + ; + ; +	this thesis	
$Cac^{mEOS4b\Delta I\text{-}IIA}$	$\frac{\text{w CacmEOS4b } \Delta I-IIA}{\text{w CacmEOS4b } \Delta I-IIA}$; + ; + ; +	this thesis	
Cac^{H18}	$\frac{CacH18}{CacH18}$; + ; + ; +	Smith *et al.*, 1998), Bloomington Stock Center #42245	
Fm7cTb	$\frac{\text{Fm7c P\{2xTbRFP\}}}{\text{Fm7c P\{2xTbRFP\}}}$; + ; + ; +		Used to balance exon out stocks for experiments with L3 larvae
$Cac^{FlpStop}$	$\frac{yw\ CacFlpStop}{yw\ CacFlpStop}$; $\frac{OK6-GAL4}{OK6-GAL4}$; + ; +	Fisher *et al.*, 2017	Used for experiments to elucidate IS4B function
UAS-Flp	+ ; $\frac{UAS-Flp.D1}{UAS-Flp.D1}$; +		Needed for Flp-induced disruption of $Cac^{FlpStop}$
UAS-cac1	w^{-}; + ; P{w^{+mc} UAS-cac1-EGFP}786C	Bloomington Stock Center #8581	Needed for cac1 overexpression in cac^{null} background
$Elav^{c155}$-GAL4 cac^{HC129}	$\frac{p\{GawB\}Elavc155-GAL4\ cacHC129\ sd1,f1}{Fm7i,P\{ActGFP\}JMR3}$	Bloomington Stock Center #8579	Needed for cross into UAS-cac1 to create cac^{null} background

2.3 CRISPR/Cas9 mediated exon excision

As mentioned before, we employed CRISPR/Cas9 mediated exon excision of one exon of a mutually exclusive pair to force isoform expression with the remaining exon. CRISPR/Cas9 has been described firstly by Doudna and Charpentier, 2014 and has since become a standard procedure for DNA manipulation and modification. In this study, two guide RNAs (gRNAs) complementary to a target sequence on either side of the exon that needs to be cut out was

designed and injected into the germline of suitable flies, generating transgenic fly strains that express gRNA under the control of the U6 promoter that is active during germline development in the early embryo. A co-expressed Cas9 enzyme in the same fly line is able to bind to this specific gRNA and cleave the double stranded DNA, which is subsequently repaired autonomously via homologous DNA repair by the cell. Thereby, we were able to cut out specific exons of *cacophony* with exon specific gRNAs. The process of designing gRNA *in silico* was done by a former member in our lab, Lukas Kilo. For the exact sequences and target sites of gRNA and gene region respectively, please see the Ph.D thesis of Lukas Kilo (2021) or Bell *et al.* (2024).

Below is a crossing scheme, which was used to generate new fly lines with exon excisions:

1. $\frac{w- \; cacsfGFP}{FM7a}$; $\frac{nosCas9}{CyO}$ x $\frac{y1 \; cho2 \; v1}{Y}$; $\frac{gRNA \; \Delta exon}{CyO}$
2. $\frac{vnd}{FM6 \; grh \; lacZ}$; $\frac{SnaSco}{CyO}$ x F1 ♂ $\frac{w- \; cacsfGFP}{Y}$; $\frac{nosCas9}{gRNA \; \Delta exon}$
3. F1 ♀ $\frac{w- \; cacsfGFP(\Delta exon)}{FM6 \; grh \; lacZ}$; $\frac{nosCas9 \; or \; gRNA \; \Delta exon}{CyO}$ x $\frac{FM6 \; grh \; lacZ}{Y}$; $\frac{SnaSco}{CyO}$ | Single crosses

The CRISPR event may happen in the germline of the F1 generation of cross 2, when nosCas9 and the gRNA of the specific exon are present in the same animal. Since this happens in the germline, virgin females of the subsequent F1 generation were singled out and re-crossed one on one with males of the balancer fly line (see cross 3). As soon as plenty of larvae were visible in the F2 generation, the mothers were squished (see 2.9.1) for DNA isolation and exon excision was screened for by using PCR (see 2.9.2). Positive fly lines were kept for experiments while negative fly lines were discarded. We noticed different probabilities for exon excision: while exons IS4A, IS4B and I-IIA yielded positive samples in around 5 - 20%, I-IIB had below 0.5% probability of exon excision (Stefanie Ryglewski, personal communication). Therefore, a large quantity of animals (at least 300) is recommended to be crossed as single crosses for effective exon excision of I-IIB.

We employed the approach to cut out exons either of sfGFP-, tagRFP or mEOS4b-tagged *cacophony* fly lines. This results in *cacophony* exon-out variants that express a fluorescent tag in the remainder of all isoforms, thus enabling subsequent localization and organization analyses via confocal laser scanning microscope (CLSM) or total internal reflection microscopy (TIRFM).

2.4 Dissection of L3 larvae:

Wandering L3 larvae were taken from the vial and placed on a dish, filled with sylgard-silicone, on the ventral side, thus the dorsal side was facing upwards. Metal pins were pierced through the head and the posterior side of the abdomen to immobilize the larva. After covering the larva with standard ringer saline, it was cut open along the dorsal midline. After stretching the body walls on the lateral sides and fixating those with two additional metal pins per side, the organs and trachea were carefully removed to reveal the crawling muscles. If needed for current clamp or two electrode voltage clamp recordings, the VNC was removed to reduce spontaneously induced movement of the crawling muscles while nerves containing the MNs innervating the crawling muscles were left long for stimulation with a suction electrode.

2.5 Electrophysiology

2.5.1 Larval crawling muscle recordings of muscle 6 (TEVC)

Wandering L3 larvae were dissected as described in 2.4 in HL 3.1 saline. Experiments were conducted in 0.5 mM extracellular Ca^{2+}. Electrodes for intracellular recordings needed during TEVC were pulled by using borosilicate glass and filled with 3M KCl. Suction electrodes were pulled with borosilicate glass and their tips were broken off individually with forceps and filled with HL 3.1 saline. These glass electrodes were pulled using a Flaming/Brown Micropipette Puller Model P-97 by Sutter Instruments with a 2.5 mm box filament.

Settings for the current passing electrodes (CPE) were: pressure 400, heat 507, pull 60, velocity 75, delay 120, ramp value 500, using WPI 1B100 F-4 borosilicate glass (World Precision Instruments Inc.).

Settings for the recording electrodes (RE) were: pressure 500, heat 507, pull 40, velocity 75, delay 120, ramp value 500 using WPI 1B100 F-4 borosilicate glass (World Precision Instruments Inc.).

Settings for the suction electrodes were: pressure 500, heat 532, pull 0, velocity 150, delay 100, ramp value 500 using Sutter BF100-50-10 borosilicate glass by Sutter Instruments/Science Products.

Dishes containing the larvae were mounted on an Olympus upright epifluorescence microscope and observed via a 20x objective (Olympus UMPlan FI). After placing the ground wire into the saline, the nerve containing motoneurons innervating muscle 6 (M6) of abdominal

segments 2 or 3 (A2/3) was sucked in with a suction electrode. Subsequently, CPE and RE were offset to 0 mV, tested for resistance (CPE: 8-15 MΩ, RE: 20-40 MΩ) and their capacitance neutralized. Both electrodes were then carefully placed into M6, beginning with the CPE. The holding position was adjusted to achieve a ramp balance between both electrodes before switching from bridge to TEVC mode using the respective dial on the intracellular amplifier. Using the software Clampex, the holding voltage was set to the membrane voltage recorded by the RE and then set to -70 mV. Voltage clamp gain was set manually to a range between 8x and 25x. Recordings were then conducted using Clampex.

Recordings were deemed acceptable if the membrane voltage was below -50 mV in bridge mode and holding current was below 5 nA in TEVC mode. Stimulation of the motoneurons was elicited with a duration of 0.1 ms with 1V above firing threshold. The firing threshold was exceeded if a stimulus elicited a distinct postsynaptic response. Afterwards, the stimulation protocol was conducted. In succession, recordings were analyzed via Clampfit 11.2 (Molecular Devices) after they were filtered with a 360 Hz Gaussian filter. The acquired data were analyzed using Microsoft Excel and statistically tested with GraphPad Prism (Version 9).

All TEVC recordings were conducted using an Axoclamp 2B amplifier by Axon Instruments, whose data were digitized by an Axon Digidata 1550 by Axon Instruments. We used an isolated pulse stimulator model 2100 by A-M Systems, amplified by a differential AC amplifier model 1700 by A-M Systems. Both head stages for TEVC were HS-2A head stages (gain: x 0.1 LU) by Axon CNS, Molecular Devices. Micromanipulators MPC-200 and MP-225, both by Sutter Instruments, were used to finely steer the three electrodes for TEVC and suction. The light source was a TH4-100 by Olympus.

The protocol during each recording started with 2 min of no stimulation in order to observe spontaneous activity and analyze frequency and amplitude of miniature excitatory postsynaptic currents (mEPSCs or ‘minis’). The firing threshold was elucidated by stimulating in a train of 1 Hz and manually increasing voltage in between stimulations. When stimulations evoked a response, voltage was briefly increased to a maximum of 10 V to ensure that all MNs in the sucked nerve are stimulated. The threshold for maximum evoked current was then exceeded by 1 V for all subsequent stimulations. All stimulations were applied with a duration of 0.1 ms. A train of 7 stimulations over 60 seconds with an inter pulse interval of 10 seconds was applied to record evoked currents. Paired pulses with inter pulse intervals of 10 ms, 15 ms, 20 ms, 25 ms, 30 ms, 50 ms and 100 ms were applied with 5 paired pulses each. Exploratively, 10 second trains of 1 Hz, 5 Hz, 10 Hz, 20 Hz and 40 Hz were applied.

The relevance of changes in mEPSCs and evoked currents as well as different means of short-term plasticity are explained in 3.2.3 (EPSCs) and 3.2.7 (short-term plasticity).

2.5.2 TEVC of muscle 12 – heterozygous exon out mutants

$Cac^{FlpStop}$ contains a cassette, which is located in a non-coding intron of the gene and is orientated in a non-disruptive state. Using a flippase, the cassette can be cut and reintegrated by chance in the disruptive direction, which will then be coded due to splice acceptor sites inside the cassette. This will lead to a premature stop of *cacophony* and as a reporter, the affected cells will express td-tomato (Fisher *et al.*, 2017). Wandering female, non-tubby L3 larvae were dissected as described in 2.4 in HL 3.1 saline with 0.5 mM extracellular Ca^{2+}. Non-tubby larvae were chosen since the absence of a tubby phenotype indicated the presence of the chromosome with the respective exon excision inherited from the mother (see fly strains in 5.5). For this experiment, all tested animals needed to be female in order to record homozygous and hemizygous lethal exon-out fly strains, in this case ΔIS4B. By expression of the exon excision on the X chromosome together with the other X chromosome containing $Cac^{FlpStop}$, we created a genetic mosaic of few motoneurons, which expressed a selective exon-out variant without functional cacophony from the $Cac^{FlpStop}$ chromosome. Thus, we were able to record the effects of the respective exon excision in single cells while circumventing the lethality if said exon excision was globally expressed.

After dissection, animals needed to be checked for RFP signal under fluorescent light since successful reintegration of the $cac^{FlpStop}$ cassette in disruptive orientation forces expression of td-tomato in neuronal membrane as described above (Fisher *et al.*, 2017). We chose to target M12 after explorative dissections since it was the muscle with the highest chance to reintegrate the cassette in both MNs projecting onto it, which is necessary to ensure that all presynaptic MNs are cac^{null} on the $cac^{FlpStop}$ chromosome. Additionally, it is still relatively easily accessible. The TEVC recordings were conducted as described in 2.5.1. Only muscles with clear fluorescent RFP signals from two motoneurons were recorded. The flies' genotype with exon-out variants was as follows: $\frac{cacsfGFP\ \Delta exon}{cacFlpStop}$; $\frac{UAS-Flp.D1}{OK6-GAL4}$. It was noticeable that M12 recordings often showed more positive membrane potentials and increased holding currents in TEVC mode when compared to M6. Thus, recordings with a membrane potential below -40 mV and holding current up to 10 nA were deemed acceptable. For this experiment, I recombined UAS-Flp.D1 with the driver OK6-GAL4 on the second chromosome while the $cac^{FlpStop}$ cassette was located on the X chromosome. After recording the experimental larvae for several weeks, no RFP-positive motoneurons were visible anymore using the aforementioned stocks for experimental crossing. During subsequent PCR and gel electrophoresis as troubleshooting, we noticed that the stocks had lost either the GAL4 driver or the UAS-Flp construct. I then employed a new strategy and constructed stocks that separately carried either the exon-out variant and UAS-

Flp ($\frac{cac\Delta exon}{cac\Delta exon/Fm7cTb}$; $\frac{UAS-FLP}{UAS-FLP}$) or the $cac^{FlpStop}$ cassette and the OK6-GAL4 driver ($\frac{cacFlpStop}{Y}$; $\frac{OK6-GAL4}{OK6-GAL4}$). Thus, only after the experimental cross, all constructs were present in the same animal. I observed no difference in amplitudes between both approaches in the genotypes, hence all data were pooled. Stimulation protocols were conducted as described in 2.5.1.

2.5.3 Electrophysiological recordings of adults:

NMJ current clamp recordings in adult animals were obtained from the DLM flight muscles 1 – 5 in adult animals aged 2 days. Here, the giant fiber pathway can be utilized to indirectly stimulate the MNs through the flies' eyes (King and Wyman, 1980). Adult females were anesthetized via cooling on ice. Legs and wings were removed, and the fly was immobilized with metal pins pierced through the proboscis and the abdomen. Furthermore, two metal pins were pushed to either side of the neck between head and thorax to provide physical resistance and facilitate penetration of the eye with tungsten wires. Vaseline via a syringe was used around the neck area to avoid saline contact to the eye, thus avoiding an electrical short while recording. Saline was applied to the thorax and had to cover at least the point of penetration in order to enable an input offset for the recording electrode.

Tungsten wires (electrolytically sharpened with KOH – NaNO2) were pushed into the eyes. Voltage threshold was tested by increasing the stimulation voltage until the flight and jump muscles in the thorax started twitching (between 2 – 10 V). Stimulation voltage was then set 1 V above threshold. The recording electrode was subsequently pushed into the thorax directly beneath the scutellum from the posterior. The first obtained membrane potential after piercing the cuticle is determined as the one of unit 5, which is innervated by MN5. By pushing the electrode further to the anterior side, membrane potentials and therefore recordings of DLMs 4, 3, 2 & 1 can be obtained, respectively. The penetration of the more anterior muscle membrane can be perceived by observation of the recorded potential – the membrane potential will fade towards more positive values followed by a sudden change to a more negative potential as soon as the next muscle membrane is penetrated. Ideally, the stimulation protocol can then be run for all five units. All recordings were filtered with a 360 Hz Gaussian filter using Clampfit 11.2.

2.5.4 Electroretinograms (ERGs)

For ERGs, the adult flies were cooled on ice and their wings and legs removed with scissors. Flies were then immobilized via two metal pins, one in the abdomen and another in the proboscis to leave the head and eyes unscathed. To enable a closed circuit, a grounding wire was placed into a hole in the abdomen, which had to be cut open. Recording electrodes (glass pulling details below) were filled with 3 M KCL and placed carefully into the eye via a micromanipulator under a 10x air lens. The recording was deemed acceptable if the amplitude of the 50 Hz mains hum oscillation was below 1 mV.

Settings for the recording electrodes (RE) were: pressure 500, heat 507, pull 40, velocity 75, delay 120, ramp value 500 using WPI 1B100 F-4 borosilicate glass (World Precision Instruments Inc.).

An LED was placed in front of the flies' eyes at approx. 1 cm. The same light stimulation protocol was run twice, once in the dark and once with the room's lights turned on. The fly was given 2 min in the dark to adapt before the protocol was conducted. In succession, the fly was given 2 min again to adapt to the light and the same protocol was repeated. Every light stimulus was applied via a pulse stimulator at 4.2 V, which was the voltage at which the light intensity was at 100%. 10 single stimuli of 1 s were given with an interpulse interval (IPI) of 1 s.

Recordings were acquired via Axoscope and analyzed via Clampfit 11.2 after filtering with a 360 Hz Gaussian filter and 50 Hz filter for electrical interference. The acquired receptor potential, lamina on and off responses were analyzed using Microsoft Excel and statistically tested via GraphPad Prism.

2.6 Immunohistochemistry and single particle tracking

2.6.1 Establishment of immunohistochemistry of L3 larvae for cac^{sfGFP} expression

Since cac^{sfGFP}-signals could not be detected under a CLSM after fixation of L3 larvae in 4% paraformaldehyde (PFA) in phosphate buffered saline (PBS), I tried different fixation approaches to establish a reliable method for cac^{sfGFP} detection. The highest staining quality could be obtained if L3 larvae were fixed in Bouin's fix for 25 min. The latter was washed out for at least 2h with PBS 0.1% Triton X (Tx), which was replaced every 20 min. Since Bouin's fix is yellow, the larvae were washed until the solution was transparent again. Although we

prefer Bouin's solution due to even better quality, preparations may alternatively be fixed in ice-cold Ethanol (100%, -30°C) for 5 to 7 min in order to ensure sufficient GFP labelling.

The preparation was then incubated in 0.4% BlockAce (in PBS 0.1% Tx) solution at 4°C overnight. After another washing step of 1 h (change every 10 min) with PBS 0.1% Tx, the preparations were put into the same dish to save antibody (AB). The primary AB (α-GFP chicken) was applied at 4°C at 1:1000 in PBS 0.1% Tx overnight. The primary AB was washed out with PBS for at least 4 h after which the secondary AB (α-chicken Alexa 488) was applied at 1:500 in PBS for 4 h in darkness at room temperature. Next, an ethanol (EtOH) series was conducted to dehydrate the preparations. Each step with increasing EtOH concentration (50%, 70%, 90%, 100%) was conducted for 10 min. Lastly, the preparations were mounted on slides and sealed with a cover (high precision glass cover slip 175 µm ± 5 µm) by nail polish. After 1 h of drying the polish, slides were scanned under a CLSM.

2.6.2 Comparative immunohistochemistry of L3 larvae for cac^{sfGFP} exon-out variants

For the comparative immunohistochemical stainings of different exon-out variants, L3 larvae were dissected as previously described in 2.4. Fixation was accomplished by fully immersing the larvae for 7 min in 100% EtOH, which was previously cooled at -30°C. Consecutively, samples were washed thrice for 10 min with PBS 0.3% Tx. Primary ABs (α-brp mouse 1:400 and α-HRP rabbit 1:1000) were applied overnight at 4°C in PBS 0.3% Tx. The next morning, samples were washed again thrice for 10 min with PBS 0.3% Tx and secondary ABs (donkey α-mouse Alexa 555, donkey α-rabbit Alexa 488 and Fluotag X4 α-GFP Alexa 647, all 1:500) were applied for 2 hrs at RT in PBS 0.3% Tx. After washing out the secondary ABs with PBS thrice for 10 min, an ethanol series with increasing concentrations (50%, 70%, 90%, 100% for 10 min each) was conducted to dehydrate the samples. Eventually, the samples were mounted in methylsalycylate on metal slips with high precision cover slips (170 µm), which were then sealed with nail polish. After drying for 1 h, samples were ready to be scanned under a CLSM microscope.

2.6.3 Immunohistochemistry of L3 larvae for NMJ morphology

L3 larvae were dissected as previously described in 2.4. Fixation was accomplished using 4% PFA for 30 min. Subsequently, the samples were washed for 10 min (changed twice). Initial tissue penetration was achieved by placing the larvae in an Eppendorf tube and using PBS 0.2% Tx for 20 min. Primary AB application (α-brp mouse 1:300 and α-HRP rabbit 1:600 in

PBS 0.2% Tx) was carried out for 60 min at RT. Then, samples were washed with PBS 0.2% Tx for 20 min (changed three times). Secondary ABs (goat α-mouse Alexa 647 and donkey α-rabbit Alexa 488, both 1:400 in PBS 0.2% Tx) were applied overnight at 4°C in darkness. After washing twice with PBS 0.2% Tx for 20 min and once with PBS for 20 min, larvae were mounted on slides and embedded in Vectashield. Slides were sealed using a coverslip, which was attached to slides and sealed via nail polish. After 1 h of drying the polish, slides were ready to be scanned under a CLSM.

2.6.4 STED microscopy and subsequent analysis

Wandering L3 larvae were dissected as previously described in 2.4. Fixation was conducted by immersing the larvae in ice-cold 100% EtOH for 7 minutes. After several rounds of washing with PBS, all dissected and fixated larvae were transferred into the same sylgard dish to ensure similar conditions for all larvae during antibody application. Penetration of the tissue was ensured by washing with PBS 0.2% Tx for 10 minutes (changed three times). Incubation of the primary antibodies (α-brp mouse and α-HRP both at 1:500 in PBS 0.2% Tx) was applied overnight at 4°C on a shaker. After three rounds of washing with PBS 0.2% Tx the next day, the secondary antibodies (Fluotag X4 α-GFP Atto 647N, α-mouse goat IgG Atto 594 and Fluotag-X4 α-rabbit IgG Atto 488, all at 1:250 in PBS 0.2% Tx) were applied for 2 h in darkness at room temperature. Then, three rounds of washing with PBS 0.2% Tx followed. Eventually, the larvae were mounted as described in 2.6.3 and were scanned using a Leica Stellaris 8 STED microscope.

2D STED scanning was carried out using the following settings: voxel size: 25 nm * 25 nm, z-step size 200 nm, magnification 93x (objective HC PL APO CS2 93x/1.30 glycerol), laser intensities: white light laser 85%, 775 nm laser 100%, 488 nm laser 10%.

3D STED scanning was conducted using the following settings: voxel size 24 nm * 24 nm, z-step size 105 nm, magnification 93x (objective HC PL APO CS2 93x/1.30 glycerol), laser intensities: white light laser 85%, 775 nm laser 100%, 488 nm laser 10%.

Subsequently, the acquired images were deconvoluted using the software Huygens Essential version 21.10 by Scientific Volume Imaging. The resulting .tif-images were then imported into a Python script created by XXXXX, which used the HRP staining as a mask. This script was then able to locate the brightest spots in a maximum projection and calculate the distance between cacophony spots and its closest brp spots. For more information on the exact use of this Python script or STED scanning, see the Master's thesis of XXXXX or Bell *et al.* (2024).

2.6.5 Single particle tracking via TIRFM

Wandering L3 larvae were dissected as described in 2.4, but with HL 3.1 Ca^{2+} saline to minimize muscle movements and therefore drift during imaging. We used Alexa 488 Goat α-HRP at a concentration of 1:300 for 5 min at RT to help localizing neuromuscular junctions since α-HRP binds to neuronal membrane (see 5.4). After rinsing the opened larva, it was placed on a custom fabricated glass slide with the ventral side facing down and fixed by using magnetic hooks.

To estimate channel numbers via TIRFM, we used the monomeric EOS4b tag, which constitutes a green-to-red photoconvertible fluorescent protein (Paez-Segala *et al.*, 2015). This tag exhibits a high thermodynamic stability, photostable green and red states, good photoconversion between both photo states and a resistance to fixatives, according to Paez-Segala *et al.*, 2015. Photoconversion of the mEOS4b tag can be initiated by using a laser at 405 nm (we used 402 nm, see below), while excitation of the converted red fluorophores can be elicited by using a laser at 561 nm (Paez-Segala *et al.*, 2015). We collaborated with Martin Heine on this project from whom we received flies with endogenously tagged cacophony^{mEOS4b} variants. Using the CRISPR/Cas9 method described in 2.3, we excised different exons and subsequently estimated the remaining channel numbers via TIRFM (for details, see below).

All experiments were conducted by use of a total internal reflection microscope. We used a 60x objective with oil immersion and 1.5x additional zoom as well as 2x2 binning, resulting in a pixel size of 144 nm. Images were scanned at a frame rate of 20 Hz. The endogenously expressed mEOS4b tags at the N-terminus of each cacophony channel were excited by sustained illumination with a 402nm UV laser (10% laser power) and a 561nm laser (100% laser power). Before recording, NMJs were localized by usage of 488nm laser (80% laser power), which excites the fluorophores of the α-HRP antibody. Additionally, lasers were magnified by 4x fold. The first 250 frames, only 561 nm laser was used to obtain baseline illumination. At frame 251, UV laser excited mEOS4b tags for 5000 frames with 402 nm laser illuminating junctions in parallel. The continuous excitation of mEOS4b will bleach the fluorophores over time, yet some single fluorophores will revert back to a red illumination state. This ‘blinking’ can then be used as a reference since it represents the illumination value of a single channel. Division of peak illumination values by the illumination value of a single channel will yield an estimate of the cacophony channels in a single AZ.

Image processing of the obtained scans was accomplished with ImageJ. We drift corrected the images with the software plugin NanoCore and subtracted the background for better contrast. Subsequently, we used a Python script designed by courtesy of XXXXX to detect regions of interests (ROIs), in this case single AZs. The script automatically detects ROIs in maximum

projection views of all 5250 frames. To be included into quantal analysis, illumination curves had to match the following criteria:

- An illumination maximum within the first 500 frames of UV light onset
- More than 300 values above baseline noise, which was calculated with a 500 frame sliding window – the lowest average of 500 frame window was considered as baseline
- Distinguishable single events

Subsequently, the .png-files generated by the Python script were thoroughly sorted out by hand according to the criteria listed above, and I analyzed the first five ROIs of each recording. We used the .csv-files generated by the Python script to analyze the quanta of the remaining illumination curves. The script normalized all values to the maximum illumination peak and subtracted the average of the aforementioned sliding window, which we considered as baseline noise, from all values. We considered the largest negative value in the baseline as noise since illumination could only result in positive values. We then looked for single distinguishable events above noise. Ideally, there were events, which were roughly common multiples of single events to ensure that the latter were not part of the noise. If possible, we averaged three of these events. If it was not possible to distinguish three similar single events, two events were averaged. Eventually, we divided the largest peak in the recording by the three or two smallest events and thus estimated the number of channels in an AZ. The Python script can be requested from XXXXX, who designed it.

Carsten Duch exploratively analyzed two recordings per genotype, but analyzed all, not just the first five regions. After comparing the analyzed data by both, we concluded that the data could be pooled since both investigators came to similar results across all genotypes. Values of the few regions that were analyzed by both investigators were averaged.

2.7 Behavioral assays

2.7.1 Fecundity Assay

To assess the ability to produce progeny in exon-out mutants and thus get an insight on one aspect of their fitness, a fecundity experiment was conducted. Pupae in late stages where sex determination via sex combs on the first leg pair was clearly possible (P12-P15) were collected from vials as the future parent generation. Pairs of a female and male (parental generation) each were placed in fresh vials to mate for 30 hours. This parental generation was between 25 and 69 hours old. We used 10 vials per genotype, thus having 10 pairs of parental flies each. Consequently, after mating the male was removed from the vial to

facilitate egg laying by the female. The female was given 27 hours from 8:30 a.m. on day 0 to 11:30 am on day 1, thus excluding the possibility of restricting experimental hours to certain daily times since *D. melanogaster* egg laying has been shown to be susceptible to circadian rhythm (Howlader and Sharma, 2006). The number of laid eggs per vial was counted and over the successive 17 days, vials were checked each morning at 10 a.m. and developmental stages of the fastest developing individuals were noted. Additionally, each freshly hatched adult fly was counted each day and removed from the vial.

2.7.2 Larval Crawling

This experiment was done in the Silies lab with a tracking apparatus capable of tracking multiple larvae at once, thus facilitating this experiment (courtesy of Marion Silies). Wandering L3 larvae were selected off vial walls for crawling experiments and starved in empty vials for 5 minutes. Afterwards, they were placed in the middle of a plasticine square on an agarose gel (1% in H_2O dest) using a brush. This square itself was placed on a tracking table with an acrylic glass plate. Usually, 10 larvae of the same genotype were recorded at a time. Occasionally, less than 10 larvae were available, in which case fewer larvae were recorded. Dishes were freshly poured each day before starting experiments. To prevent the larvae from escaping the boundary, an electrically charged wire was placed inside the square boundaries. Crawling pictures were obtained with a camera (Basler acA2040-90µm) from below the glass plate at a frame rate of 4 Hz for 5 minutes via pylon viewer (Version 6). Since some larvae were able to dig into the gel through small holes, only larvae that stayed inside the arena for 5 minutes were included into analysis. Tracking data of larval crawling (crawling distance and maximum speed) were analyzed via the free software FIMtrack (Universität Münster, Computer Vision and Machine Learning Systems).

2.8 Data analysis and statistics

All obtained data were analyzed using Microsoft Excel. Statistics were done using GraphPad Prism (Version 9). Further figure editing was completed with Corel Draw (Version X7). The significance level for all tests, including normality tests, was set at a p-value < 0.05. All data were statistically tested for normal distribution via a Shapiro-Wilk test. Comparison of two groups was done with an unpaired t-test if normally distributed and a Mann-Whitney-U-test if not normally distributed. If an experiment investigated at least three groups, t-tests and Mann-Whitney-U tests were not qualified for statistical analysis. Consequently, if data were normally

distributed, ANOVA tests with Tukey post-hoc tests were done to compare single groups. Not normally distributed data were compared via a Kruskal-Wallis ANOVA with Dunn's post-hoc test. For some analyses, Šidák or Dunnett post-hoc tests were performed. Test details are listed in figure captions.

2.8.1 Data availability statement

Data and analyses have been deposited with Stefanie Ryglewski and Carsten Duch (Institute for Developmental Biology and Neurobiology, JGU Mainz) and are made available upon reasonable request. The Python scripts for estimating channel numbers via single particle tracking and for detecting GFP-signal inside bruchpilot-masks were created by and are deposited with XXXXX (Institute for Developmental Biology and Neurobiology, JGU Mainz). In addition, the data from this study, which are published in Bell *et al.*, 2024 will be made available in a public repository.

2.9 Molecular Biology

2.9.1 DNA isolation from adult flies

The first step to obtain information on the presence of DNA constructs is to isolate DNA from the flies' genome. Therefore, single adult flies needed to be anesthetized with CO_2 and were then homogenized with a pipette tip containing 50 µL of squishing buffer (see appendix) with protease K to prevent contamination of the samples with too much protein. Samples were kept at RT for 20 min and were then heated up to 95°C in a water bath for 2 min to inactivate protease K. Subsequently, such obtained samples could be stored for several months in a -28°C freezer or at 4°C in a fridge.

2.9.2 PCR

Polymerase Chain reactions (PCR) were performed to either confirm successful exon excision for sfGFP$^{N\text{-}term}$- or mEOS4b-tagged exon-out variants or to validate presence of certain integrated constructs needed for experiments. All PCRs were carried out using a common thermocycler (BIO-RAD, T-100 Thermal Cycler). Taq-polymerase (New England Biolabs, #M0267S) was used for all PCRs.

Table 3: Protocol of a standard PCR. Annealing temperature & extension period are variable depending on primer sequence & construct of interest's length.

No. cycles	Temperature [C°]	Duration [s]	Description
None	95	30	Initial DNA denaturation
30	95	15	Denaturation per cycle
	Depending on primer	30	Annealing
	68	60/kb DNA	Extension
None	68	300	Concluding extension
None	12	∞	Holding temperature

2.9.3 Gel electrophoresis

Standard gel electrophoresis is conducted to visualize PCR amplification products. An 0.5% to 2.0% agarose gel in TAE Buffer (see appendix), depending on construct length, was poured for electrophoresis. For small constructs, e.g., 300 bp, 2.0% agarose gel was used, while for 3000 bp, 0.5% agarose gel was used. The gel was then heated with a microwave for 90 to 120 sec and cooled down for several minutes after which GelRed Stain (Roth, 0984.1) was added to visualize amplified DNA fragments. The casting chamber was provided with combs before gel casting to create the wells needed for sample loading. After 20 – 30 min, the gel was hard enough to be transferred into the electrophoresis chamber filled with TAE buffer. Before loading the wells, the samples were mixed with loading dye. At least one well per sample row was loaded with a DNA ladder (NEB, 1kb: #N3232S, 1kb plus: #N0550S) to estimate construct length appropriately. After connecting the chamber to the power source, electrophoresis was started at 80 V. Runtime varied between 1 to 2 h depending on the expected band size. Eventually, the gel was transferred into the documentation device (PeqLab, EBOX VX5), where DNA could be visualized via UV light. Images were created to document the resulting bands and afterwards, the gel was discarded.

3 Results

3.1 While the IS4B exon is essential for survival, the IS4A exon is needed for a healthy life and normal lifespan

3.1.1 Exon IS4A is essential for normal life expectancy

Since the homozygous loss of cacophony is lethal, a longevity study was conducted in order to obtain insight into effects of exon excision on life expectancy. When observing the different exon-out strains in their food vials, it is clearly noticeable that the homozygous removal of exon IS4A affects the animals severely: they are lethargic, often fall off the vial wall and die due to getting stuck on the food. Death due to being stuck on the food is not an uncommon sight in food vials but is normally observed in older animals. However, it was noticeable, that ΔIS4A animals often died at younger ages. Some of the above mentioned behavioral defects have been studied and quantified in the Ph. D. thesis of Lukas Kilo (2021). Figure 4 depicts the surviving flies in percent of the initial cohort sorted per genotype, which were obtained over a span of 88 days, in a Kaplan-Meier-Curve. All cacophony variants were tagged with sfGFP.

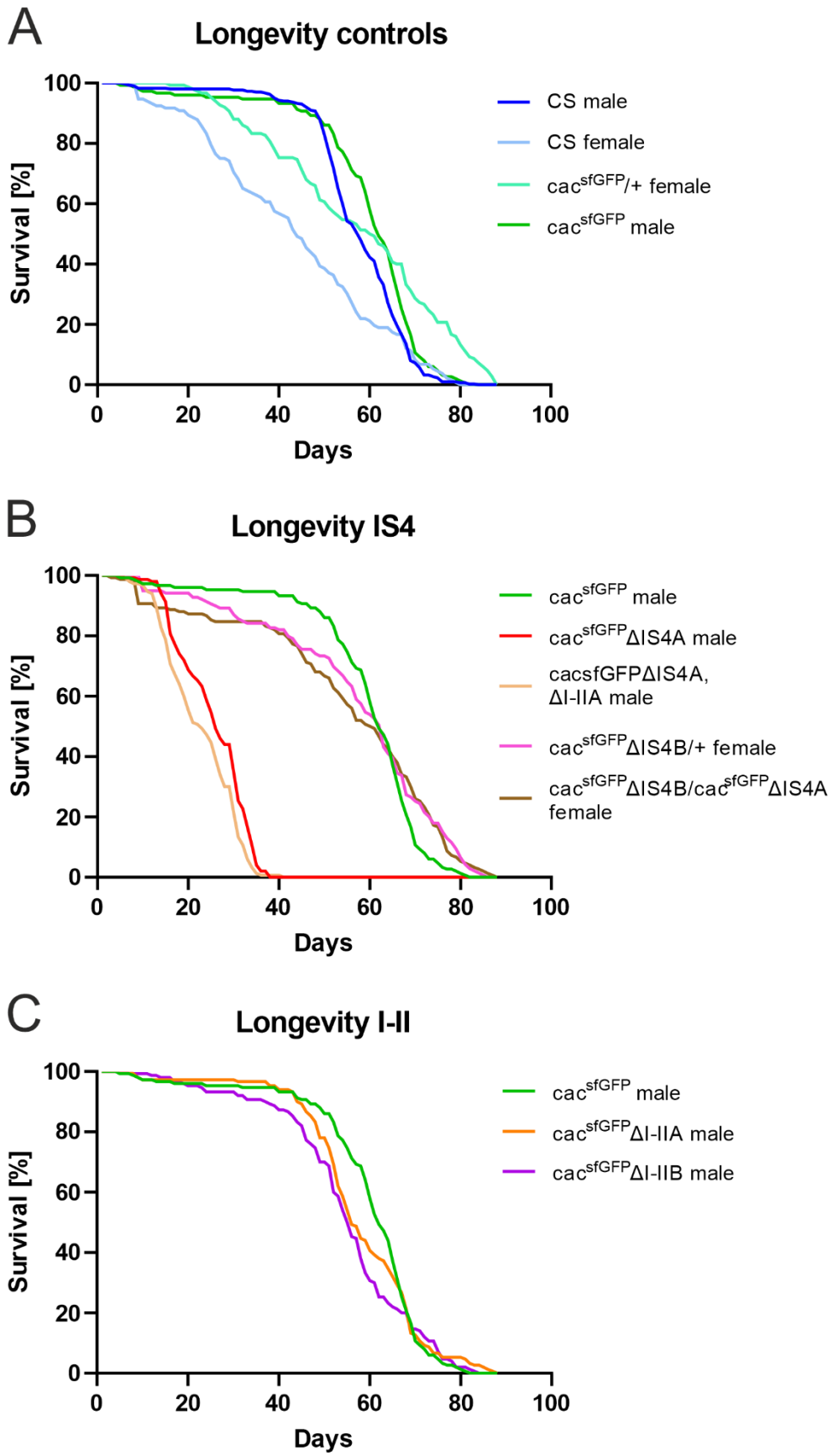

Figure 4: Survival rate of different exon-out variants and controls visualized in a Kaplan-Meier-curve. The survival rate is depicted in percent over the course of 88 days in all panels. **A** depicts longevity data of several controls: Canton S male (navy

blue) n= 300, Canton S female (light blue) n= 132, $\frac{cacsfGFP}{+}$ female (teal) n= 150 and cac^{sfGFP} (green) n= 150. **B** depicts longevity data of animals containing exon excisions at the IS4 locus: cac^{sfGFP} male as control (green), cac^{sfGFP}ΔIS4A male (red) n= 150, cac^{sfGFP}ΔIS4A, ^{sfGFP}ΔI-IIA male (tan) n= 150, $\frac{sfGFP\Delta IS4B}{+}$ female (pink) n= 139 and $\frac{sfGFP\Delta IS4B}{sfGFP\Delta IS4A}$ female (brown) n= 150. **C** depicts longevity data of animals containing exon excisions at the I-II locus: cac^{sfGFP} male as control (green), cac^{sfGFP}ΔI-IIA male (orange) n= 150 and cac^{sfGFP}ΔI-IIB male (magenta) n= 150.

The severely reduced life span of ΔIS4A male animals quantified in Figure 4 is striking: the entire cohort is dead after 38 days while in all other genotypes, including both controls Canton S and cac^{sfGFP} males, 96.33% and 94.67% of the cohorts are still alive at that point in time, respectively. The additional removal of I-IIA, resulting in the double exon-out ΔIS4A, ΔI-IIA, has no additional effect on longevity when compared to single IS4A excision as both curves are very similar. This is intriguing since the removal of IS4A leaves 13 of 18 isoforms possible for transcription while removal of both, IS4A and I-IIA, leaves only 4 isoforms. This provides evidence for the theory that effects of exon removal are more due to specific exon function rather than variability of many available isoforms. Transheterozygous expression of $\frac{\text{cacsfGFP}\Delta IS4B}{\text{cacsfGFP}\Delta IS4A}$ enables a full rescue for animals, thereby giving rise to the theory that animals can assemble the needed composition of isoforms from two differently severed genes on different chromosomes. Furthermore, heterozygous expression of ΔIS4B over a wild-type chromosome ($\frac{\text{cacsfGFP}\Delta IS4B}{+}$) does not alter life expectancy. Taken the last two findings together, it can be concluded that a distinct exon excision in only one of two chromosomes (thus only in females) does not influence life expectancy. A similar observation was already made in climbing behavior where the performance of ΔIS4A animals was detrimental while $\frac{\Delta IS4B}{\Delta IS4A}$ climbing performance was rescued to control levels (Ph.D. thesis Lukas Kilo, 2021). Additionally, Lukas Kilo observed increased calcium signals via calcium imaging in ΔIS4A pupae (P8) (Ph.D. thesis Lukas Kilo, 2021). Since intracellular Ca^{2+} levels are tightly regulated and increased Ca^{2+} levels can be toxic (Brini and Carafoli, 2009; Krebs, 2022), this might provide an explanation as to why ΔIS4A animals show such a severely decreased lifespan compared to other genotypes.

Removal of either I-II exon has no effect on survival rate when compared to the respective control, which is cac^{sfGFP}. This provides evidence that alternative splicing of the IS4 locus is essential for a normal life expectancy with regular fitness while alternative splicing at the I-II locus is not influential regarding life expectancy and fitness. Interestingly, Canton S females show a tendency to die earlier than their male counterparts when comparing cac^{sfGFP} females to males of the same genotype. It has been published that *Drosophila melanogaster* females can show a reduced lifespan compared to males of the same genotype (Gaitanidis ***et al.***, 2019), which provides an explanation on why in this experimental series, female cohorts died earlier than males of the same genotype. However, this is not subject to this thesis. Please note, that these observations were made under laboratory conditions and may not be transferable to

wild-type longevity in conditions outside of the lab, where lack of I-II exons may very well be detrimental due to predators for example. This point is elaborated on in more detail in section 4.1.

3.1.2 Removal of IS4A and I-IIA have effects on flies' hatching rate and speed, respectively

Over the course of this study, it was noticeable that in some exon-out variants, ΔIS4A adults seemed to hatch faster than Canton S and cac^{sfGFP} while ΔI-IIA animals hatched slower under the same conditions. To quantify these effects and to observe hatching rate and egg laying, an experiment on fecundity was conducted. All cacophony variants in this experiment were tagged with an sfGFP-tag.

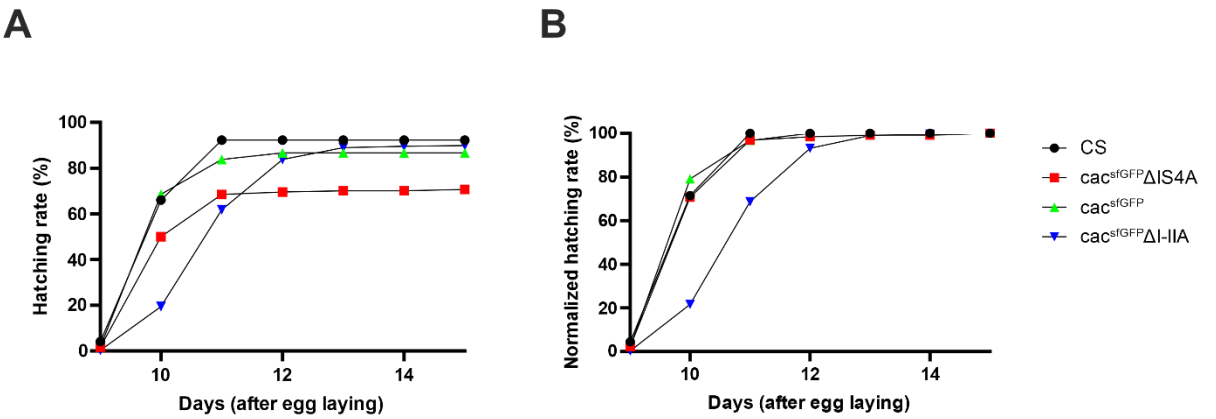

Figure 5: Line chart of absolute and normalized hatching rates of exon-out variants and controls. A depicts the absolute hatching rate in percent of Canton S (black), cacs^{fGFP} (green), cac^{sfGFP}ΔIS4A (red) and cac^{sfGFP}ΔI-IIA (blue). Eggs hatched: Canton S n= 179, cac^{sfGFP} n= 91, ΔIS4A n= 130, ΔI-IIA n= 310. **B** depicts the hatching rate normalized to the number of all eggs that eventually developed into adulthood. All cacophony variants were sfGFP-tagged.

It is noticeable that in ΔIS4A animals only 70% of layed eggs developed into adulthood as compared to 92% in Canton S, 87% in cac^{sfGFP} and 90% in ΔI-IIA (Figure 5). This hints at a reduced viability of animals expressing cacophony isoforms containing only IS4B exons, which is supported by a severely reduced lifespan (Figure 4). Furthermore, it is clearly visible that ΔI-IIA animals are hatching a day later on average than ΔIS4A and control animals. This is quite curious as animals containing cacophony isoforms with only I-IIB seem to have wild-type like survivability. This hints at possible functions of both exons in development, but only IS4A is needed for a wild-type like absolute hatching rate. The previous observation that ΔIS4A animals hatched earlier than other fly strains could not be validated with this experiment.

The reduced rate of ΔIS4A eggs developing into adulthood is in accordance with a reduced lifespan (Figure 4) and may be the result of increased calcium signals in ΔIS4A pupae (P8) as observed by Lukas Kilo via calcium imaging (Ph.D. thesis Lukas Kilo, 2021). Increased calcium levels are toxic (Brini and Carafoli, 2009; Krebs, 2022) and thus, removal of IS4A could

negatively impact development. This is supported by the fact that Ca^{2+} is an essential player in neural outgrowth during development (Hutchins and Kalil, 2008; Rosenberg and Spitzer, 2011).

3.2 Effects of reduced isoform variability on localization and synaptic transmission at NMJs

3.2.1 Detection of all exons in the NMJ, yet ΔIS4B and ΔI-IIB exhibit less protein label intensity

Since my focus of electrophysiology was on the NMJ of L3 larvae, immunohistochemistry with successive CLSM was conducted to explore whether all exon-out variants localize to presynaptic terminals of NMJs. All cacophony variants were tagged with an sfGFP-tag.

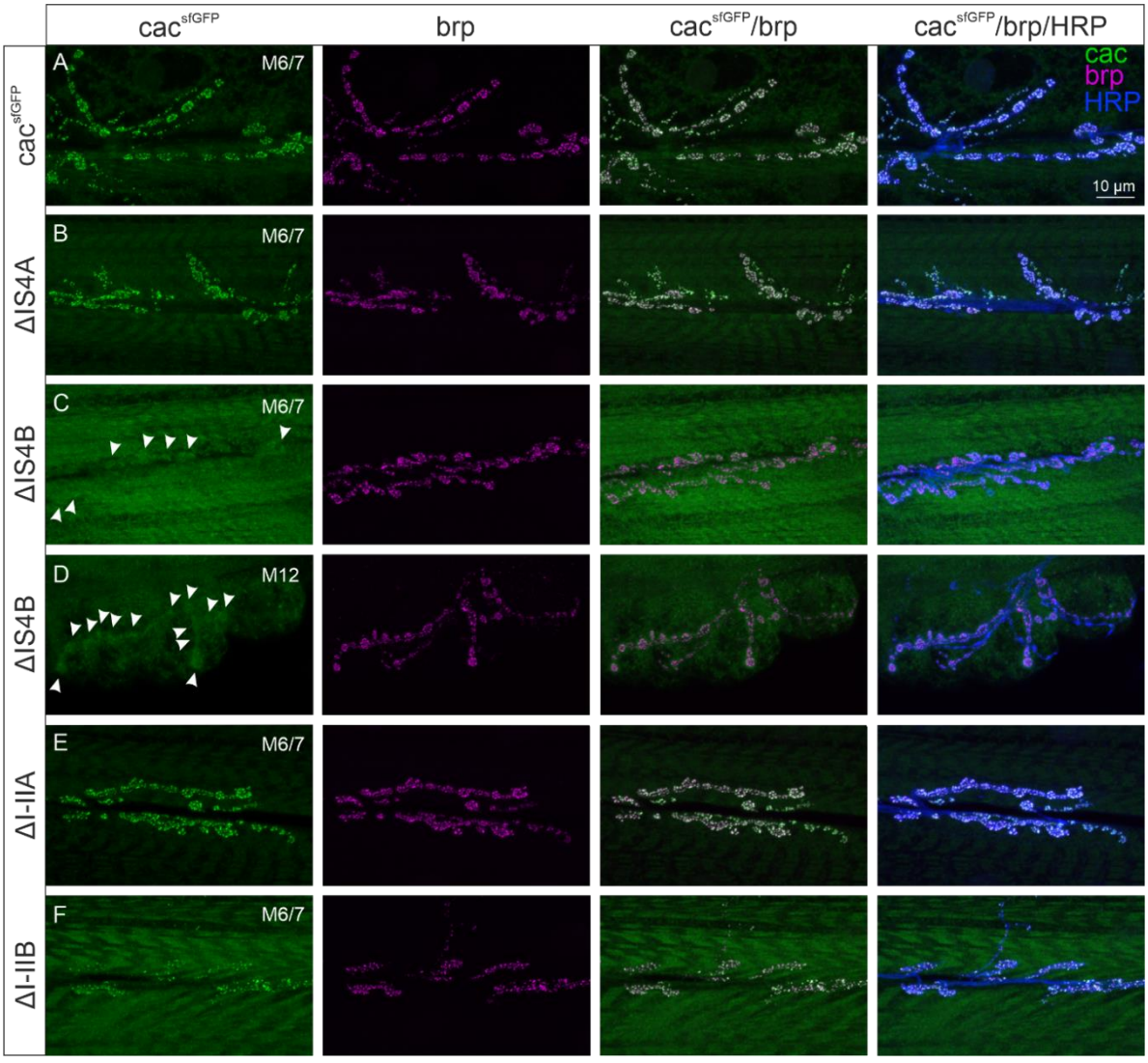

Figure 6: Representative immunohistochemistry stainings of NMJs on M6/7 and M12 in L3 larvae of different exon-out variants. The left panel depicts cac^{sfGFP} in green, the second to the left bruchpilot in magenta, the second to the right is a

merge of cac^{sfGFP} (green) and bruchpilot (magenta) and the right panel is a merge between cacsfGFP (green), bruchpilot (magenta) and HRP (blue) to outline the entire terminal. **A** depicts cac^{sfGFP}, **B** cac^{sfGFP}ΔIS4A, **C** $\frac{cacsfGFP\Delta IS4B}{+}$ on M6, **D** $\frac{cacsfGFP\Delta IS4B}{Fm7c}$ on M12, **E** cac^{sfGFP}ΔI-IIA and **F** cac^{sfGFP}ΔI-IIB. White arrows indicate very subtle, yet recognizable cac^{sfGFP} label in presynaptic terminals in $\frac{\Delta IS4B}{+}$ animals (C, D). Colocalization of cac^{sfGFP} and brp in the panel second to the right is indicated by white spots. Colocalization of cac^{sfGFP}, brp and HRP in the right panel is indicated by teal spots. Scalebar: 10 µM. All cacophony variants were sfGFP-tagged. Data by XXXXX (Bachelor's thesis) and Bell *et al.*, 2024.

Representative immunohistochemistry stainings (Figure 6) conducted by XXXXX, whom I supervised during his Bachelor's thesis, demonstrate that reduction of isoform variability by means of exon excision of IS4B and I-IIB leads to clearly less GFP label when compared to control. However, cac spots still co-localize with brp in ΔI-IIB but not in ΔIS4B. This lack of co-localization hints towards the possibility, that ΔIS4B cannot be tethered to the release site via brp. However, it needs consideration that ΔIS4B was only scanned in a heterozygous animal ($\frac{cacsfGFP\Delta IS4B}{+}$), meaning that there could be cacophony channels in the NMJs, which are undetectable due to the missing GFP-tag on the wild-type chromosome. ΔIS4A and ΔI-IIA larvae noticeably show a similar GFP-tagged cacophony label. These findings support our theory that IS4B is crucially needed at presynaptic terminals, although the missing GFP label could be due to the aforementioned heterozygosity. Lastly, there are no glaring differences in bouton shape, confirming previous experimental results on this obtained by Bachelor students (XXXXX, XXXXX, XXXXX) in our lab (results not shown). The data in Figure 6 have been published in Bell *et al.*, 2024.

3.2.2 Quantification of sfGFP label intensity suggests reduced I-IIB expression in presynaptic terminals

As stated above, immunolabeling demonstrates that all exons seem to encode for isoforms that localize to presynaptic terminals of NMJs, although it is unclear and therefore debatable whether cac channels containing IS4A actually localize properly (Figure 6). Still, ΔI-IIB apparently shows reduced label intensity. Since these immunohistochemistry stainings were not conducted in a comparable manner, we designed an experiment to soundly quantify cac^{sfGFP} label intensities. Subsequently, we can compare possible effects of certain exon excisions on synaptic transmission with protein label intensity. It has been previously described that the fluorescence intensity of this specific sfGFP-tag seems to correlate with the amount of cacophony in active zones (Gratz *et al.*, 2019).

All larvae were handled in the same dish after fixation and scanned on the same day with identical laser and detector settings to ensure comparability between the different genotypes (Figure 7). Analysis was partially automized with a Python script (courtesy of XXXXX), that detected brp staining and created a mask. Subsequently, sfGFP staining from a maximum

projection view inside that mask was considered as functional cacophony inside AZs. This is important since cac^{sfGFP} outside of the brp mask should not be functional and should not contribute to synaptic transmission. cac^{sfGFP} outside AZs could be in transport to the axon terminals for example. cac^{sfGFP} label intensity from maximum projection view inside the brp mask was eventually compared to the exon out variants to gain insight on isoform expression.

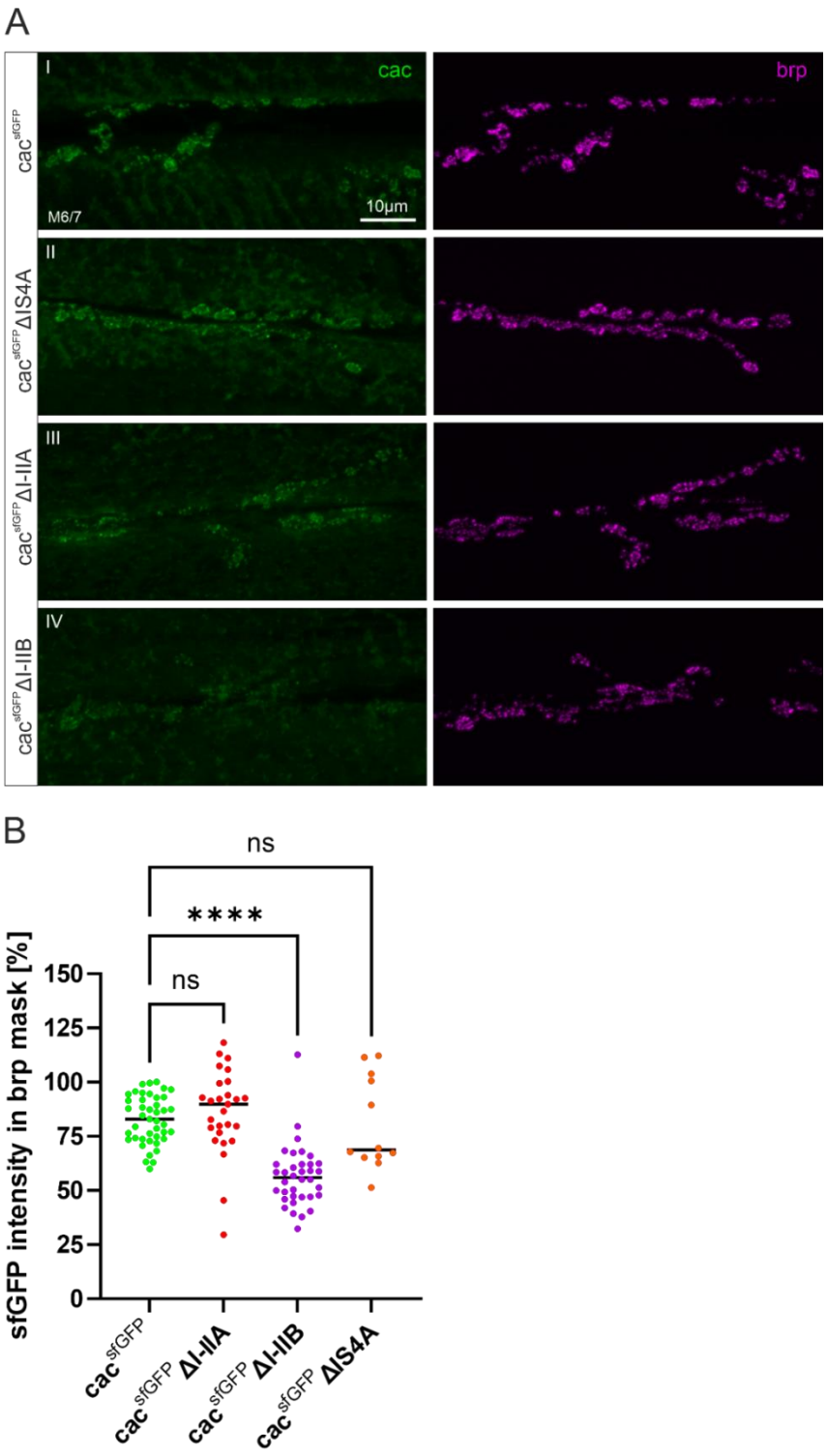

Figure 7: Representative comparable immunohistochemistry stainings of NMJs onto M6/7 and relative cac^{sfGFP} fluorescence intensities of different exon-out variants normalized to control. A depicts cacs^{fGFP} (green) in the left panel and

bruchpilot (magenta) in the right panel. Scalebar: 10 µm. A_I depicts cac^{sfGFP}, A_{II} cac^{sfGFP}ΔIS4A, A_{III} cac^{sfGFP}ΔI-IIA and A_{IV} cac^{sfGFP}ΔI-IIB. **B** depicts a scatter plot of normalized quantified cac^{sfGFP} label intensities for control and several sfGFP-tagged exon-out variants. Each data point represents one NMJ. Shown are cac^{sfGFP} (green) n= 8, cac^{sfGFP}ΔI-IIA (red) n= 8, cac^{sfGFP}ΔI-IIB (purple) n= 5 and cac^{sfGFP}ΔIS4A (orange) n=3. Each value was normalized to the highest control value of each experiment. Statistics: all groups were normally distributed; therefore, a one-way ANOVA was conducted, comparing exon-out variants only to control: p=, Šidák post-hoc test: cac^{sfGFP} vs. ΔIS4A p= 0.9998, cac^{sfGFP} vs. ΔI-IIA p= 0.8072, cac^{sfGFP} vs. ΔI-IIB p= 0.0464. Median shown for all data (Bell *et al.*, 2024).

It can be seen, that animals lacking exon I-IIB have reduced cacophony label in NMJs of M6/7 ($p< 0.0001$, Figure 7). As explained above, the label intensity of cac^{sfGFP} may correlate with protein in AZs. Therefore, it is likely that ΔI-IIB animals lack a substantial number of cacophony channels in AZs. ΔI-IIA meanwhile shows no significant decrease in sfGFP intensity ($p= 0.8072$), but the distribution of intensity value is quite high compared to control. ΔIS4A is also not significantly different from control ($p= 0.9998$). Thus, I-IIB may be needed for normal cacophony channel number at the NMJ of M6/7. A channel estimation via photoconvertible mEOS4b-tags was conducted to estimate these channel numbers more directly (see Figure 22). The data shown in Figure 7 have been published in Bell *et al.* (2024).

3.2.2 Cacophony isoforms do not localize differently inside AZs at the NMJ

As described above, cacophony isoforms likely vary in their abundance in presynaptic terminals. It is established in mammalian systems that presynaptic calcium channels in the AZ can localize closer to or further away from SVs and therefore to the vesicular release machinery (Wadel, Neher and Sakaba, 2007; Eggermann *et al.*, 2012). It has been suggested by R. J. Kittel *et al.*, 2006, that the longer rise time of EPSCs in *brp* deficiency mutants at *Drosophila* NMJs is consequential to an increase in distance between VGCCs and SVs.

Thus, an attractive hypothesis would be that different cacophony isoforms could be coupled more tightly or loosely with the vesicular release machinery, which in turn would increase the dynamic range of MNs. To explore this theory, Master student XXXXX studied tagged different exon-out variants with two channel stimulus emission depletion microscopy (dual channel STED) and calculated the distance between every cacophony and the next bruchpilot spot. All cacophony variants were sfGFP-tagged.

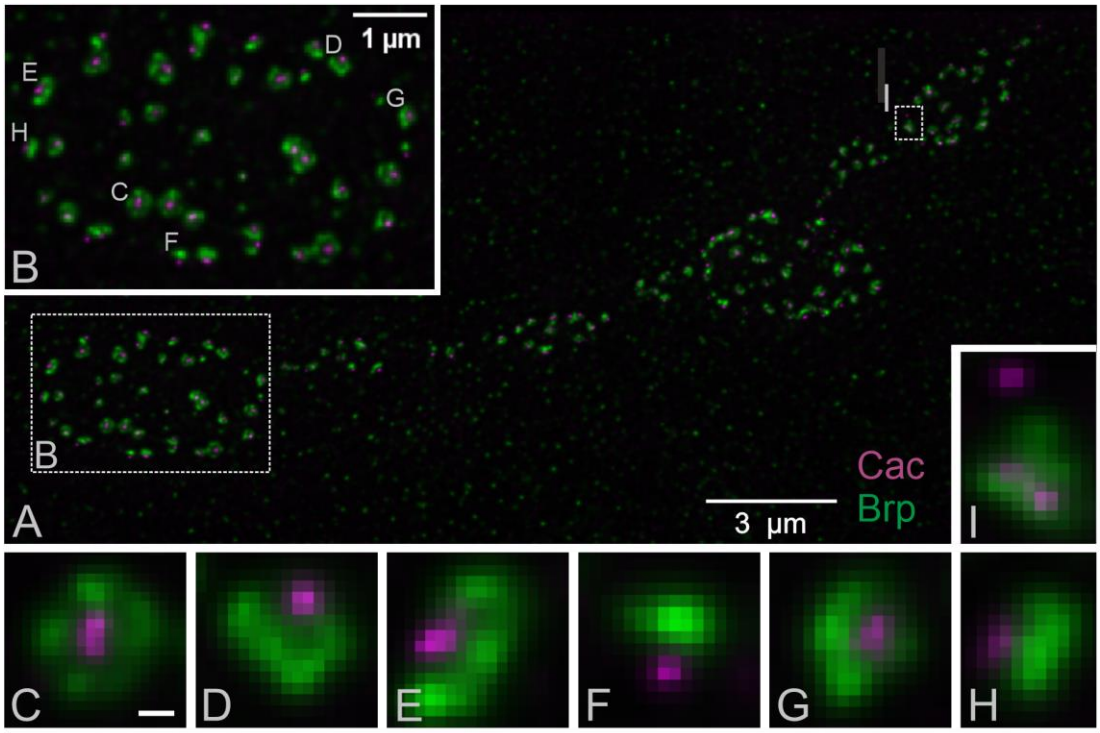

Figure 8: Localization of cacophony exon-out variants inside AZs of larval NMJs (M6) via STED microscopy of immunocytochemistry stainings after deconvolution. A depicts several junctions of a control animal with brp labeled in green and GFP labeled in magenta (scale bar 3µM). **B** shows an enlargement of a selection of AZs (scale bar 1µM). **C-I** depict several enlarged AZs, in which brp molecules form a 'donut' shape around cacophony channels (scale bar 100nm). Not all brp molecules can be displayed in the same focal plane, seven different AZs are shown. Figure modified after XXXXX (Master's thesis) and Bell *et al.* (2024).

Figure 8 displays several AZs within representative 1b boutons at NMJs of M6/7 from different angles, depending on how the AZs within the sphere-shaped boutons are oriented relative to the focal plane. When looked upon from a top view (Figure 8C), it is visible that several brp puncta (green) surround a single cacophony punctum (magenta), thereby shaping a donut-like structure. Figure 8D-H show different cacophony puncta (magenta) surrounded by brp label (green) from different angles. Consequently, having perspective on multiple AZs within a single bouton from different angles allows a first visual estimate of the distance between the active zone protein brp (green) and the cac channel cluster (magenta) that form a punctum. A quantification of the data that are shown in Figure 8 is depicted in Figure 9. The data in Figure 8 have been published in Bell *et al.*, 2024.

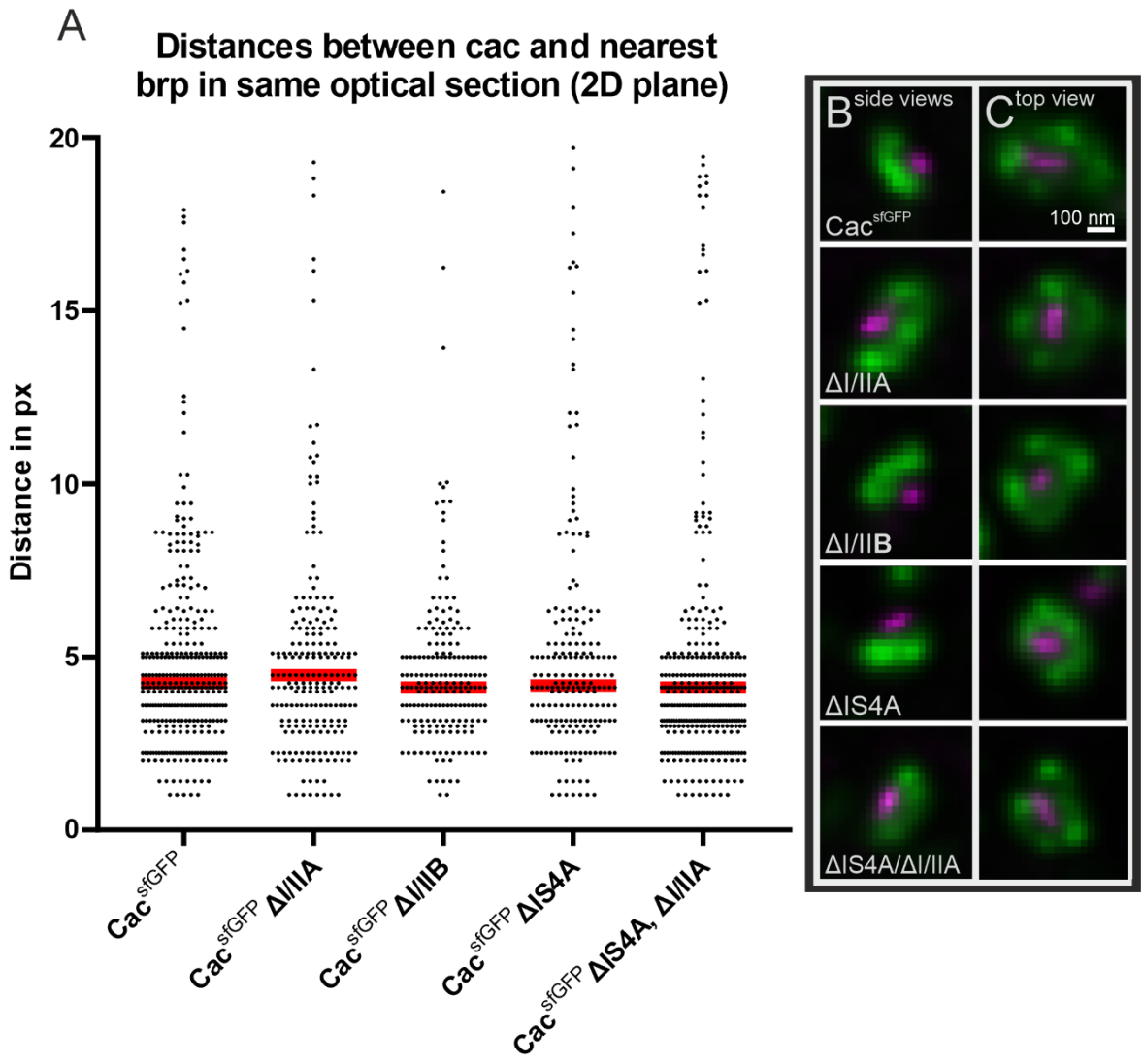

Figure 9: Quantification of the distance of cacophony spots to the closest bruchpilot spots in the same optical section. The quantification is shown in a scatter plot in **A**. Genotypes shown are cac^{sfGFP}, cac^{sfGFP} ΔI-IIA, cac^{sfGFP} ΔI-IIB, cac^{sfGFP} ΔIS4A & cac^{sfGFP}ΔIS4A, I-IIA. **B** and **C** show several AZs from side views and top views, respectively. All cacophony variants were sfGFP-tagged. The average for each genotype is represented by the horizontal red bar. Figure modified after XXXXX (Master's thesis) and Bell *et al.*, 2024.

There is no difference in distance between cac and brp spots, no matter the point of view, indicating that once cacophony channels are inside the AZ, isoform variability does not determine the coupling distance (Figure 9). Since the resolution of these STED images is 25 nm and the median distance of cac and brp is around 4 – 5 pixels, the average distance is estimated to be around 100 to 125 nm (Bell *et al.*, 2024). From these images, we estimated the AZ diameter to be around 250 nm due to viewpoints from different angles between cac and brp (XXXXX, Master's thesis). This is in accordance with recent studies that have investigated Ca_V2 channel clusters in *C. elegans* (Mueller *et al.*, 2023). Thus, it can be assumed that cacophony in a distance above 250 nm away from the next brp spot is not in a functional relationship with brp. It needs to be considered that there could be cacophony channels in reserve

located intracellularly, which are also endogenously tagged with sfGFP, but are not yet located in the membrane. The data in Figure 9 have been published in Bell *et al.* (2024)

3.2.3 Synaptic transmission is abolished in MNs upon IS4B exon excision

Since excision of the IS4B exon is homozygous lethal and the expression of one single isoform containing IS4B, *cac1*, rescues synaptic transmission and viability, we hypothesized that IS4B is needed for neurotransmitter release at *Drosophila* NMJs. Since heterozygous expression of ΔIS4B over a balancer chromosome enables females to express wild-type *cac*, we had to take a different experimental angle: we crossed ΔIS4B over $cac^{Flpstop}$ to achieve a hemizygous ΔIS4B expression in a mosaic *cac* knockout. A flippase under UAS-control, here driven by a larval crawling MN driver (OK6-GAL4) so that it is only expressed in these MNs, binds to specific target sites in the $cac^{Flpstop}$ cassette that resides within the cac gene and can invert a transcriptional terminator from a non-disruptive to a disruptive state. This will stochastically cause premature termination of transcription and thus result in a cac null phenotype in some but not all motoneurons (Fisher *et al.*, 2017). Successful flip events were monitored by td-tomato expression in the respective MNs (see 2.5.2). This approach allows to generate viable mosaic animals with cac^{null} over ΔIS4B in few motoneurons by employing the OK6-GAL4 driver, which drives most effectively in motoneurons onto muscle 12. Therefore, for experiments involving the cacFLPStop approach, only muscle 12 was recorded (Figure 10). In this experiment, all cacophony variants were sfGFP-tagged except for ΔIS4A in the $\frac{\Delta IS4B}{\Delta IS4A}$ animals, which was tagRFP-tagged. The presence of UAS-Flp is not listed in the label of the scatter plots as well as in the caption below the figure (Figure 10) for reasons of clarity. Please note that all animals that carried a $cac^{Flpstop}$ on the X chromosome also carried a UAS-Flp on the 2nd chromosome. The animals labeled as '$\frac{cacsfGFP\Delta IS4B}{cacFlpStop}$ – no driver' did not carry a driver on the second chromosome, their genotype is $\frac{cacsfGFP\Delta IS4B}{cacFlpStop}$; $\frac{+}{UAS-Flp}$. Please see section 5.5 or a full list of genotypes used in this experiment.

We analyzed evoked release, quantal size and mean quantal content (MQC). Evoked release is the transmission amplitude, that is released upon an action potential invasion of the presynaptic terminal, which in this case is artificially evoked via a suction electrode. Quantal size is characterized as the transmission amplitude generated by fusion of a single synaptic vesicle and typically recorded by observing spontaneous release without stimulation. The smallest transient amplitude was determined as quantal size. MQC is the amount of SVs released upon an action potential and is calculated by dividing the transmission amplitude of

evoked release by the amplitude of quantal size (one single SV). Please note that the amplitudes recorded in TEVC represent negative inward currents, thus lower values represent a higher transmission amplitude.

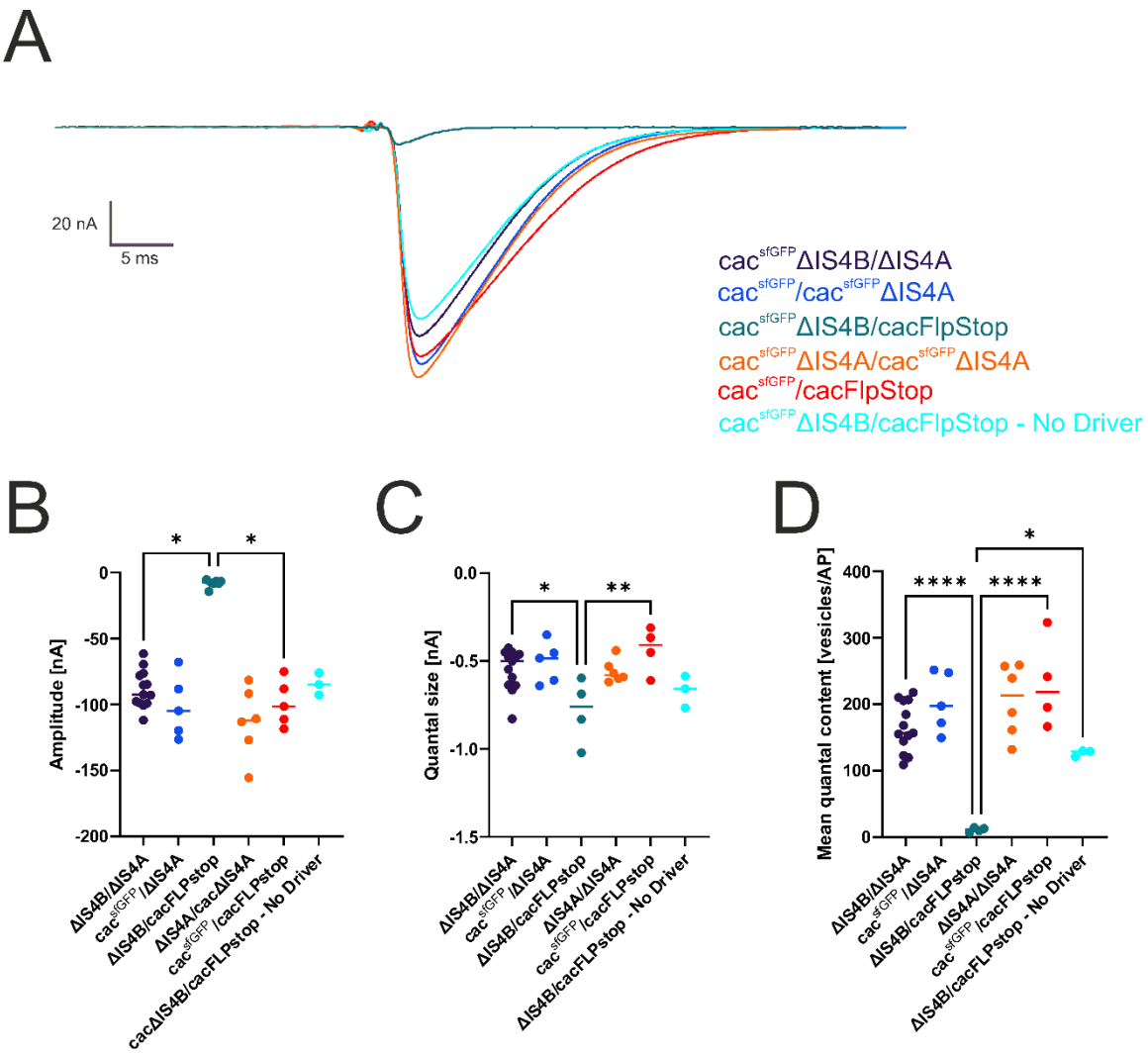

Figure 10: Traces and scatter plots of evoked release, quantal size and mean quantal content (MQC) of different cacophony variants in the NMJ onto M12. A depicts traces of evoked EPSC amplitudes of several cacophony variants: $\frac{cacsfGFP\Delta IS4B}{cacRFP\Delta IS4A}$ (dark blue), $\frac{cacsfGFP}{cacsfGFP\Delta IS4A}$ (navy blue), $\frac{cacsfGFP\Delta IS4B}{cacFlpStop}$ (dark green), $\frac{cacsfGFP\Delta IS4A}{cacsfGFP\Delta IS4A}$ (orange), $\frac{cacsfGFP}{cacFlpStop}$ (red) and $\frac{cacsfGFP\Delta IS4B}{cacFlpStop}$ – no driver (light blue). **B** depicts amplitudes of evoked responses of all analyzed genotypes organized in a scatter plot: $\frac{\Delta IS4B}{\Delta IS4A}$ n 10, $\frac{cacsfGFP}{cacsfGFP\Delta IS4A}$ n= 2, $\frac{cacsfGFP\Delta IS4B}{cacFlpStop}$ n= 5, $\frac{cacsfGFP\Delta IS4A}{cacsfGFP\Delta IS4A}$ n= 4, $\frac{cacsfGFP}{cacFlpStop}$ n= 5 and $\frac{cacsfGFP\Delta IS4B}{cacFlpStop}$ – no driver n= 2. Statistics: Group $\frac{cacsfGFP\Delta IS4B}{cacFlpStop}$ was not normally distributed (p= 0.0302), therefore a Kruskal-Wallis-ANOVA was conducted: p= 0.0009, Dunn's post-hoc test: $\frac{cacsfGFP\Delta IS4B}{cacRFP\Delta IS4A}$ vs. $\frac{cacsfGFP\Delta IS4B}{cacFlpstop}$ p= 0.0205, $\frac{cacsfGFP\Delta IS4B}{cacsfGFP\Delta IS4A}$ vs. $\frac{cacsfGFP}{cacsfGFP\Delta IS4A}$ p> 0.9999, . $\frac{cacsfGFP\Delta IS4B}{cacFlpstop}$ vs. $\frac{cacsfGFP}{cacFlpstop}$ p= 0.0135, $\frac{cacsfGFP\Delta IS4B}{cacFlpstop}$ vs. $\frac{cacsfGFP\Delta IS4B}{cacFlpstop}$ – no driver p= 0.8113, . $\frac{cacsfGFP}{cacsfGFP\Delta IS4A}$ vs. $\frac{cacsfGFP}{cacFlpstop}$ p> 0.9999, $\frac{cacsfGFP\Delta IS4B}{cacRFP\Delta IS4A}$ vs. $\frac{cacsfGFP}{cacFlpstop}$ p> 0.9999, $\frac{cacsfGFP\Delta IS4B}{cacsRFP\Delta IS4A}$ vs. $\frac{cacsfGFP\Delta IS4A}{cacsfGFP\Delta IS4A}$ p= 0.8666, $\frac{cacsfGFP}{cacsfGFP\Delta IS4A}$ vs. $\frac{cacsfGFP\Delta IS4A}{cacsfGFP\Delta IS4A}$ p> 0.9999, $\frac{cacsfGFP\Delta IS4A}{cacsfGFP\Delta IS4A}$ vs. $\frac{cacsfGFP}{cacFlpstop}$ p> 0.9999. **C** shows the quantal size of all analyzed genotypes organized in a scatter plot. Statistics: All groups were normally distributed. Ordinary one-way ANOVA p= 0.0043, Šidák post-hoc test: $\frac{cacsfGFP\Delta IS4B}{cacRFP\Delta IS4A}$ vs. $\frac{cacsfGFP}{cacsfGFP\Delta IS4A}$ p= 0.9982, $\frac{cacsfGFP\Delta IS4B}{cacRFP\Delta IS4A}$ vs. $\frac{cacsfGFP\Delta IS4B}{cacFlpstop}$ p= 0.0163, $\frac{cacsfGFP\Delta IS4B}{cacRFP\Delta IS4A}$ vs. $\frac{cacsfGFP\Delta IS4A}{cacsfGFP\Delta IS4A}$ p> 0.9999, $\frac{cacsfGFP\Delta IS4B}{cacFlpstop}$ vs. $\frac{cacsfGFP}{cacFlpstop}$ p= 0.0024, $\frac{cacsfGFP\Delta IS4B}{cacFlpstop}$ vs. $\frac{cacsfGFP\Delta IS4B}{cacFlpstop}$ – no driver p= 0.8927, $\frac{cacsfGFPcacGFP}{cacsfGFP\Delta IS4A}$ vs. $\frac{cacsfGFP\Delta IS4A}{cacsfGFP\Delta IS4A}$ p= 0.9977, $\frac{cacsfGFP\Delta IS4B}{cacRFP\Delta IS4A}$ vs. $\frac{cacsfGFP}{cacFlpstop}$ p= 0.6153, $\frac{cacsfGFP}{cacsfGFP\Delta IS4A}$ vs. $\frac{cacsfGFP}{cacFlpstop}$ p= 0.9839, $\frac{cacsfGFP\Delta IS4A}{cacsfGFP\Delta IS4A}$ vs.

$\frac{cacsfGFP}{cacFlpstop}$ p= 0.6822. **D** depicts the vesicles released per evoked action potential, also known as the mean quantal content, of all analyzed genotypes organized in a scatter plot. Statistics: All groups were normally distributed. Ordinary one-way ANOVA p< 0.0001, Šidák post-hoc test: $\frac{cacsfGFP\Delta IS4B}{cacRFP\Delta IS4A}$ vs. $\frac{cacsfGFP}{cacsfGFP\Delta IS4A}$ p= 0.6218, $\frac{cacsfGFP\Delta IS4B}{cacRFP\Delta IS4A}$ vs. $\frac{cacsfGFP\Delta IS4B}{cacFlpstop}$ p< 0.0001, $\frac{cacsfGFP\Delta IS4B}{cacFlpstop}$ vs. $\frac{cacsfGFP}{cacFlpstop}$ p< 0.0001, $\frac{cacsfGFP\Delta IS4B}{cacFlpstop}$ vs. $\frac{cacsfGFP\Delta IS4B}{cacFlpstop}$ – no driver p= 0.0121, $\frac{cacsfGFP\Delta IS4B}{cacRFP\Delta IS4A}$ vs. $\frac{cacsfGFP}{cacFlpstop}$ p= 0.0989, $\frac{cacsfGFP}{cacsfGFP\Delta IS4A}$ vs. $\frac{cacsfGFP}{cacFlpstop}$ p= 0.9752, $\frac{cacsfGFP\Delta IS4B}{cacRFP\Delta IS4A}$ vs. $\frac{cacsfGFP\Delta IS4A}{cacsfGFP\Delta IS4A}$ p= 0.4567, $\frac{cacsfGFP}{\Delta IS4A}$ vs. $\frac{cacsfGFP\Delta IS4A}{cacsfGFP\Delta IS4A}$ p> 0.9999, $\frac{cacsfGFP\Delta IS4A}{cacsfGFP\Delta IS4A}$ vs. $\frac{cacsfGFP}{cacFlpstop}$ p= 0.9825. The line in each column depicts the median in all scatter plots. Depictions of not significant test results were not included in B-D to avoid loss of overview due to many compared groups. All genotypes were tested against one another, because the exon out variants are concerning the same locus (IS4) and there are multiple controls ($\frac{cacsfGFP}{cacsfGFP\Delta IS4A}$, $\frac{cacsfGFP}{cacFlpstop}$ and $\frac{cacsfGFP\Delta IS4B}{cacFlpstop}$). All cacophony variants were sfGFP-tagged except for ΔIS4A in the $\frac{\Delta IS4B}{\Delta IS4A}$ animals, which was tagRFP-tagged. Animals containing cac^{FlpStop} on the X chromosome also carried a UAS-Flp to induce a premature stop in the FlpStop cassette; this was not included in the naming of genotypes for reasons of clarity (please see 5.5 for complete genotypes). Tags were not listed for every genotype in the label of the scatter plots' y-axes for clarity (Bell *et al.*, 2024).

We employed TEVC of muscle 12 as described in 2.5.2 to record evoked postsynaptic currents. As all genotypes are concerning the same locus (IS4) and we tested three controls ($\frac{cacsfGFP}{cacsfGFP\Delta IS4A}$, $\frac{cacsfGFP}{cacFlpstop}$ and $\frac{cacsfGFP\Delta IS4B}{cacFlpstop}$), it is suitable and necessary to compare all genotypes with each other.

Evoked synaptic transmission data obtained by TEVC onto M12 clearly show a severe reduction of both transmission amplitude (p= 0.0135) and mean quantal content (MQC, p< 0.0001) in animals with the ΔIS4B chromosome and a factual cac knockout via cac^{FlpStop} in the respective crawling motoneurons when compared to the control $\frac{cacsfGFP}{cacFlpStop}$ (Figure 10). This is evidence for the hypothesis that IS4B is essential for synaptic transmission at the NMJ, since there are only very few SVs fusing with the presynaptic membrane (MQC $\frac{\Delta IS4B}{cacFlpStop}$: ~13 SVs vs. MQC $\frac{cacsfGFP}{cacFlpStop}$: 218 SVs; Figure 10D) upon stimulation. Expression of $\frac{\Delta IS4B}{cacFlpStop}$ without a driver to initiate the mosaic knockout shows a normal transmission amplitude, indicating that the knockout works as intended. The strong reduction in transmission amplitude and MQC can be rescued to control levels by transheterozygous expression of $\frac{\Delta IS4B}{\Delta IS4A}$ (evoked p> 0.9999, MQC p= 0.0989). Additionally, homozygous expression of ΔIS4A as well as $\frac{cacsfGFP}{\Delta IS4A}$ yield no significantly different transmission amplitudes (ΔIS4A p> 0.9999, $\frac{cacsfGFP}{\Delta IS4A}$ p> 0.9999) or MQC (ΔIS4A p= 0.9825, $\frac{cacsfGFP}{\Delta IS4A}$ p= 0.9752) when compared to control, further indicating that motoneurons only need IS4B isoforms at presynaptic terminals for proper neurotransmission onto muscle 12.

IS4B removal results in increased quantal size (Figure 10C), which could be a form of homeostatic compensation since the cacophony isoforms responsible for SV release are severely reduced. The change in the size of one quantum ('quantal size') indicates either a higher

number of neurotransmitters per SV or an increased response of postsynaptically located glutamate receptors (GluR). This would therefore counteract the impairment in an attempt to maintain synaptic stability (Lazarevic *et al.*, 2013; James, Zwiefelhofer and Frank, 2019; Rozenfeld *et al.*, 2023). However, it is quite clear, that increasing the quantal size in response to IS4B removal is not able to rescue evoked transmission amplitude.

A limiting factor of this experiment is the low number of tested animals, especially for $\frac{cacsfGFP\Delta IS4B}{cacFlpstop}$ and $\frac{cacsfGFP\Delta IS4B}{cacFlpstop}$; $\frac{+}{UAS-FLP}$. Therefore, the statistical analyses may need to be observed with caution. This may in fact also be an alternative explanation for the reduced quantal size in $\frac{cacsfGFP\Delta IS4B}{cacFlpstop}$ animals as there are only four data points available for analysis. The data shown in Figure 10 have been published in Bell *et al.* (2024).

3.2.4 Synaptic transmission is abolished in flight MNs upon IS4B exon excision in adults

We investigated IS4B excision not only in L3 larval crawling MNs, but also wanted to explore effects on adult flight MNs. We therefore used the aforementioned cacFlpStop technique, but with a flight MN driver, 23H06-GAL4, which drives expression of GAL-4 in flight motoneurons. Animals expressing $\frac{\Delta IS4B}{cacFlpStop}$; $\frac{UAS-FLP}{+}$ $\frac{23H06-GAL4}{+}$ were not able to fly, providing an indicator, that IS4B is also essential for neuromuscular synaptic transmission in adult animals. This was then further tested exploratively by using current clamp recordings for the adult flight muscle NMJ (see 2.5.3). In this experiment, the ΔIS4B exon-out variant was sfGFP-tagged. Please note that the Canton S trace was omitted for clarity. The quantification of amplitudes of Canton S can be observed in Figure 11A.

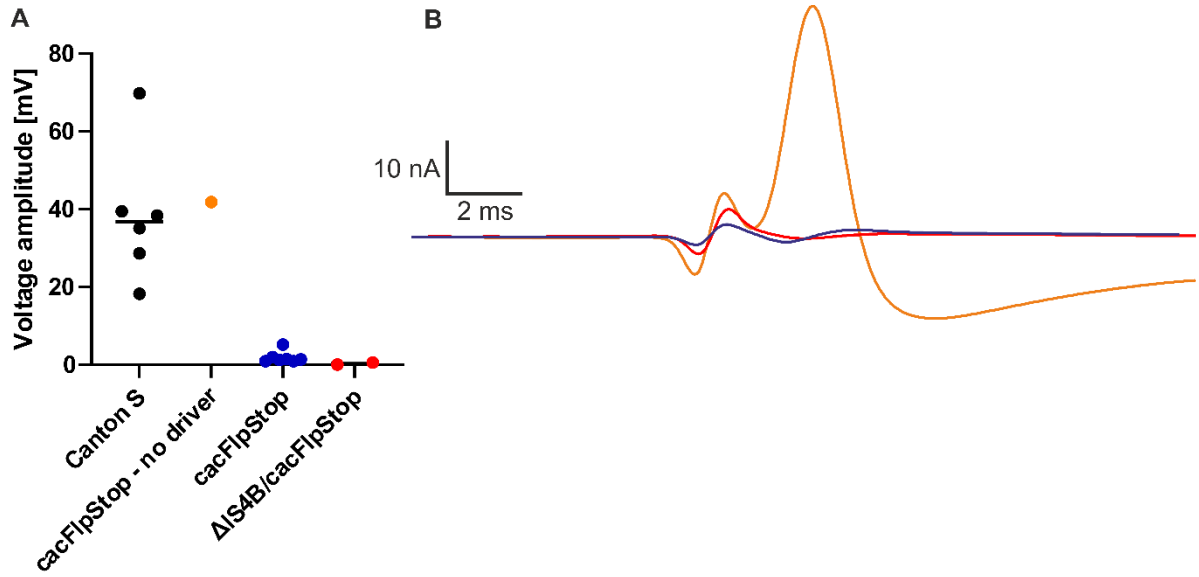

Figure 11: Scatter plot and representative traces of voltage amplitudes in flight DLMs of adult flies. A depicts a scatter plot with the voltage amplitude [mV] recorded in current clamp mode: Canton S (black) n= 4, cacFlpStop without a driver (orange) n= 1, cacFlpStop; UAS-Flp; 23H06-GAL4 (blue) n=3 and $\frac{cacsfGFP\Delta IS4B}{cacFlpStop}$; UAS-Flp; 23H06-GAL4 (red) n= 2. B shows representative traces in amplitude for cacFlpStop without a driver (orange), cacFlpStop; UAS-Flp; 23H06-GAL4 (blue) and $\frac{cacsfGFP\Delta IS4B}{cacFlpStop}$; UAS-Flp; 23H06GAL4 (red). The Canton S trace was omitted for clarity. Median shown for all data. ΔIS4B was sfGFP-tagged.

As can be seen in Figure 11, flight muscles in Canton S and the one recorded in cacFlpStop without a driver, synaptic transmission could still be evoked reliably, though with a high variability in Canton S. This provides evidence, that the insertion of the FlpStop-cassette as described in 2.5.2 alone has no effect on synaptic transmission amplitude. Still, a hyperpolarization after return to baseline is clearly visible (Figure 11). Since this was one recorded animal in an explorative experimental approach, I cannot state with certainty if this is an outlier or true for all animals. In contrast, cacFlpStop with a driver and $\frac{\Delta IS4B}{cacFlpStop}$; $\frac{23H06-GAL4}{+}$ showed no or tiny responses upon stimulation through the giant fiber pathway. This provides further evidence that IS4B is crucial for synaptic transmission in both larvae and adult neurons. In consequence, animals without functional IS4B cacophony isoforms cannot fly (visual, qualitative observation).

3.2.5 Both I-II exons are required for normal synaptic transmission

Homozygous viable cacophony exon out variants do not need the Flp stop approach due to their viability. To test the effects of these exon out variants on synaptic transmission, we used TEVC on M6, since it is a very large muscle, that is easily accessible and NMJ experiments are usually conducted in this muscle (Imlach and McCabe, 2009). It is reasonable and necessary to compare all genotypes against one another since both I-II exon out variants exhibit

opposing effects on transmission amplitude while the transheterozygous mutant rescues transmission amplitude.

In contrast to ΔIS4A animals, ΔI-IIA and ΔI-IIB animals show no obvious behavior impairments in food vials. In accordance, ΔI-IIA animals have a similar life expectancy (Figure 4). Additionally, previous studies in our lab have shown that courtship success, flight initiation and duration, as well as larval crawling distance, are not significantly different compared to control (Lukas Kilo, Ph.D. thesis 2021, data not shown). To assess effects of exon excision on synaptic transmission, I conducted a TEVC experiment on muscle 6. In this experiment, all cacophony variants were sfGFP-tagged except for ΔIS4A in the $\frac{\Delta IS4B}{\Delta IS4A}$ animals, which was tagRFP-tagged.

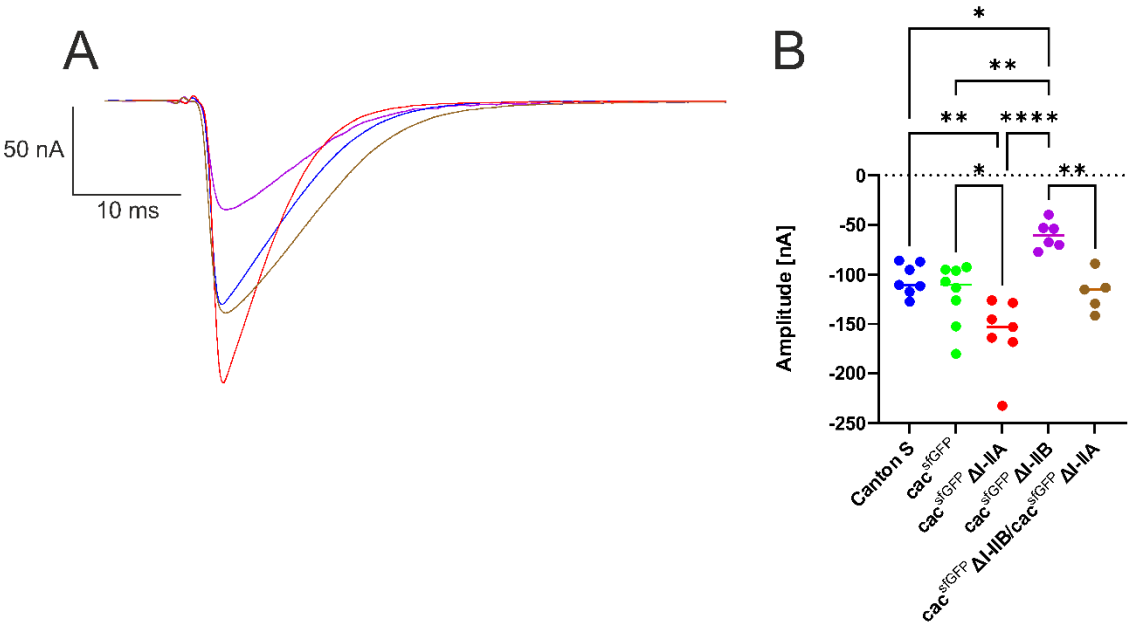

Figure 12: Synaptic transmission in animals with reduced isoform variability due to excisions at the I-II locus. A shows traces representative for the amplitude of evoked inward currents in muscle 6 generated by stimulation of the presynaptic motoneuron: Canton S (blue), ΔI-IIA (red), ΔI-IIB (purple) and $\frac{\Delta I-IIA}{\Delta I-IIB}$ (brown). The green trace for cac^{sfGFP} is not shown in this figure for clarity since it is similar in amplitude to CS. **B** depicts amplitudes of evoked responses of all analyzed genotypes organized in a scatter plot: CS n= 5, cac^{sfGFP} n= 6, ΔI-IIA n= 6, ΔI-IIB n= 5, $\frac{\Delta I-IIA}{\Delta I-IIB}$ n= 4. The line in each plot is the median. Statistics: all groups were normally distributed. Ordinary one-way ANOVA p< 0.0001, Tukey post-hoc test: CS vs cac^{sfGFP} p= 0.7775, CS vs ΔI-IIA p= 0.0039, CS vs ΔI-IIB p = 0.0307, CS vs $\frac{\Delta I-IIA}{\Delta I-IIB}$ p= 0.9156, cac^{sfGFP} vs ΔI-IIA p= 0.0465, cac^{sfGFP} vs ΔI-IIB p= 0.0015, cac^{sfGFP} vs $\frac{\Delta I-IIA}{\Delta I-IIB}$ p= 0.9997, ΔI-IIA vs ΔI-IIB p< 0.0001, ΔI-IIA vs $\frac{\Delta I-IIA}{\Delta I-IIB}$ p= 0.0667, ΔI-IIB vs $\frac{\Delta I-IIA}{\Delta I-IIB}$ p= 0.0079. All genotypes were tested against one another, because Canton S and cac^{sfGFP} both serve as controls, while the exon out variants are concerning the same locus (I-II) and show different effects on evoked release. Not significant test results were not included in B to avoid loss of overview due to many compared groups. All cacophony variants were sfGFP-tagged (Bell *et al.*, 2024).

When looking at evoked synaptic transmission amplitude, a one-way ANOVA showed highly significant differences between the tested groups with p< 0.0001 (Figure 12). Unexpectedly, ΔI-IIA showed significantly higher amplitude evoked transmission by approximately 40 % as compared to control (Tukey post-hoc p= 0.0465). ΔI-IIB showed significantly lower evoked transmission amplitude as compared to control (p= 0.0015). Expressing both exon excisions

as a transheterozygous mutant ($\frac{\Delta I-IIA}{\Delta I-IIB}$) results in a control-like current amplitude (cac^{sfGFP} vs. $\frac{\Delta I-IIA}{\Delta I-IIB}$ p= 0.9997). These data indicate that both exons are needed for a normal synaptic transmission amplitude and that isoform composition for a normal synaptic transmission amplitude can still be assembled from two chromosomes with different I-II exon excisions as we found for the IS4 locus (Figure 10). However, we also published these data pooled together with recordings conducted by a colleague in our lab, XXXXX, and do not observe the significantly increased synaptic transmission amplitude in ΔI-IIA (Bell *et al.*, 2024). A tendency to increased transmission amplitude remains, however. Therefore, the data concerning ΔI-IIA might need more careful interpretation. In contrast, the effect of significantly decreased amplitude persists in ΔI-IIB animals (Bell *et al.*, 2024).

Please note, that the amplitudes shown are only representative in amplitude, but not necessarily representative in shape with regard to kinetics (Figure 12). This is due to the fact that there were no traces in the recordings, which were representative for the median transmission amplitudes as well as for the kinetics. Analysis of said kinetics and representative traces will be shown later in Figure 17 of section 3.2.8. The data in Figure 12 have been published in Bell *et al.* (2024).

3.2.6 Synaptic transmission is unaltered in animals lacking IS4A exon.

Animals lacking the IS4A exon show a significantly reduced lifespan as well as impaired motor behavior such as in flight or during larval crawling (Bachelor Thesis XXXXX, Lukas Kilo, Ph.D. thesis). Consequently, synaptic transmission from the MN to the crawling muscle is an obvious target of research to elucidate the source of these impairments. We again tested this by TEVC recordings from M6 in L3 larvae. A one-way ANOVA of synaptic transmission amplitude yielded significant differences between the tested groups (Figure 13, p= 0.0011). ΔIS4A animals do not show statistically significantly different currents in amplitude compared to control (p= 0.3048). Still, variability of current amplitude is higher than in control – an effect that other members of our lab have confirmed in different experiments, for example in current patch clamp recordings from motoneuron somata in pupae (Stefanie Ryglewski, personal communication).

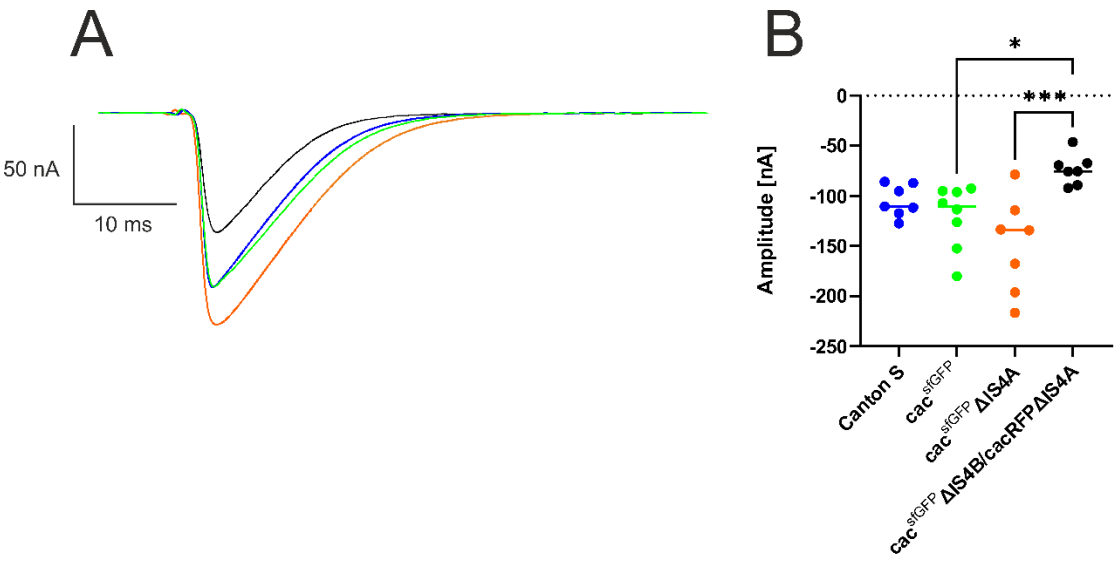

Figure 13: Synaptic transmission in ΔIS4A & transheterozygous mutant. A shows traces representative for the amplitude of evoked inward currents in muscle 6 generated by stimulation of the presynaptic motoneuron. Canton S (blue), cac^{sfGFP} (green), ΔIS4A (orange) and $\frac{\Delta IS4A}{\Delta IS4B}$ (black). **B** depicts amplitudes of evoked responses of all analyzed genotypes organized in a scatter plot: CS n= 5, cac^{sfGFP} n= 6, ΔIS4A n= 6, $\frac{\Delta IS4A}{\Delta IS4B}$ n= 6. The line in each plot is the median. Statistics: all groups were normally distributed. Ordinary one-way ANOVA p= 0.0011, Tukey post-hoc test: CS vs cac^{sfGFP} p= 0.7683, CS vs ΔIS4A p= 0.0601, CS vs $\frac{\Delta IS4A}{\Delta IS4B}$ p= 0.2483, cac^{sfGFP} vs ΔIS4A p= 0.3048, cac^{sfGFP} vs $\frac{\Delta IS4A}{\Delta IS4B}$ p= 0.0327, ΔIS4A vs $\frac{\Delta IS4A}{\Delta IS4B}$ p= 0.0006. Not significant test results were not included in B to avoid loss of overview due to many compared groups. All genotypes were tested against one another, because Canton S and cac^{sfGFP} both serve as controls, while the exon out variants are concerning the same locus (IS4). All cacophony variants were sfGFP-tagged except for ΔIS4A in the $\frac{\Delta IS4B}{\Delta IS4A}$ animals, which was RFP-tagged (Bell *et al.*, 2024).

To check for a possible rescue effect of the severe behavioral phenotype in ΔIS4A animals, we crossed a transheterozygous mutant ($\frac{\Delta IS4A}{\Delta IS4B}$). As a result, neurons may in theory express all possible isoforms, but complementary from different chromosomes instead of enabling all isoforms to be transcribed from one chromosome. This led to highly significantly reduced currents compared to ΔIS4A (p= 0.0006) as well as significantly reduced currents as compared to cac^{sfGFP} (p= 0.0327). Albeit current amplitudes are not on control level, transheterozygous adults show a remarkably different viability and fitness compared to ΔIS4A animals. The partial rescue of synaptic transmission amplitude however seems to be sufficient to ensure a normal lifespan (Figure 4) and normal climbing behavior (Ph.D. thesis Lukas Kilo, 2021). The reduced amplitude in transheterozygous mutant of IS4 is particularly noticeable when compared to the one of I-II. Interestingly, this reduced amplitude in transheterozygous mutants of IS4 is only true for muscle 6 since data of muscle 12 indicate a full rescue as can be seen in Figure 10. This might be due to the possibility that MNs recruit different compositions of cacophony channels for the AZs depending on the muscle, which I deem rather unlikely since there is no obvious benefit to equipping different crawling muscles, which work peristaltically, with different Ca_V2 channel isoforms. Another more plausible explanation would be the comparison of the transheterozygous mutant to different genotypes between experiments. This might result in statistical differences when compared to homozygous cacophony exon out

variants (Figure 10), while comparison to heterozygous exon out variants with $cac^{FlpStop}$ results in no significant differences (Figure 13). Additionally, a tendency of increased synaptic transmission amplitude can also be observed in homozygous ΔIS4A animals compared to the transheterozygous mutant for M12, although not statistically significant. This might simply be due to a higher variance and increased number of recorded animals in the transheterozygous group for the TEVC experiment on M12 (Figure 10, n= 10 vs. n= 6).

We have pooled my TEVC data with those acquired by my colleague in our lab, XXXXX, and are in the process of publishing these results (Bell *et al.*, 2024). These data still indicate a slight tendency, albeit not significant, towards a higher transmission amplitude in ΔIS4A animals compared to Canton S and cac^{sfGFP}. In addition, the transheterozygous mutant exhibits significantly lower transmission amplitudes when compared to cac^{sfGFP} (Bell *et al.*, 2024). Therefore, these pooled data strengthen the observations made in Figure 13.

Please note, that like in Figure 12, the traces depicted in Figure 13 are only representative for the median transmission amplitude, not the activation or inactivation kinetics. These will be analyzed in Figure 17 of section 3.2.8. The data in Figure 13 have been published in Bell *et al.* (2024).

3.2.7 Short-term plasticity, mEPSC amplitude & frequency at NMJ onto M6 unaffected by most exon excisions

Short-term plasticity is a mechanism by the nervous system in response to recent synaptic activity (von Gersdorff and Borst, 2002). This process is typically studied by stimulation via so-called paired pulses (PP) in certain temporal distances, in which the second vesicle release is still influenced by the previous release. A reduced amplitude of the second pulse compared to the first one is called synaptic depression whilst an increased amplitude is called synaptic facilitation. Both are constantly countering each other simultaneously (Jackman and Regehr, 2017). To study especially the effects of reduced isoform variability on short-term plasticity, PPs with various interpulse intervals (IPI) between 10 and 100 ms were elicited. In this experiment regarding PP, mEPSC amplitude and frequency, all cacophony variants were sfGFP-tagged except for ΔIS4A in the $\frac{\Delta IS4B}{\Delta IS4A}$ animals, where it was tagged with an RFP-tag. The data in Figure 14, Figure 15 and Figure 16 have been published in Bell *et al.* (2024).

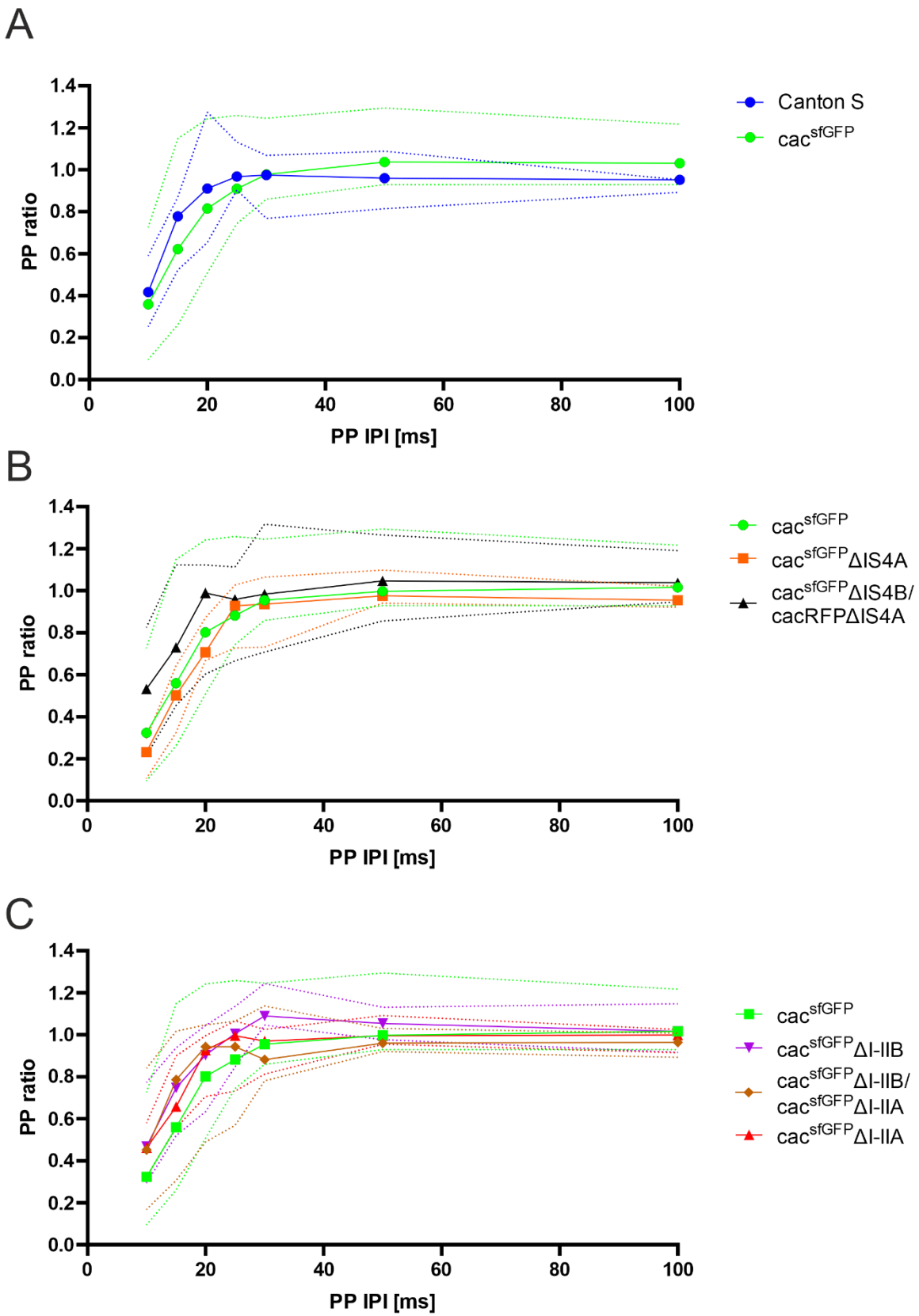

Figure 14: Line chart with the paired pulse ratio of interpulse intervals of 10, 15, 20, 25, 30, 50 and 100 ms. A depicts PP ratios of Canton S (blue), cac^{sfGFP} (green), ΔIS4A (orange) and $\frac{\Delta IS4B}{\Delta IS4A}$ (black) in a line chart. **B** shows PP ratios of cac^{sfGFP} (green), ΔIS4A (orange) and $\frac{\Delta IS4B}{\Delta IS4A}$ (black). **C** depicts PP ratios of cac^{sfGFP} (green), ΔI-IIB (purple), $\frac{\Delta I-IIB}{\Delta I-IIA}$ (brown) and ΔI-IIA (red). Median shown for all charts. The dotted lines display the upper and lower range of data distribution and were chosen over error bars

for clarity. All cacophony variants were sfGFP-tagged except for ΔIS4A in the $\frac{\Delta IS4B}{\Delta IS4A}$ animals, which was RFP-tagged (Bell *et al.*, 2024).

It can be deduced from Figure 14, that both controls (Canton S and cac^{sfGFP}) as well as the different exon-out variants show no obvious differences in PP ratio when IPIs are set from 25 ms to 100 ms. However, especially at time points closely after the first pulse at 10 ms and 15ms IPI, PP ratio can vary quite strongly between the genotypes with exon excisions at locus IS4. I therefore quantified the PP ratios and statistically tested the time points of IPIs 10 and 15 ms to look at these time points in more detail (Figure 15).

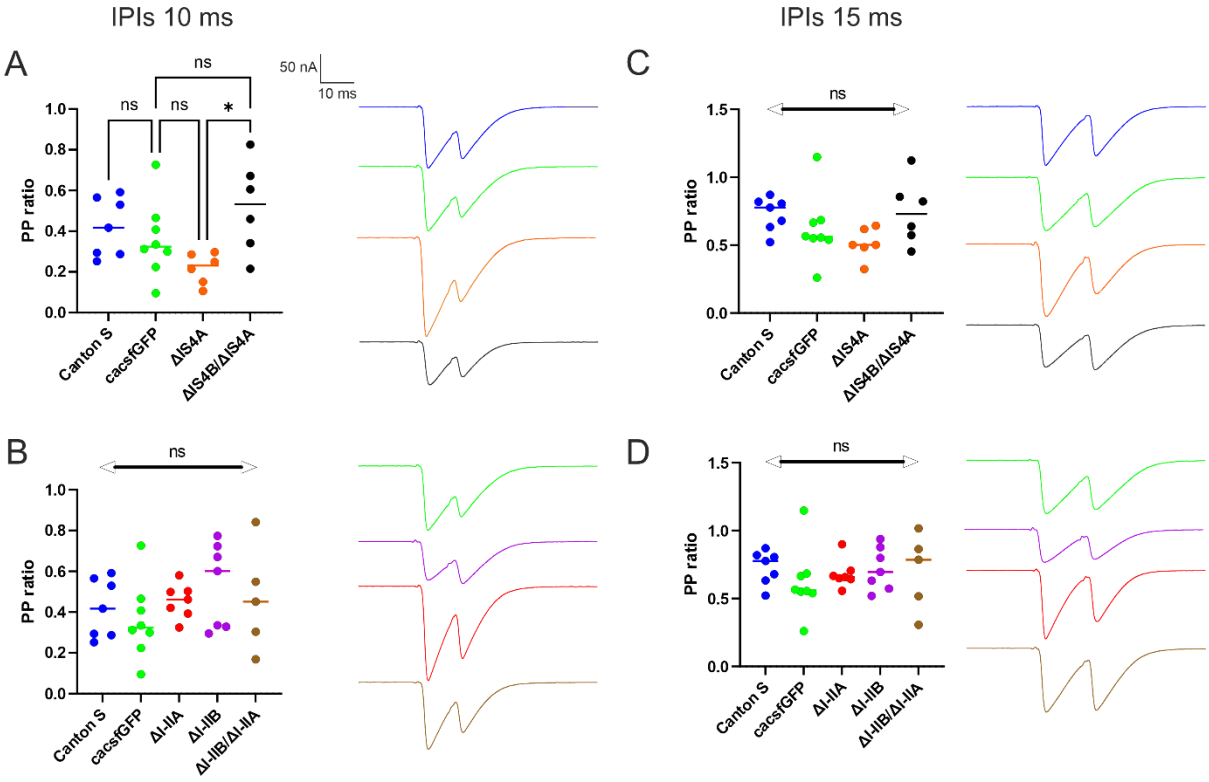

Figure 15: Quantification and comparisons of paired pulse ratios at different IPIs. A depicts a scatter plot and representative traces of PP ratios of controls and exon-out variants considering locus IS4 at 10 ms IPI: Canton S (blue), cac^{sfGFP} (green), ΔIS4A (orange) and $\frac{\Delta IS4B}{\Delta IS4A}$ (black). Ordinary one-way ANOVA: p= 0.0333, Šidák post-hoc test: CS vs. cac^{sfGFP} p= 0.9308, cac^{sfGFP} vs. cac^{sfGFP}ΔIS4A p= 0.4361, cac^{sfGFP}ΔIS4A vs. $\frac{cacsfGFP\Delta IS4B}{cacRFP\Delta IS4A}$ p= 0.0189, cac^{sfGFP} vs. $\frac{cacsfGFP\Delta IS4B}{cacRFP\Delta IS4A}$ p= 0.3070. **B** depicts a scatter plot and representative traces of PP ratios of controls and exon-out variants considering locus I-IIA at 10 ms IPI: Canton S (blue), cac^{sfGFP} (green), cac^{sfGFP}ΔI-IIA (red), cac^{sfGFP}ΔI-IIB (purple) and $\frac{cacsfGFP\Delta I-IIB}{cacsfGFP\Delta I-IIA}$ (brown). Ordinary one-way ANOVA: p= 0.9433, Šidák post-hoc test: CS vs. cac^{sfGFP} p= 0.9935, cac^{sfGFP} vs. cac^{sfGFP}ΔI-IIA p= 0.9216, cac^{sfGFP} vs. cac^{sfGFP}ΔI-IIB p= 0.3956, cac^{sfGFP} vs. $\frac{cacsfGFP\Delta I-IIB}{cacsfGFP\Delta I-IIA}$ p= 0.9272, cac^{sfGFP}ΔI-IIA vs. cac^{sfGFP}ΔI-IIB p= 0.9785, cac^{sfGFP}ΔI-IIA vs. $\frac{cacsfGFP\Delta I-IIB}{cacsfGFP\Delta I-IIA}$ p> 0.9999, cac^{sfGFP}ΔI-IIB vs $\frac{cacsfGFP\Delta I-IIB}{cacsfGFP\Delta I-IIA}$ p= 0.9933. **C** depicts a scatter plot and representative traces of PP ratios of controls and exon-out variants considering locus IS4 at 15 ms IPI: Canton S (blue), cac^{sfGFP} (green), cac^{sfGFP} ΔIS4A (orange) and $\frac{cacsfGFP\Delta IS4B}{cacRFP\Delta IS4A}$ (black). Ordinary one-way ANOVA: p= 0.1563, Šidák post-hoc test: CS vs. cac^{sfGFP} p= 0.7528, cac^{sfGFP} vs. cac^{sfGFP} ΔIS4A p= 0.7744, cac^{sfGFP} vs. $\frac{cacsfGFP\Delta IS4B}{cacRFP\Delta IS4A}$ p= 0.6927, ΔIS4A vs. $\frac{cacsfGFP\Delta IS4B}{cacRFP\Delta IS4A}$ p= 0.1884. **D** depicts a scatter plot and representative traces of PP ratios of controls and exon-out variants considering locus I-IIA at 15 ms IPI: Canton S (blue, scatter plot only), cac^{sfGFP} (green), ΔI-IIA (red), ΔI-IIB (purple) and $\frac{cacsfGFP\Delta I-IIB}{cacRFP\Delta I-IIA}$ (brown). CS is not shown for clarity and due to its similarity with cac^{sfGFP}**.** Ordinary one-way ANOVA: 0.3780, Šidák post-hoc test: CS vs. cac^{sfGFP} p= 0.9032, cac^{sfGFP} vs. cac^{sfGFP}ΔI-IIA p= 0.9956, cac^{sfGFP} vs. cac^{sfGFP}ΔI-IIB p= 0.9388, cac^{sfGFP} vs. $\frac{cacsfGFP\Delta I-IIB}{cacsfGFP\Delta I-IIA}$ p= 0.9905, cac^{sfGFP}ΔI-IIA vs. $\frac{cacsfGFP\Delta I-IIB}{cacsfGFP\Delta I-IIA}$ p> 0.9999, cac^{sfGFP}ΔI-IIB vs. $\frac{cacsfGFP\Delta I-IIB}{cacsfGFP\Delta I-IIA}$ p> 0.9999, cac^{sfGFP}ΔI-IIA vs. cac^{sfGFP}ΔI-IIB p= 0.9999. All data from plots **A-D** were normally distributed, therefore

only ordinary one-way ANOVAs were conducted. Median shown for all data. All cacophony variants were sfGFP-tagged except for ΔIS4A in the $\frac{\Delta IS4B}{\Delta IS4A}$ animals, which was RFP-tagged. Tags were not listed for every genotype in the label of the scatter plots' y-axes for clarity (Bell *et al.*, 2024).

There are no significant differences between all genotypes at an IPI of 15 ms (Figure 15C p= 0.1563, Figure 15D p= 0.3780). Additionally, at 10 ms IPI, no significant differences between genotypes considering the locus I-IIA can be observed (Figure 15B p= 0.9433). However, ΔIS4A shows a significantly decreased PP ratio when compared to the transheterozygous mutant $\frac{\Delta IS4B}{\Delta IS4A}$ (Figure 15A). Still, both mutants show no significant differences when compared to control cac^{sfGFP} at 10 ms IPI (Figure 15A).

Changes of mEPSC amplitude and spontaneous release frequency can indicate forms of homeostatic plasticity, which are responses upon perturbation (Hanes *et al.*, 2020). An increase or decrease of mini frequency can indicate a higher release probability of SVs (Wierenga, Ibata and Turrigiano, 2005). Analyzed data regarding mini amplitude and frequency obtained via TEVC of M6 are depicted in Figure 16.

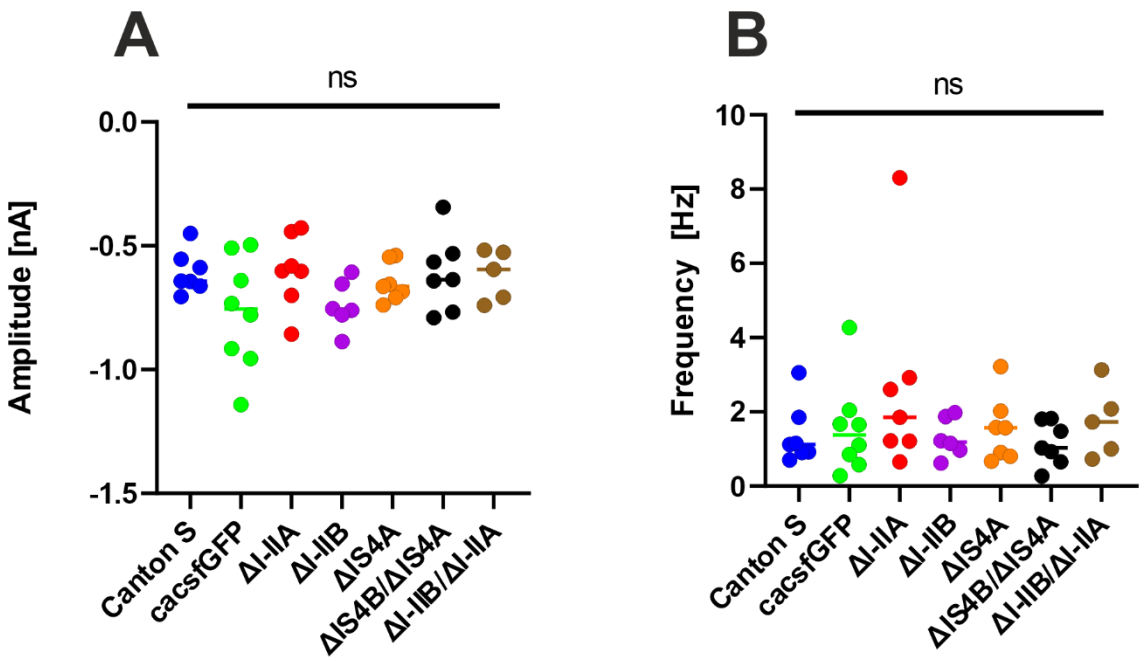

Figure 16: Quantification of mEPSC amplitude and frequency of different exon-out variants during TEVC onto M6. A depicts the smallest quantal units that occurred spontaneously during TEVC recordings organized in a scatter plot: Canton S (blue), cac^{sfGFP} (green), cac^{sfGFP}ΔI-IIA (red), cac^{sfGFP}ΔI-IIB (violet), cac^{sfGFP}ΔIS4A (orange), $\frac{cacsfGFP\Delta IS4B}{cacRFP\Delta IS4A}$ (black) and $\frac{cacsfGFP\Delta I-IIB}{cacsfGFP\Delta I-IIA}$ (brown). Statistics: all groups were normally distributed. Ordinary one-way ANOVA: p= 0.1362, Dunnett post-hoc test: Canton S vs. cac^{sfGFP} p= 0.1293, Canton S vs. cac^{sfGFP}ΔI-IIA p> 0.9999, Canton S vs. cac^{sfGFP}ΔI-IIB p= 0.3577, Canton S vs. cac^{sfGFP}ΔIS4A p= 0.9866, Canton S vs. $\frac{cacsfGFP\Delta IS4B}{cacRFP\Delta IS4A}$ p> 0.9999, Canton S vs. $\frac{cacsfGFP\Delta I-IIB}{cacsfGFP\Delta I-IIA}$ p= 0.9998. **B** depicts the frequency of all analyzed spontaneous release events during TEVC recordings organized in a scatter plot. Statistics: groups Canton S (p= 0.0317) and cac^{sfGFP}ΔI-IIA (p= 0.0091) are not normally distributed, therefore a Kruskal-Wallis-ANOVA was performed: p= 0.7178, Dunn's post-hoc test: Canton S vs. all other groups p> 0.9999. Median shown for all data. All cacophony variants were sfGFP-tagged

except for ΔIS4A in the $\frac{cacsfGFP\Delta IS4B}{cacRFP\Delta IS4A}$ animals, which was RFP-tagged. Tags were not listed for every genotype in the label of the scatter plots' y-axes for clarity (Bell *et al.*, 2024).

As can be seen in Figure 16, neither exon-out variant shows a significantly different mEPSC amplitude or frequency (amplitude: $p > 0.05$ for all groups, frequency $p > 0.9999$ for all groups). The similar quantal size provides evidence against homeostatic compensation by postsynaptic receptors or number of neurotransmitters per vesicle. Additionally, the unaltered mini frequency across all genotypes supports the theory, that there is no homeostatic compensation upon exon-out excision apart from IS4B, which showed an increased mEPSC amplitude at the NMJ of M12 (Figure 10).

3.2.8 Analysis of kinetics reveal inconclusive data on decay τ

To get an idea on channel kinetics, the rise and decay tau (τ) of single pulses are usually considered. In Figure 17, I depicted the τ_{rise} and τ_{decay} of exon-out variants of both loci. Please note that these kinetics reflect postsynaptic current, which is therefore only an indirect reflection of presynaptic current through cacophony channels. Therefore, we can only draw conclusions from these kinetics data if several other variables contributing to synaptic transmission are identical across all genotypes. These variables include but are not limited to: similar postsynaptic membrane shape and properties including the receptors, distances between cac and SVs and similar RRP sizes. So far, we have no evidence on alteration of said parameters, which is why we can carefully consider differences in rise and decay times as reflections of presynaptic channel activation and inactivation. As mentioned before in sections 3.2.5 and 3.2.6, the depicted traces in Figure 12 and Figure 13 are representative for transmission amplitudes, but not activation and inactivation kinetics. The traces depicted in Figure 17C/F are representative for these kinetics, but not for the transmission amplitude.

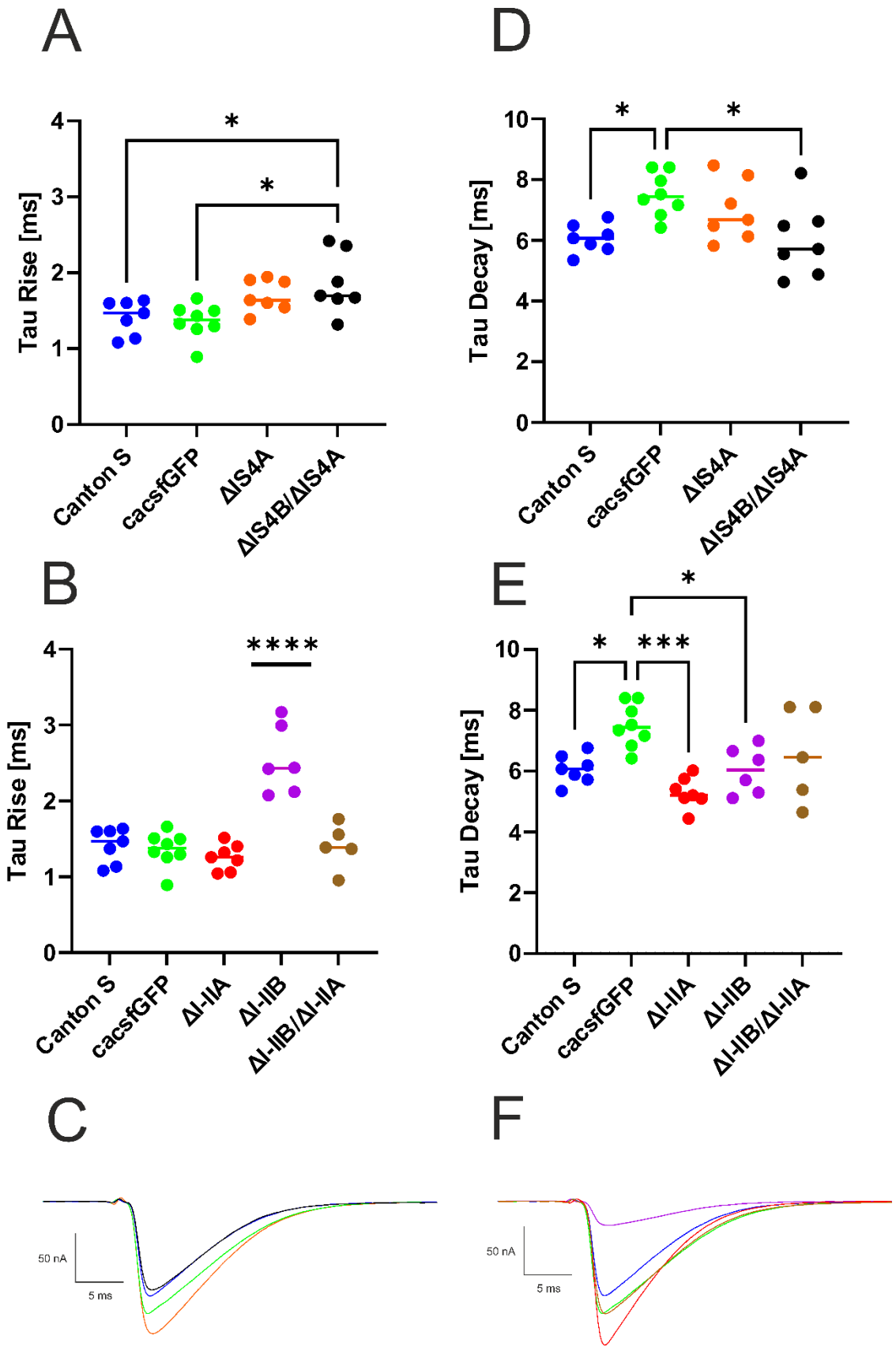

Figure 17: Rise and decay τ for different exon-out variants and their controls. Across all panels, the following genotypes are depicted: Canton S (blue), cac^{sfGFP} (green) n=5, ΔIS4A (orange) n=6, $\frac{cacsfGFP\Delta IS4B}{cacRFP\Delta IS4A}$ (black) n=6, cac^{sfGFP}ΔI-IIA (red) n= 6, cac^{sfGFP}ΔI-IIB (purple) n=5 and $\frac{cacsfGFP\Delta I-IIB}{cacsfGFP\Delta I-IIA}$ (brown) n=4. **A** depicts the τ_{rise} of controls and exon-out variants concerning the IS4 locus. Statistics: all groups were normally distributed. Ordinary one-way ANOVA p< 0.0001, Šidák post-hoc test: Canton S

vs. cac^{sfGFP} p= 0.9995, Canton S vs. cac^{sfGFP}ΔIS4A p= 0.3727, Canton S vs. $\frac{cacsfGFP\Delta IS4B}{cacRFP\Delta IS4A}$ p= 0.0434, cac^{sfGFP} vs. cac^{sfGFP}ΔIS4A p= 0.1683, cac^{sfGFP} vs. $\frac{cacsfGFP\Delta IS4B}{cacRFP\Delta IS4A}$ p= 0.0131, cac^{sfGFP}ΔIS4A vs. $\frac{cacsfGFP\Delta IS4B}{cacRFP\Delta IS4A}$ p= 0.0964. **B** depicts the τ_{rise} of controls and exon-out variants concerning the I-II locus. Statistics: all groups were normally distributed. Ordinary one-way ANOVA p< 0.0001, Šidák post-hoc test: Canton S vs. cac^{sfGFP} p= 0.9957, Canton S vs. cac^{sfGFP}ΔI-IIA p= 0.8453, Canton S vs. cac^{sfGFP}ΔI-IIB p< 0.0001, Canton S vs. $\frac{cacsfGFP\Delta I-IIB}{cacsfGFP\Delta I-IIA}$ p> 0.9999, cac^{sfGFP} vs. cac^{sfGFP}ΔI-IIA p= 0.9594, cac^{sfGFP} vs. cac^{sfGFP}ΔI-IIB p< 0.0001, cac^{sfGFP} vs. $\frac{cacsfGFP\Delta I-IIB}{cacsfGFP\Delta I-IIA}$ p= 0.9984, cac^{sfGFP}ΔI-IIA vs. cac^{sfGFP}ΔI-IIB p< 0.0001, cac^{sfGFP}ΔI-IIA vs. $\frac{cacsfGFP\Delta I-IIB}{cacsfGFP\Delta I-IIA}$ p= 0.9014, cac^{sfGFP} ΔI-IIB vs. $\frac{cacsfGFP\Delta I-IIB}{cacsfGFP\Delta I-IIA}$ p< 0.0001. **C** depicts traces representative for the postsynaptic activation and inactivation currents of genotypes concerning the IS4 locus. **D** depicts the τ_{decay} of controls and exon-out variants concerning the IS4 locus. Statistics: all groups were normally distributed. Ordinary one-way ANOVA p= 0.0075, Šidák post-hoc test: Canton S vs. cac^{sfGFP} p= 0.0220, Canton S vs. cac^{sfGFP}ΔIS4A p= 0.2361, Canton S vs. $\frac{cacsfGFP\Delta IS4B}{cacRFP\Delta IS4A}$ p= 0.9995, cac^{sfGFP} vs. cac^{sfGFP}ΔIS4A p= 0.6854, cac^{sfGFP} vs. $\frac{cacsfGFP\Delta IS4B}{cacRFP\Delta IS4A}$ p= 0.0167, cac^{sfGFP}ΔIS4A vs. $\frac{cacsfGFP\Delta IS4B}{cacRFP\Delta IS4A}$ p= 0.1947. **E** depicts the τ_{decay} of controls and exon-out variants concerning the I-II locus. Statistics: all groups were normally distributed. Ordinary one-way ANOVA p= 0.0004, Šidák post-hoc test: Canton S vs. cac^{sfGFP} p= 0.0177, Canton S vs. cac^{sfGFP}ΔI-IIA p= 0.4235, Canton S vs. cac^{sfGFP}ΔI-IIB p> 0.9999, Canton S vs. $\frac{cacsfGFP\Delta I-IIB}{cacsfGFP\Delta I-IIA}$ p= 0.8628, cac^{sfGFP} vs. cac^{sfGFP}ΔI-IIA p= 0.0002, cac^{sfGFP} vs. cac^{sfGFP}ΔI-IIB p= 0.02, cac^{sfGFP} vs. $\frac{cacsfGFP\Delta I-IIB}{cacsfGFP\Delta I-IIA}$ p= 0.2711, cac^{sfGFP}ΔI-IIA vs. cac^{sfGFP}ΔI-IIB p= 0.5155, cac^{sfGFP}ΔI-IIA vs. $\frac{cacsfGFP\Delta I-IIB}{cacsfGFP\Delta I-IIA}$ p= 0.1033, cac^{sfGFP}ΔI-IIB vs. $\frac{cacsfGFP\Delta I-IIB}{cacsfGFP\Delta I-IIA}$ p= 0.8412. **F** depicts traces representative for the postsynaptic activation and inactivation currents of genotypes concerning the I-II locus. Median shown for all data. Not significant test results were not included in B to avoid loss of overview due to many compared groups. All cacophony variants were sfGFP-tagged except for ΔIS4A in the $\frac{\Delta IS4B}{\Delta IS4A}$ animals, which was RFP-tagged. Tags were not listed for every genotype in the label of the scatter plots' y-axes for clarity (Bell *et al.*, 2024).

The removal of IS4A does not seem to affect activation kinetics (vs. Canton S p= 0.3727, vs. cac^{sfGFP} p= 0.1683) whereas curiously, the transheterozygous mutant $\frac{\Delta IS4B}{\Delta IS4A}$ shows a slightly prolonged activation time when compared to both controls (vs. Canton S p= 0.0434, vs. cac^{sfGFP} p= 0.0131, Figure 17). This indicates that although transheterozygous expression of both exon-out variants rescues viability (see Figure 4) and synaptic transmission amplitude to an extent (see Figure 10 and Figure 12), for normal synaptic transmission, a full set of possible isoforms needs to be available on both chromosomes. Additionally, since ΔIS4A shows no difference in activation kinetics, it may be assumed that the alteration stems from the chromosome lacking exon IS4B, which is needed for synaptic transmission and therefore viability. Furthermore, the removal of exon I-IIB leads to distinctly slower activation kinetics when compared to both controls (vs. Canton S p< 0.0001, vs. cac^{sfGFP} p< 0.0001). Interestingly, the transheterozygous mutant $\frac{\Delta I-IIB}{\Delta I-IIA}$ fully rescues this effect (vs. ΔI-IIB p< 0.0001).

One effect is very noticeable upon looking at the inactivation time: cac^{sfGFP}, which serves as a control to the GFP-tagged exon-out variants, shows significantly longer inactivation times (vs. Canton S p= 0.0177). It has been shown that the interaction of $G_{\beta\gamma}$-subunits and VGCCs may involve the binding site encoded by exon I-IIB as well as the N-terminus of the α_1-subunit (Zamponi *et al.*, 1997; Cantí *et al.*, 1999; Zamponi and Currie, 2013). Considering the fact that this sfGFP-tag is located N-terminally these data may suggest a possible impairment in this regard. Curiously, the sfGFP-tagged exon-out variants, which were constructed from cac^{sfGFP} via CRISPR/Cas9, do not show this effect of slower inactivation.

To test whether $G_{\beta\gamma}$-subunit interaction possibly affects transmission, we employed an RNAi knockdown of $G_{\beta\gamma}$-subunits. We predict that a knockdown of $G_{\beta\gamma}$ phenocopies the effects on synaptic transmission upon removal of I-IIB (seen in Figure 12), since I-IIB carries a binding site for these $G_{\beta\gamma}$-subunits. Accordingly, knockdown of $G_{\beta\gamma}$-subunits in control and ΔI-IIA should result in a reduced transmission amplitude while a knockdown in ΔI-IIB should have no further effect on synaptic transmission amplitude. Although the data in Figure 17 were not published as such in Bell *et al.* (2024), please note that these data were extracted and analyzed from evoked transmission amplitudes, which were published in said publication.

3.3.1 Knockdown of 76C isoform of $G_{\beta\gamma}$-subunit increases synaptic transmission

Following the 50% decrease in evoked transmission amplitude in ΔI-IIB mutants, we explored two possible explanations. Firstly, channel numbers could be reduced, thereby proportionally reducing Ca^{2+} influx and consequently SV release. Secondly, the reduced amplitude could be the result of acute effects of sole expression of isoforms containing I-IIA. An acute effect could be caused by the fact that in ΔI-IIB mutants, only I-IIA cacophony channels can be expressed, which do not have an interaction motif for $G_{\beta\gamma}$-subunits (Smith *et al.*, 1998). $G_{\beta\gamma}$-subunits are known to increase Ca^{2+}-dependent inactivation of the channel after dissociation from a G-protein coupled receptor in the membrane (Agler *et al.*, 2005). Due to possible effects of the N-terminal GFP-tag, the exon-out variants that are endogenously tagged with sfGFP are explicitly named as such in this experiment to increase comprehension.

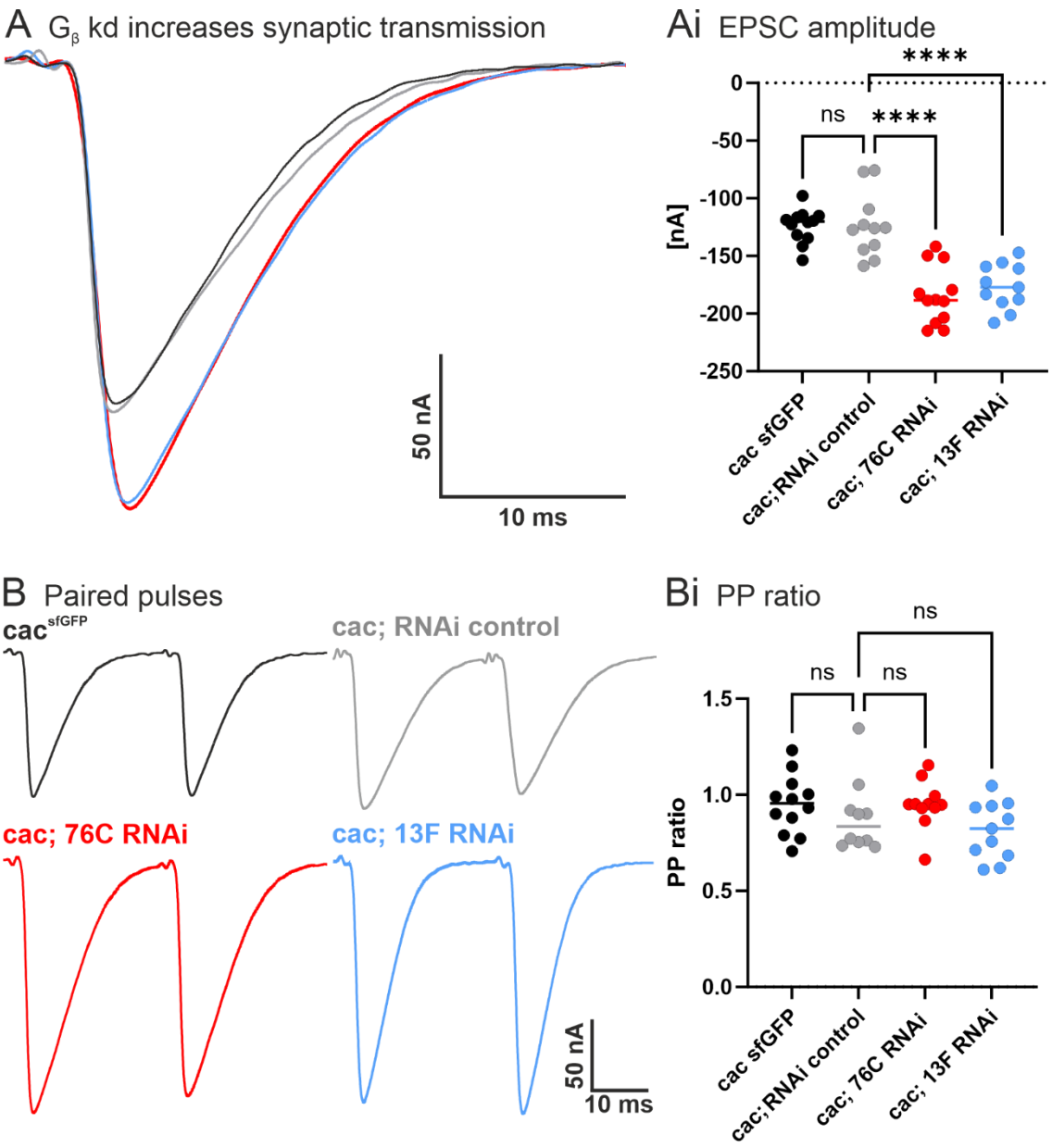

Figure 18: Visualization of evoked single pulses and paired pulses during TEVC of M6 in knockdown of two $G_{\beta\gamma}$-subunits, 76C & 13F. A depicts representative traces of evoked inward currents in muscle 6 generated by stimulation of the presynaptic motoneuron. The traces shown are cacsfGFP (black) and cac; RNAi control (gray) as well as cac; 76C RNAi (red) and cac; 13F RNAi (light blue). **Ai** depicts amplitudes of evoked responses of all analyzed genotypes organized in a scatter plot: cacsfGFP n= 6, cac; RNAi control n= 5, cac; 76C RNAi n= 6, cac; 13F RNAi n= 5. The line in each plot is the median. Statistics: all groups were normally distributed. Ordinary one-way ANOVA p< 0.0001, Šidák post-hoc test: cacsfGFP vs cac; RNAi control p> 0.9999, cac; RNAi control vs cac; 76C RNAi p < 0.0001; cac; RNAi control vs. cac; 13F RNAi p < 0.0001. **B** shows representative traces of responses to paired pulse stimulation (IPI: 30 ms). The traces shown are cacsfGFP (black) and cac; RNAi control (gray) as well as cac; 76C RNAi (red) and cac; 13F RNAi (light blue). **Bi** depicts paired pulse ratios of all analyzed genotypes organized in a scatter plot. cacsfGFP n= 6, cac; RNAi control n= 5, cac; 76C RNAi n= 5, cac; 13F RNAi n= 5. The line in each plot is the median. Statistics: Group cac; RNAi control was not normally distributed (p= 0.0132), therefore a Kruskal-Wallis ANOVA was conducted: p= 0.0963, Dunn's post-hoc test: cacsfGFP vs cac; RNAi control p= 0.5067, cac; RNAi control vs cac; 76C RNAi p= 0.4098; cac; RNAi control vs. cac; 13F RNAi p> 0.9999. Figure by XXXXX (Bachelor's thesis).

To explore this theory, XXXXX (Bachelor student under my supervision) first expressed an RNAi-knockdown of two G_{β}-subunits, 76C and 13F, via the driver OK371-GAL4. The OK371-GAL4 driver construct drives the RNAi-knockdown in all glutamatergic neurons, thus including but not limited to crawling muscle MNs. The G_{β}-subunits 76C

(flybase.org/reports/FBgn0004623.htm) and 13F (flybase.org/reports/FBgn0001105.htm) were chosen among 3 possible subunits after considering strong neuronal expression data, whereas $G_{\beta}5$ is supposedly less strongly expressed (flybase.org/reports/FBgn0030011.htm). $G_{\beta\gamma}$-subunits consist of a G_{β} and a G_{γ}-subunit (McCudden *et al.*, 2005; Zamponi and Currie, 2013) and as far as we are aware, both subunits always act as a dimer. Consequently, knock-down of the G_{β}-subunit such as conducted for this experiment should result in a knockdown of the whole dimer.

As can be seen in Figure 18, 76C RNAi & 13F RNAi expression increase evoked synaptic transmission amplitudes by approx. 40% compared to control (both comparisons $p< 0.0001$), thereby contradicting our initial hypothesis. In fact, this provides evidence that at least the investigated $G_{\beta\gamma}$-subunits containing G_{β}76C and G_{β}13F are involved in reducing the transmission amplitude at the larval NMJ of muscle 6. These findings suggest that the reduced transmission amplitude in ΔI-IIB larvae (Figure 12) is not caused by $G_{\beta\gamma}$-subunit binding.

cac^{sfGFP} and cac; RNAi control are not significantly different from one another, thus indicating that the insertion of the P-element alone doesn't cause any alterations in synaptic transmission.

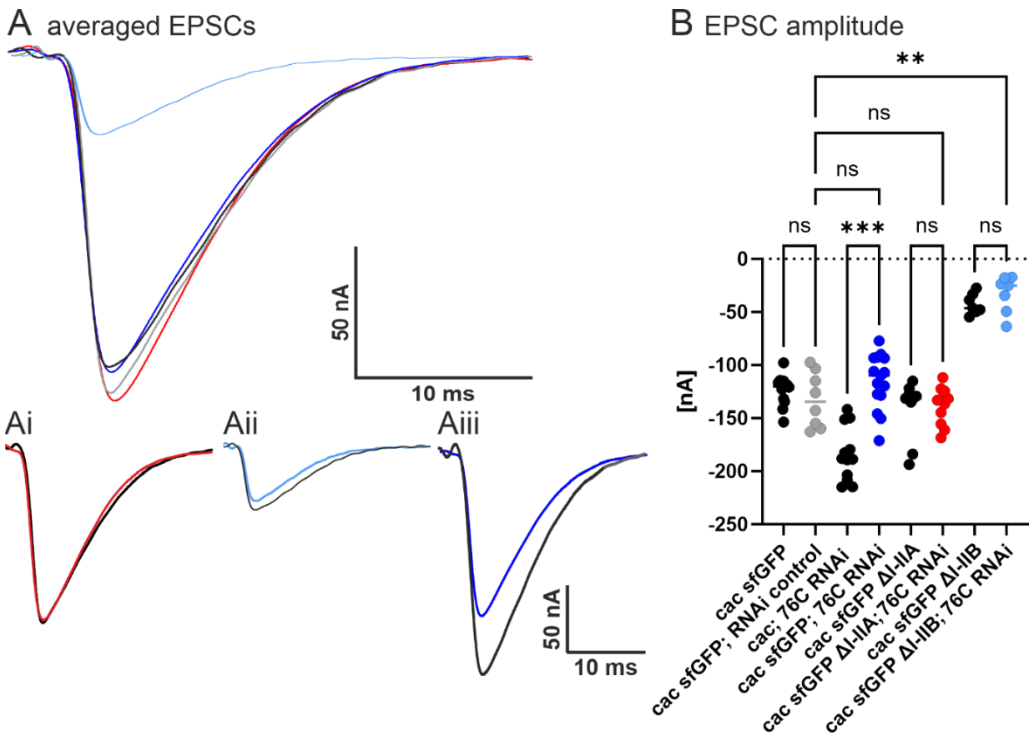

Figure 19: Visualization of evoked single pulses in 76C-RNAi knockdowns with and without GFP-tagged cacophony as well as RNAi co-expression with exon-out mutants. A depicts representative evoked inward currents of cac^{sfGFP} (black), cac^{sfGFP}; RNAi control (gray), cac^{sfGFP}; 76C RNAi (blue), $cac^{sfGFP\ \Delta I\text{-}IIA}$; 76C RNAi (red) and $cac^{sfGFP\ \Delta I\text{-}IIB}$; 76C RNAi (light blue). **Ai** shows representative traces of $cac^{sfGFP\ \Delta I\text{-}IIA}$ (black) and $cac^{sfGFP\ \Delta I\text{-}IIA}$; 76C RNAi (red), **Aii** shows representative traces of $cac^{sfGFP\ \Delta I\text{-}IIB}$

(black) and $cac^{sfGFP\ \Delta I\text{-}IIB}$; 76C RNAi (light blue) and **Aiii** shows cac^{sfGFP} (black) and cac^{sfGFP}; 76C RNAi (blue). **B** depicts amplitudes of evoked single pulses of all analyzed genotypes organized in a scatter plot: cac^{sfGFP} n= 6, cac^{sfGFP}; RNAi control n= 8, cac; 76C RNAi n= 6, cac^{sfGFP}; 76C RNAi n= 5, $cac^{sfGFP\ \Delta I\text{-}IIA}$ n= 4, $cac^{sfGFP\ \Delta I\text{-}IIA}$; 76C RNAi n= 5, $cac^{sfGFP\ \Delta I\text{-}IIB}$ n= 6, $cac^{sfGFP\ \Delta I\text{-}IIA}$; 76C RNAi n= 5. The line in each plot is the median. Statistics: Group $cac^{sfGFP\ \Delta I\text{-}IIA}$ was not normally distributed (p= 0.0054), therefore a Kruskal-Wallis ANOVA was conducted: p< 0.0001, Dunn's post-hoc test: cac^{sfGFP} vs. cac^{sfGFP}; RNAi control p> 0.9999, $cac^{sfGFP\ \Delta I\text{-}IIA}$ vs. $cac^{sfGFP\ \Delta I\text{-}IIA}$; 76C RNAi p> 0.9999, $cac^{sfGFP\ \Delta I\text{-}IIB}$ vs. $cac^{sfGFP\ \Delta I\text{-}IIB}$; 76C RNAi p> 0.9999, cac; 76C RNAi vs. cac^{sfGFP}; 76C RNAi p= 0.0002, cac^{sfGFP}; RNAi control vs. cac^{sfGFP}; 76C RNAi p> 0.9999, cac^{sfGFP}; RNAi control vs. $cac^{sfGFP\ \Delta I\text{-}IIA}$; 76C RNAi p> 0.9999, cac^{sfGFP}; RNAi control vs. $cac^{sfGFP\ \Delta I\text{-}IIB}$; 76C RNAi p= 0.0077. Figure by XXXXX (Bachelor's thesis).

Consecutively, the 76C knockdown was co-expressed together with GFP-tagged control (cac^{sfGFP}) and the exon-out variants of the I-II exon, which is associated with $G_{\beta\gamma}$-binding (Figure 19). In contrast to both $G_{\beta\gamma}$-subunit knockdowns in animals without an N-terminal GFP-tagged cacophony (Figure 18), animals with GFP-tag and a co-expressed 76C knockdown no longer show an increased transmission amplitude (cac^{sfGFP}; RNAi control vs. cac^{sfGFP}; 76C RNAi p> 0.9999 (Figure 19, gray vs. dark blue). This hints at a counteracting mechanism of the GFP-tag to 76C RNAi, but only with simultaneously reduced $G_{\beta\gamma}$-subunit expression since the GFP-tag at the N-terminus of cacophony alone does not alter synaptic transmission amplitude as described above (Figure 12). Comparatively, the $cac^{sfGFP\ \Delta I\text{-}IIA}$ animals with 76C knockdown also do not exhibit an increase in amplitude (p> 0.9999). Opposed to this, $cac^{sfGFP\ \Delta I\text{-}IIB}$; 76C RNAi shows a strongly reduced transmission amplitude when compared to the RNAi control (p= 0.0077), but not to $cac^{sfGFP\ \Delta I\text{-}IIB}$ without a 76C RNAi (p> 0.9999). We did not expect a further reduction in $cac^{sfGFP\ \Delta I\text{-}IIB}$; 76C RNAi animals compared to $cac^{sfGFP\ \Delta I\text{-}IIB}$ due to the lacking $G_{\beta\gamma}$-binding site in the remaining I-IIA isoforms. Yet, increased transmission amplitudes in cac; 76C RNAi and cac; 13F RNAi animals (Figure 18) and possible confounding effects of the sfGFP-tag (Figure 19) do not support our initial hypothesis, that the significantly reduced evoked transmission amplitude in ΔI-IIB is due to a lack of $G_{\beta\gamma}$-binding.

Something to keep in mind while investigating $G_{\beta\gamma}$-subunit function as described above is that these subunits are knocked down globally in the affected neurons, thereby possibly affecting G-protein function not only in the specific binding to sites in the α1-subunit of cacophony, but other proteins as well. Furthermore, we only knocked down one of three $G_{\beta\gamma}$-subunits at a time. We cannot rule out an overexpression of the other subunits as a homeostatic response to $G_{\beta\gamma}$-knockdown and thus masking possible effects.

3.3.2 $G_{\beta\gamma}$-subunit knockdown doesn't affect presynaptic MN morphology

Based on the findings that $G_{\beta\gamma}$ subunit knockdowns of 76C and 13F increase synaptic transmission (Figure 18), immunohistochemistry and subsequent CLSM were used to evaluate possible altered NMJ or AZ morphology due to developmental defects. Since calcium influx through VGCCs is known to influence neuronal growth (Kater and Mills, 1991), investigating

morphology was essential upon observing effects in synaptic transmission. Besides, an increased number of release sites on the muscle could also cause increased transmission amplitudes. Additionally, G-proteins are known to play a role in many more processes than VGCC inactivation like cell growth or protein synthesis (Zachariou, Duman and Nestler, 2012). Neuronal membrane was labeled with an α-HRP antibody and α-brp antibody was used to mark AZs. A Python script (see 2.6.4) by XXXXX was then used to generate a 3D-mask of the hrp-staining and thereby, the membrane of the larval crawling motoneuron. Additionally, the script was able to count the brp-spots inside the 3D mask as well as the number of boutons. We only included 76C RNAi and not 13F RNAi into this experiment due to the fact that both groups were almost statistically identical and therefore assumed that the same mechanism would be responsible for increased synaptic transmission.

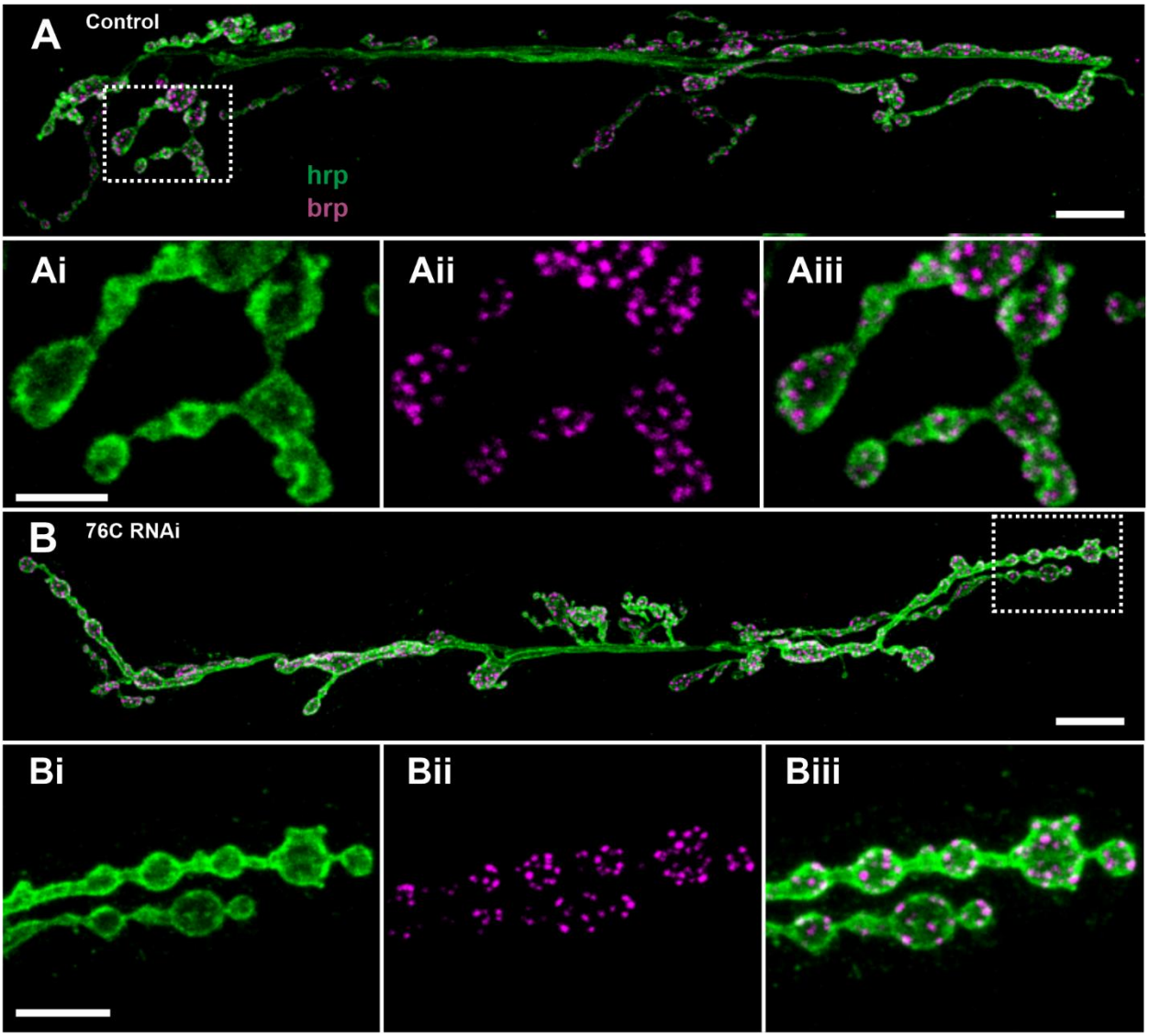

Figure 20: Representative confocal microscopy images of larval NMjs onto M6/7 in a maximum projection view. A shows genotype cac; RNAi control while **B** shows genotype cac; 76C RNAi, scale bar: 10 µm. Immunolabeling of hrp is in green, brp in magenta. **Ai**- **Aiii** & **Bi**- **Biii** depict zoomed junctions of both genotypes (Ai & Bi: hrp), (Aii & Bii: brp), (Aiii & Biii: merge), scale bar: 5 µm. Figure modified after XXXXX (Bachelor's thesis).

We couldn't observe any obvious differences in NMJ morphology (Figure 20). To obtain statistically sound evidence on this, different relevant values like NMJ volume, AZ numbers and bouton numbers were quantified (Figure 21).

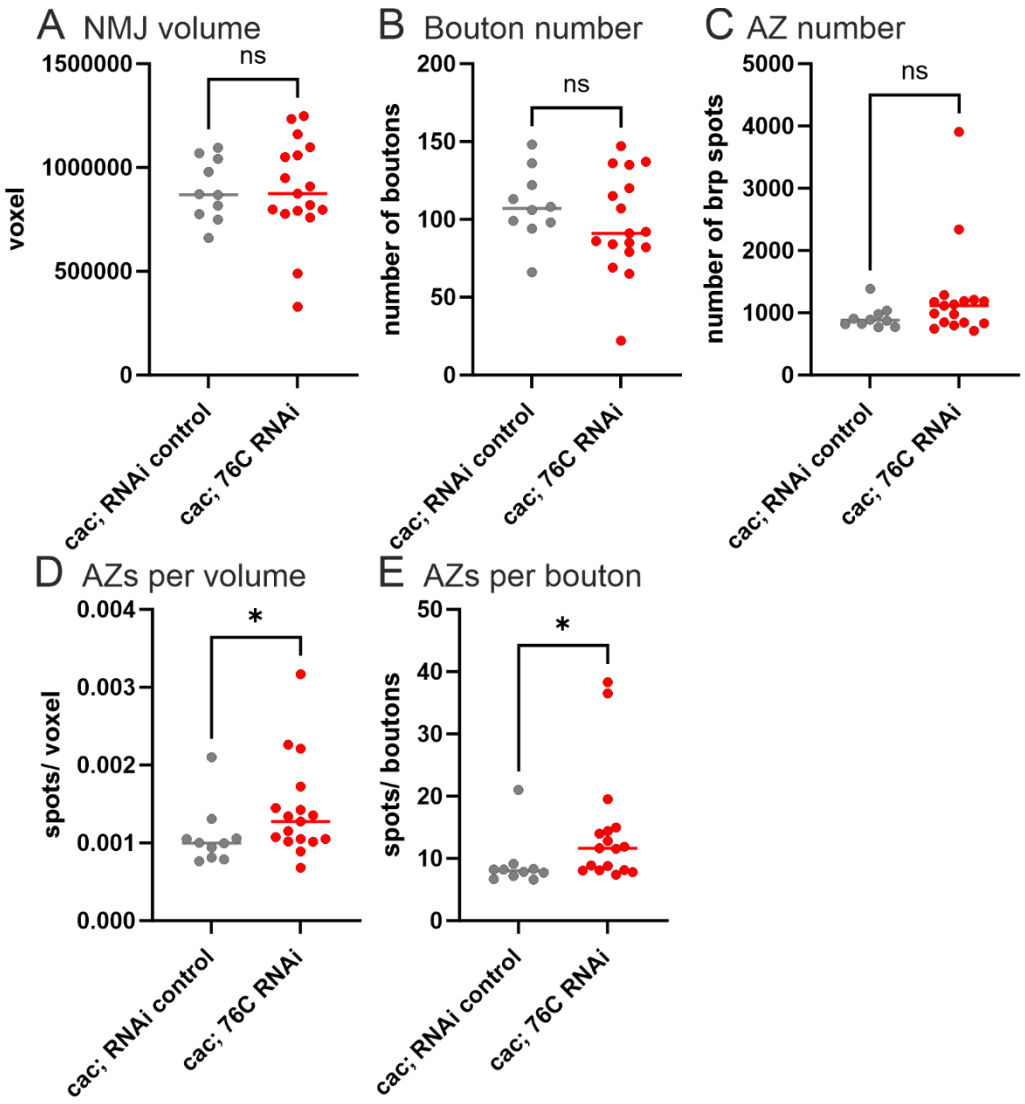

Figure 21: Quantification of NMJ volume, bouton number and AZ number of immunolabeled hrp & brp at the larval NMJ onto M6 of A3. All plots show cac; RNAi control (n= 4) & cac; 76C RNAi (n=5). **A** shows no statistical significance in NMJ volume in voxels (t-test, p: 0.9835). **B** shows no statistical significance in bouton number (t-test, p= 0.3184). **C** shows no statistical difference in AZ number (Mann-Whitney-U-test, p= 0.1868). **D** depicts a statistical difference in AZ number per NMJ volume (Mann-Whitney-U-test, p= 0.0310). **E** depicts a statistical difference in AZ number per bouton (Mann-Whitney-U-test, p= 0.0235). Figure by XXXXX (Bachelor's thesis).

There were no statistically significant differences between the RNAi control and 76C RNAi considering NMJ volume (p= 0.9835), bouton number (p= 0.3184) and AZ number (p= 0.1868). Consequently, we conclude that the statistical significance in AZs per volume and AZs per bouton are due to increased effect size and are therefore an artifact. These results suggest an acute effect of reduced G-protein subunits rather than a developmental effect on synaptic transmission.

3.4 Channel number in AZs is unaffected by IS4A and I-IIA exon excision

Since we had tested morphology and localization of channels inside the AZs and couldn't find any differences, the cause of effects of exon excisions on synaptic transmission were still unknown. Differences in synaptic transmission between exon-out variants could also occur due to altered channel kinetics, differences in single channel conductance, different channel numbers or a combination of all these factors. Recently, a study was conducted in which cacophony channels were approximately counted using an endogenous photoconvertible mEOS4b-tag (Ghelani *et al.*, 2023). In collaboration with Martin Heine, I used TIRF microscopy and bleached mEOS4b-tagged channels to estimate channel numbers per AZ on muscles 6 and 7 in abdominal segments 2 to 7. Please see section 2.6.5 for a detailed method description.

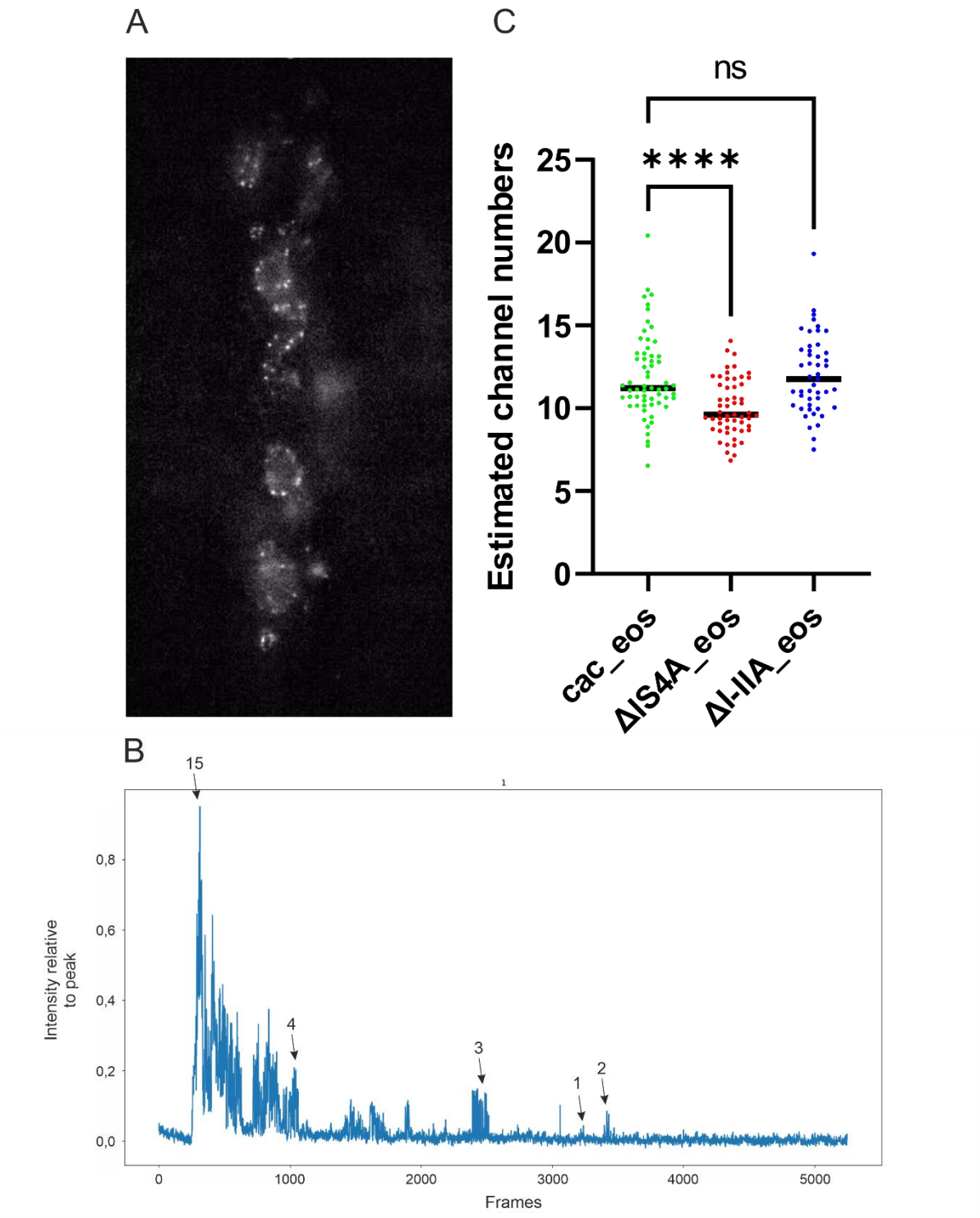

Figure 22: Quantification of estimated channels per AZ on M6/7 of L3 larvae. A depicts a slide of mEOS4b excitation via UV light in an NMJ of controls. Bright spots represent mEOS4b fluorophores and therefore, channels. As these channels are endogenously tagged, the brightness of each spot is in proportion with the number of channels. **B** depicts the excitation normalized to the highest value over time of an analyzed AZ. The x axis shows frames while the y-axis shows the light intensity relative to the peak. Several excitation events and their estimated number of photoconverted mEOS4b-tags are indicated with black arrows. Depicted in **C** are quantifications of the control cac^{eos} (green), $cac^{eosΔIS4A}$ (red) and $cac^{eosΔI-IIA}$ (blue). The y-axis shows the estimated channel numbers. Datasets of Carsten Duch and myself were pooled since independent analyses yielded similar results for all genotypes. Few spots, which were analyzed by both investigators were averaged. Statistics: group cac^{eos} was not normally distributed (p= 0.0167), therefore a Kruskal-Wallis ANOVA was conducted (p< 0.0001), Dunn's post-hoc test: cac^{eos} vs $cac^{eosΔIS4A}$ p< 0.0001, cac^{eos} vs. $cac^{eosΔI-IIA}$ p> 0.9999. Median shown for all data (Bell *et al.*, 2024).

Animals lacking exon IS4A show a significantly decreased number of eos-tagged cacophony channels when compared to control (Figure 22, green vs. red; p< 0.0001). There are around two channels less (median ΔIS4A: 9.62; cac^{eos}: 11.23) per AZ at the NMJs of larval crawling muscles. In contrast, animals lacking exon I-IIA show no significant difference when compared to control (p> 0.9999), thus channel number in AZs does not correlate with the observed effects of exon excision in current amplitude recorded via TEVC (Figure 13). The control-like amplitude in ΔIS4A animals is not reflected by a control-like number in estimated channels per AZ, thus hinting at a possible mechanism of homeostatic compensation. Yet, this possible compensation is likely not due to an increased quantal size, which we have tested previously (Figure 16). We also expected an increased channel number in ΔI-IIA animals, which is not confirmed by our data. Thus, these data suggest, that an increased transmission amplitude is the result of other mechanisms than sheer ΔI-IIA channel numbers, possibly due to altered channel properties.

Testing this hypothesis requires either patch-clamping Ca^{2+} currents from the AZs in presynaptic boutons or patch in a heterologous expression system like sf9 (*Spodoptera frugiperda*) cells. Both methods were beyond our capacities in this study. *In situ* recordings from larval crawling motoneurons revealed, that cacophony is not driving the somatodendritic calcium current in these neurons (Worrell and Levine, 2008). However, cacophony is located somatodendritically in adult flight MNs (Ryglewski *et al.*, 2012), which could be recorded to test possibly altered calcium currents, depending on cacophony variants. The complex structure of said MNs and especially their dendrites (Duch, Vonhoff and Ryglewski, 2008; Vonhoff and Duch, 2010) however may confound the results of current kinetics and other properties, thus making interpretation difficult. The data shown in Figure 22 have been published in Bell *et al.* (2024).

3.5 Both I-II exons are required for normal crawling behavior

We have tested the investigated exon-out variants for morphological and electrophysiological differences at the NMJ. Although we have shown that ΔIS4A animals have a severely reduced lifespan, it must be considered that this lifespan was observed in adult animals while the immunohistochemistry and electrophysiology data were acquired in L3 larvae. Since the changes in transmitter amplitude upon isoform reduction reflect how much neurotransmitter is transmitted onto the muscles, it is reasonable and necessary to quantify larval motor behavior, which is dependent on neuromuscular activity. Larval behavior is composed of mainly two motor activities: crawling and feeding. To obtain insight on larval motor behavior, a larval crawling experiment was conducted. Only larvae of the transheterozygous mutants $\frac{\Delta IS4B}{\Delta IS4A}$ and $\frac{\Delta I-IIB}{\Delta I-IIA}$ were

selected as females while the sex of all other genotypes was not determined. Please note, that the average crawling speed (Figure 23) is proportional to the average crawling distance as all larvae were observed for the same amount of time (5 min). I therefore omitted the depiction of average crawling distance as it would be redundant.

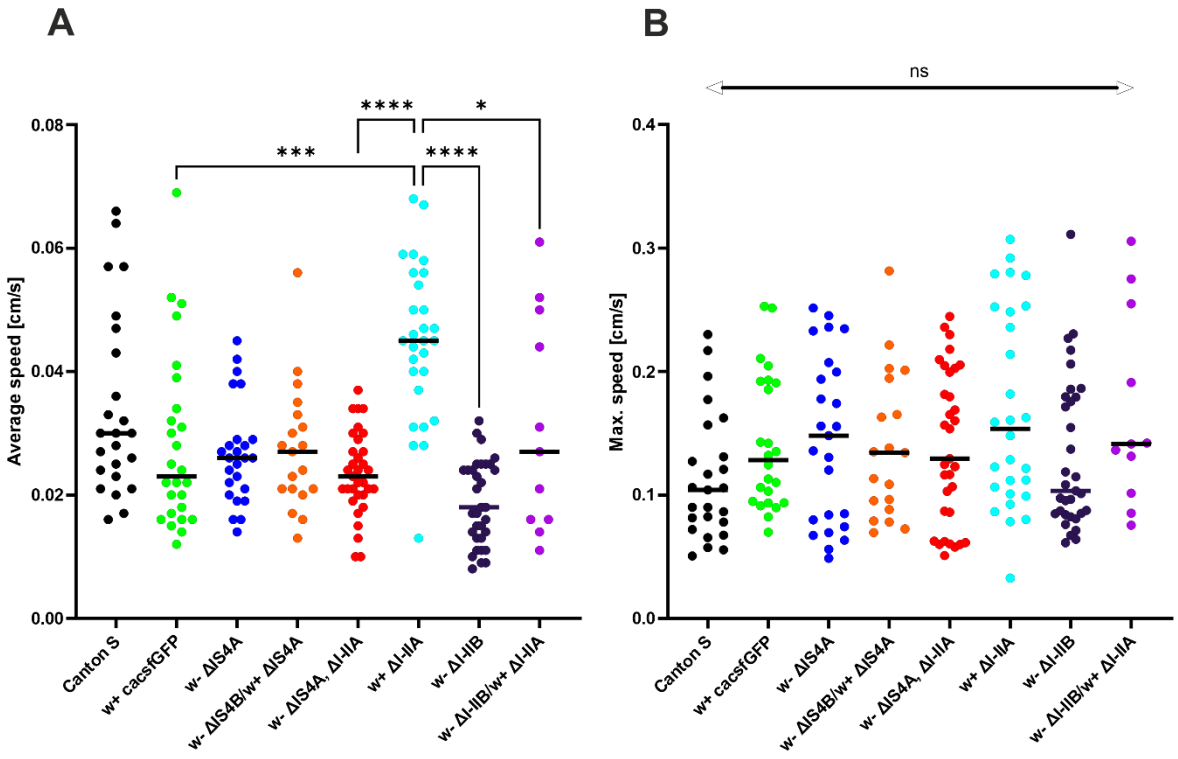

Figure 23: Quantification of crawling speed of different exon-out larvae. Depicted in **A** is the maximum crawling speed of L3 larvae in cm over 5 minutes organized in a scatter plot: Canton S (black) n= 25, cac^{sfGFP} (green) n= 24, w- cac^{sfGFP}ΔIS4A (navy blue) n= 25, $\frac{w- cacsfGFP\Delta IS4B}{cacRFP\Delta IS4A}$ (orange) n= 19, w- cac^{sfGFP}ΔIS4A, ΔI-IIA (red) n= 33, cac^{sfGFP}ΔI-IIA (light blue) n= 28, w- cac$^{sfGFP\Delta I-IIB}$ (dark blue) n= 33, $\frac{w- cacsfGFP\Delta I-IIB}{cacsfGFP\Delta I-IIA}$ (violet) n= 11. Statistics: group Canton S was not normally distributed (p= 0.0011); therefore, a Kruskal-Wallis-ANOVA was performed, Dunn's post-hoc test: p< 0.0001. Canton S vs. cac^{sfGFP} p> 0.9999, cac^{sfGFP} vs w- cac^{sfGFP}ΔIS4A p> 0.9999, cac^{sfGFP} vs. $\frac{w- cacsfGFP\Delta IS4B}{cacRFP\Delta IS4A}$ p> 0.9999, cac^{sfGFP} vs. w- cac^{sfGFP}ΔIS4A, ΔI-IIA p= 0.3377, cac^{sfGFP} vs. cac^{sfGFP}ΔI-IIA p= 0.0277, cac^{sfGFP} vs. w- cacs^{fGFP}ΔI-IIB p= 0.0005, cac^{sfGFP} vs. $\frac{w- cacsfGFP\Delta I-IIB}{cacsfGFP\Delta I-IIA}$ p> 0.9999, w- cac^{sfGFP}ΔIS4A vs. $\frac{w- cacsfGFP\Delta IS4B}{cacRFP\Delta IS4A}$ p> 0.9999, w- cac^{sfGFP}ΔIS4A vs. w- cac^{sfGFP}ΔIS4A, ΔI-IIA p> 0.9999, cac^{sfGFP}ΔI-IIA vs. w- cac^{sfGFP}ΔI-IIB p< 0.0001, w- cac^{sfGFP}ΔIS4A, ΔI-IIA vs. cac^{sfGFP}ΔI-IIA p< 0.0001, cac^{sfGFP}ΔI-IIA vs. $\frac{w- cacsfGFP\Delta I-IIB}{cacsfGFP\Delta I-IIA}$ p= 0.0234, w- cac^{sfGFP}ΔI-IIB vs. $\frac{w- cacsfGFP\Delta I-IIB}{cacsfGFP\Delta I-IIA}$ p= 0.1937 . Not significant test results were not included to avoid loss of overview due to many compared groups. Depicted in **B** is the maximum speed of the same L3 larvae in cm/s over 5 minutes organized in a scatter plot. Statistics: groups Canton S (p= 0.0246), cac^{sfGFP} (p= 0.0233), w- cac^{sfGFP}ΔIS4A, ΔI-IIA (p=0.0264), cac^{sfGFP}ΔI-IIA (0.0358) and w- cac^{sfGFP}ΔI-IIB (p= 0.0015) were not normally distributed, therefore a Kruskal-Wallis ANOVA was performed: p= 0.1363, Dunn's post-hoc test: Canton S vs. cac^{sfGFP} p= 0.8112, cac^{sfGFP} vs. w- cac^{sfGFP}ΔIS4A p> 0.9999, cac^{sfGFP} vs. $\frac{w- cacsfGFP\Delta IS4B}{cacRFP\Delta IS4A}$ p> 0.9999, cac^{sfGFP} vs. w- cac^{sfGFP}ΔIS4A, ΔI-IIA p> 0.9999, cac^{sfGFP} vs. cac^{sfGFP}ΔI-IIA p> 0.9999, cac^{sfGFP} vs. w- cac^{sfGFP}ΔI-IIB p> 0.9999, cac^{sfGFP} vs. $\frac{w- cacsfGFP\Delta I-IIB}{cacsfGFP\Delta I-IIA}$ p> 0.9999, w- cac^{sfGFP}ΔIS4A vs. $\frac{w- cacsfGFP\Delta IS4B}{cacRFP\Delta IS4A}$ p> 0.9999, cac^{sfGFP}ΔIS4A vs. w- cac^{sfGFP}ΔIS4A, ΔI-IIA p> 0.9999, cac^{sfGFP}ΔI-IIA vs. w- cac^{sfGFP}ΔI-IIB p= 0.5166, w- cac^{sfGFP}ΔIS4A, ΔI-IIA vs. cac^{sfGFP}ΔI-IIA p> 0.9999, cac^{sfGFP}ΔI-IIA vs. $\frac{w- cacsfGFP\Delta I-IIB}{cacsfGFP\Delta I-IIA}$ p> 0.9999, w- cac^{sfGFP}ΔI-IIB vs. $\frac{w- cacsfGFP\Delta I-IIB}{cacsfGFP\Delta I-IIA}$ p> 0.9999. Median shown for all data. All cacophony variants were sfGFP-tagged except for ΔIS4A in the $\frac{\Delta IS4B}{\Delta IS4A}$ animals, which was RFP-tagged. Tags were not listed for every genotype in the label of the scatter plots' y-axes for clarity (Bell *et al.*, 2024).

Average crawling speed (Figure 23A) seems to be correlated to synaptic transmission amplitude as recorded in muscle 6 (Figure 12): ΔI-IIA shows significantly increased average crawling speed when compared to control cac^{sfGFP} speed (p= 0.0277) while ΔI-IIB shows a significantly decreased average crawling speed (p= 0.0005). Notably, transheterozygous expression of ΔI-IIA and ΔI-IIB in the same animal rescues crawling speed (vs. cac^{sfGFP} p< 0.9999). This result is also in accordance with synaptic transmission data where transheterozygous expression of both I-II exon excisions in the same animal rescues synaptic transmission effects (Figure 12). I also analyzed maximum speed (Figure 23B) to elucidate whether larvae with increased average crawling speed are also able to crawl faster at maximum speed. This is not the case since all different genotypes are able to reach a similar maximum speed. Therefore, the alterations in average crawling speed might be a result of different endurance, motivation, or both. To get a glimpse on these possibilities, one would need to analyze the number of stops and the time in which larvae do not crawl. I would expect an increased number of stops as well as non-crawling time in animals that lack motivation and/or endurance.

A limitation of this experimental design was the presence of the *white*$^{-}$ (w^{-}) mutation in all animals except for those containing ΔI-IIA, cac^{sfGFP} the chromosome with ΔI-IIA in the transheterozygous variant $\frac{\Delta I-IIB}{\Delta I-IIA}$, which carried wild-type like *white* (see 5.5 for list of fly strains). This can transpire as a confounder in behavioral experiments since *white* is assumed to influence serotonin biosynthesis (Myers *et al.*, 2021) and has been shown to reduce serotonin and dopamine levels (Borycz *et al.*, 2008). This is problematic since dopamine is known to promote motivation (Yamamoto and Seto, 2014) and serotonin has been shown to modulate locomotor activity (Flaive *et al.*, 2020). For full context however, it has to be stated that the decreased levels of both biogenic amines are debated (Myers *et al.*, 2021), because others haven't found effects due to the loss of *white* function on the amounts of biogenic amines (Yarali *et al.*, 2009). It is unlikely however that the different *white* backgrounds of the genotypes are responsible for significantly different average crawling speeds. If the loss of *white* function were to lead to reduced crawling speed via reduced levels of biogenic amines, all animals containing a *white* mutation should crawl less, which is not the case. Secondly, ΔI-IIA animals, which crawl with significantly increased speed compared to Canton S as well as cac^{sfGFP}, carry the same wild-type *white* as both controls, meaning that the effect is most likely due to exon excision. The data shown in Figure 23 have been published in Bell *et al.* (2024).

3.6 Effects of reduced isoform variability on the visual system

As mentioned earlier, Smith *et al.* showed in 1998 that a point mutation in the I-II loop of *cacophony* causes defects in the visual system, hence the alternative name *nightblind A*. Since *nightblind A*^{H18} (*cac*^{H18}) carries a point mutation that causes a premature stop in exon I-IIA, we expect the ΔI-IIA variant to phenocopy the effects observed in electroretinograms (ERG) by Smith *et al.*, 1998. ERGs depict extracellularly recorded field potentials of photoreceptor cells and their postsynaptic partners in the lamina (first optic neuropil), L1 and L2 (Coombe, 1986). The tonic negative potential represents the response of photoreceptors, while the transient responses during light on- (positive potential) and offset (negative potential) represent the lamina responses, which are termed ‘lamina on’ and ‘lamina off’, respectively. An example of a typical ERG is depicted in Figure 24A in the trace of Canton S. The aforementioned observations made by (Smith *et al.*, 1998) were that cac^{H18} showed reduced tonic receptor potentials and abolished transient lamina on and off responses.

To study the effects of a lack of specific alternative exons, we conducted ERGs on the eyes of different exon-out animals. Please note that the stock of ΔIS4A mutants recorded in this experiment have later been shown via PCR to have lost their GFP-tag, which is why this group has been compared to Canton S as control instead of cac^{sfGFP}. All flies carried a wild-type *white* gene since it has been shown that *white* mutants are more sensitive to light than wild-type flies (Wu and Wong, 1977), which could confound the results of this experiment. The data shown in Figure 24 have already been shown in the Ph.D. thesis of Lukas Kilo, 2021, but were acquired and analyzed by me.

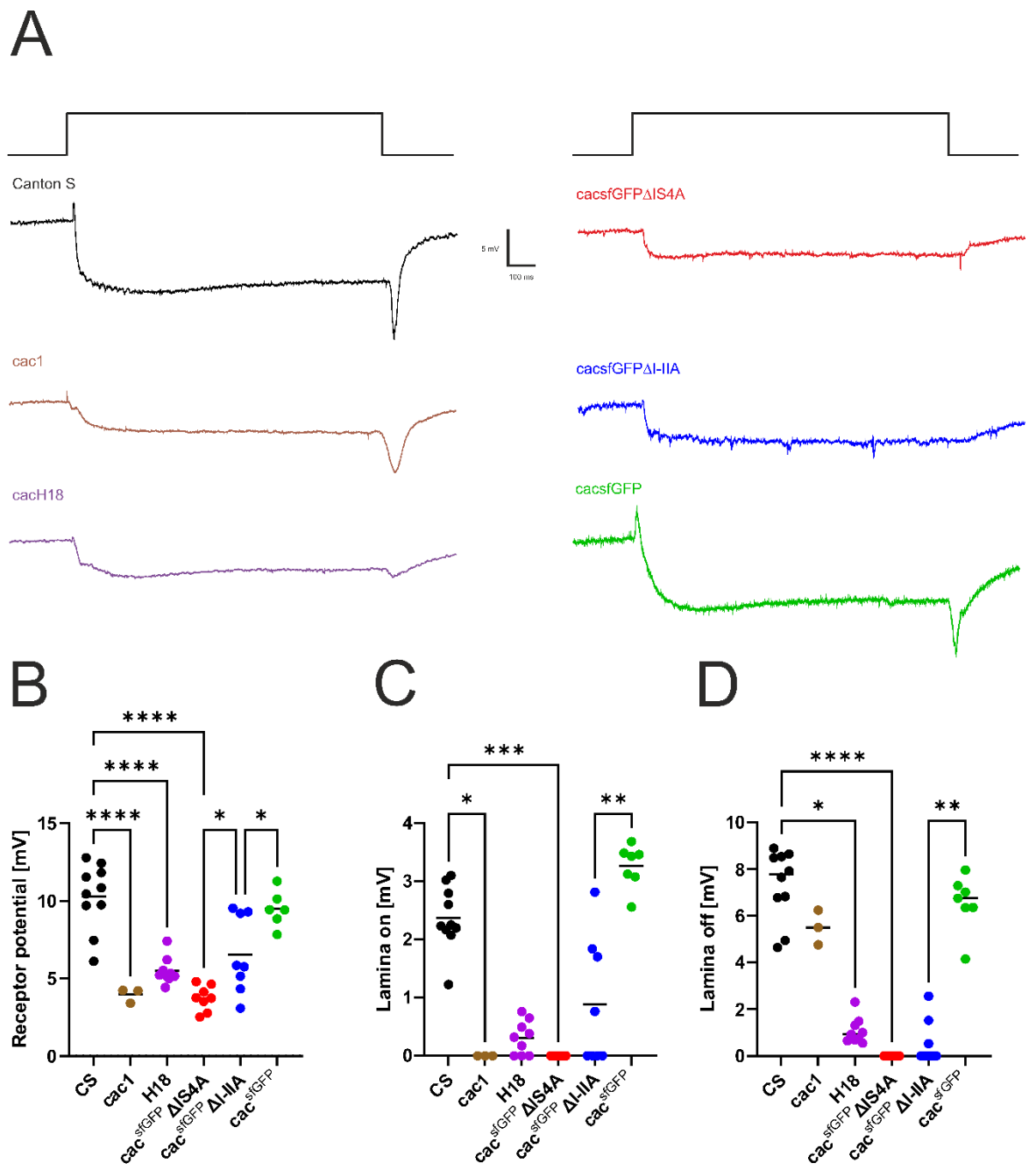

Figure 24: Traces and scatter plots of electroretinogram recordings in different cacophony variants. A depicts representative traces of electroretinograms. The traces shown are Canton S (black), cac1 (brown), cac^{H18} (purple), cac^{sfGFP}ΔIS4A (red), cac^{sfGFP}ΔI-IIA (blue) & cac^{sfGFP} (green). **B** shows the quantification of the receptor potential amplitudes organized in a scatter plot. Statistics: all groups were normally distributed. Ordinary one-way ANOVA p< 0.0001, Šidák post-hoc test: CS vs cac1 p< 0.0001, CS vs. H18 p< 0.0001, CS vs cac^{sfGFP}ΔIS4A p< 0.0001, cac1 vs H18 p= 0.8442, cac1 vs. cac^{sfGFP}ΔIS4A p> 0.9999, H18 vs. cac^{sfGFP}ΔIS4A p= 0.2927, cac^{sfGFP}ΔIS4A vs cac^{sfGFP}ΔI-IIA p= 0.0158, cac^{sfGFP}ΔI-IIA vs cac^{sfGFP} p= 0.0184, CS vs. cac^{sfGFP} p= 0.9869, H18 vs. cac^{sfGFP}ΔI-IIA p= 0.8941. **C** shows the quantification of lamina on amplitudes organized in a scatter plot. Statistics: Group ΔI-IIA was not normally distributed (p= 0.0426), therefore a Kruskal-Wallis ANOVA was conducted: p< 0.0001, Dunn's post-hoc test: CS vs. cac1 p= 0.0497, CS vs. H18 p= 0.0794, CS vs. cac^{sfGFP}ΔIS4A p= 0.001, cac1 vs H18 p> 0.9999, cac1 vs. cac^{sfGFP}ΔIS4A p> 0.9999, H18 vs. cac^{sfGFP}ΔIS4A p> 0.9999, cac^{sfGFP}ΔIS4A vs. cac^{sfGFP}ΔI-IIA p> 0.9999, cac^{sfGFP}ΔI-IIA vs. cac^{sfGFP} p= 0.0093, CS vs. cac^{sfGFP} p> 0.9999, H18 vs. cac^{sfGFP}ΔI-IIA p> 0.9999. **D** depicts the quantification of lamina off amplitudes organized in a scatter plot. Statistics: Group cac^{sfGFP}ΔI-IIA was not normally distributed (p= 0.0019), therefore a Kruskal-Wallis-ANOVA was conducted: p< 0.0001, Dunn's post-hoc test: CS vs. cac1 p> 0.9999, CS vs. H18 p= 0.0153, CS vs. cac^{sfGFP}ΔIS4A p< 0.0001, cac1 vs. H18 p> 0.9999, cac1 vs. cac^{sfGFP}ΔIS4A p= 0.0987, H18 vs. cac^{sfGFP}ΔIS4A p= 0.5475, cac^{sfGFP}ΔIS4A vs. cac^{sfGFP}ΔI-IIA p> 0.9999, cac^{sfGFP}ΔI-IIA vs. cac^{sfGFP} p= 0.0090, CS vs. cac^{sfGFP} p> 0.9999, H18 vs. cac^{sfGFP}ΔI-IIA p> 0.9999. The line in each column depicts the median in all scatter plots. The number of tested flies was equal for every analyzed value: Canton S n= 10, cac1 n= 3, H18 n= 9, cac^{sfGFP}ΔIS4A n= 8, cac^{sfGFP}ΔI-IIA n= 8, cac^{sfGFP} n= 6. Not significant test results were not included

in B-D to avoid loss of overview due to many compared groups. Please note that cac1 was GFP-tagged C-terminally as described in Kawasaki *et al.,* 2004, while H18 was not tagged at all. All cacophony exon-out variants were sfGFP-tagged. Cac1 carries an C-terminal GFP-tag, H18 is not tagged.

Figure 24 shows the effects of the lack of expression of specific cacophony isoforms on the photoreceptor potential, lamina on and off response to light stimuli of 1s. While the untagged variants H18 and ΔIS4A were compared to the wild-type like control Canton S, the tagged variant ΔI-IIA was compared to cac^{GFP} to exclude possible effects of the GFP-tag itself. Cac1 was compared to Canton S, since it carries an eGFP-tag C-terminally (Kawasaki, Collins and Ordway, 2002) while all other tagged variants carry their sfGFP-tag N-terminally. cac^{GFP} is similar in receptor potentials as well as in lamina on and off responses (rec. pot. p= 0.9869, L. on p> 0.9999, L. off p> 0.9999), indicating that the GFP-tag itself does not impair visual function in the photoreceptor and lamina cells at least on the level of extracellularly recorded field potentials.

Out of the investigated exon-out variants, ΔIS4A mutants show the most severe impairments in the visual system with a significantly reduced receptor potential (p< 0.0001) and completely abolished lamina on (p= 0.001) and off responses (p< 0.0001) compared to Canton S as control. H18 and ΔI-IIA show similar impairments: a significantly reduced receptor potential (H18 p< 0.0001, ΔI-IIA p= 0.0184) and reduced lamina on (H18 p= 0.0794, ΔI-IIA p= 0.0093) and off responses (H18 p= 0.0153, ΔI-IIA p= 0.009). Still, there is a qualitative difference between both genotypes as H18 reliably elicits a, albeit small, lamina off response whereas in ΔI-IIA, not all animals show a lamina off response. Note that H18 is a point mutation in the I-IIA exon, resulting in a premature stop of all isoforms containing said exon. Therefore, the similarities were to be expected. It is noticeable however, that ΔI-IIA animals occasionally exhibit, albeit small, lamina on and off responses in contrast to ΔIS4A animals. Since these transient lamina responses depend on the graded transmitter release of the presynaptic photoreceptors, this may hint towards either different localization and/or function of IS4A and I-IIA cacophony variants.

Cac1 however is an overexpression under the control of the GAL4-UAS system in a cac^{null} background and expresses only one single isoform (annotation on flybase.org: cac transcript variant RC) containing IS4B and I-IIB exons and representing ΔIS4A/ΔI-IIA double exon out mutants to a limited extent. These animals show a similarly reduced photoreceptor potential (p> 0.9999) and lamina on response (p> 0.9999) compared to ΔIS4A, but still elicit a control-like lamina off response (p> 0.9999) suggesting that transmission from photoreceptors is still functional. This is noteworthy since UAS-cac1 offers only one isoform while ΔIS4A mutants are still able to express four different B/B exon variants besides the 9 variants containing I-IIA. It must be considered however that the mechanisms for both mutants are different: UAS-cac1

is an overexpression of one cacophony isoform in a cac^{null} background while ΔIS4A offers a reduced isoform variability due to endogenous exon excision.

The reduced lamina on and off responses in various genotypes could either be the result of missing cacophony in the lamina itself or due to reduced vesicle release in the presynaptic photoreceptor cells. This hypothesis arises since every mutant with reduced or abolished lamina responses also shows reduced receptor potentials. To divide the effects on either side of the synapse, I reduced the light intensity gradually in Canton S animals, which in turn reduced the receptor potential. Still, the transient lamina on and off responses were observable as long as photoreceptors received photonic input (explorative, results not shown), which indicates that reduced photoreceptor potential and reduced lamina on and off potentials are separate effects. These results were validated by a second ERG approach conducted by XXXXX in his Master's thesis.

Complementarily, Lukas Kilo was able to show in his Ph.D. thesis via immunohistochemistry and subsequent CLSM, that the immunohistochemistry label of ΔIS4A is missing in most of the lamina cartridges except for the apical parts (Ph. D. thesis Lukas Kilo, 2021). Lamina cartridges are the structures, in which synapses between photoreceptor cells form synapses onto lamina cells, thereby making up the first optic neuropile (Fröhlich and Meinertzhagen, 1982). Lukas Kilo concluded that IS4A supposedly is the main reason why cacophony localizes to lamina cartridges (Ph. D. thesis Lukas Kilo, 2021). Additionally, ΔI-IIA animals show a weak, albeit distinct expression of cacophony in the lamina cartridges, thus being qualitatively different from ΔIS4A. This is in accordance with qualitative differences between ΔIS4A and ΔI-IIA in lamina on and off responses as described above (Figure 24). Which exact large monopolar cells (LMCs) in the lamina are affected by these exon excisions will be unraveled by collaborators in the lab via co-expression of RFP-derivates in the membrane of LMCs.

4 Discussion

4.1 Impairments in synaptic transmission might be responsible for effects in larval crawling, but not adult longevity and fitness

The experiments conducted in this study show severely reduced fitness and lifespan in animals (Figure 4 and Figure 5) lacking exon IS4A while the same animals show a largely wild type like synaptic transmission. In contrast, ΔI-IIB animals exhibit a strongly reduced synaptic transmission amplitude, but live a rather healthy life, which is comparable, also in its duration, to controls. This provides evidence for the first important conclusion from this study:

In principle, reduced isoform variability at the NMJ is not the fundamental impairment, which is reducing fitness and lifespan in ΔIS4A animals. Evidence gathered in this study hints towards more specific isoform function as the reason for reduced fitness and lifespan in ΔIS4A animals.

The transmitted current amplitude does not seem to be of any issue for the organism in lab conditions for as long as transmission can be elicited reliably. This is further supported by the fact that homozygous cacophony deletion or IS4B removal leads to embryonic lethality. However, it needs to be stated that this and other studies by Lukas Kilo and various bachelor students in this lab focus on behavior in lab conditions. While the removal of I-IIA and I-IIB seems to leave behavior largely unaffected in lab conditions, it does not mean that both exons are redundant or behaviorally obsolete. It is nearly impossible to simulate wildlife conditions in which predators, different weather conditions or random environmental events in the flies' surroundings are present. Therefore, while we cannot obtain data on behavioral defects except for vision in ΔI-IIA animals, this does not automatically speak for a lack of functions of the I-II exons since vision is an absolutely essential sense for fruit flies in nature. Vision impairment due to lack of I-IIA could very well be detrimental for flies in natural conditions as it could hinder them to detect predators in time. Furthermore, a rich isoform variability of cacophony at presynaptic terminals could increase the working range of synapses or the resistance to perturbations like neurotoxins or due to loss of ion channel function via e.g., a mutation.

Additionally, it needs to be considered that we have not tested synaptic transmission in adults as thoroughly as in larvae. While transmission amplitude in larvae positively correlates with higher average crawling speed, it cannot be translated as well to adult longevity data. Hence, it is also possible that cacophony is spliced differentially when comparing larval and adult life. Possibly, IS4A could just be essential in adult neurons for more nuanced functions in different compartments like integration of complex dendritic input in a much more complex nervous system than in larvae. While larval behavior is almost solely composed of feeding and crawling,

adult flies have a very broad variety of motoric behaviors like walking, flying, climbing, feeding, grooming and courtship. This more complex behavioral pattern might need a more diverse variety of Ca_V2 channels than larvae. Still, it needs to be stated that my data obtained in the larval crawling experiment contradict the data of my collaborator Lukas Kilo. He found a significantly decreased crawling distance in ΔIS4A animals when compared to Canton S. Additionally, Lukas Kilo found larger calcium signals (broader calcium shoulder) during calcium imaging of pupal (stages P8 and P9) MN5 and double spikes in ΔIS4A animals as well as ΔI-IIA animals during whole cell patch clamp recordings, which contradicts the theory that IS4A could just be essential in adult neurons (Ph.D. thesis, Lukas Kilo, 2021). Application of the calcium channel blocker cadmium abolished the double spikes, thus providing evidence that these double spikes are calcium dependent (Ph.D. thesis, Lukas Kilo, 2021). However, specific cacophony isoform expression could still be developmentally regulated as larvae are able to exhibit normal behavior while adults are behaviorally impaired and die rather early (Figure 4).

4.2 How do specific exon encoded cacophony isoforms affect synaptic transmission?

As already stated before, fast, action potential-triggered synaptic transmission at the larval NMJ in ΔIS4A animals was not significantly different from control, albeit with a tendency towards a slightly increased transmission amplitude, which would correlate with increased calcium signals in P8/9 as observed by Lukas Kilo in his Ph.D. thesis (2021). ΔI-IIA animals showed a significantly increased synaptic transmission amplitude in my experiment, while others in this lab have obtained data, which are not significantly different from control (Bell *et al.*, 2024; XXXXX, XXXXX, personal communication). Curiously, my transmission amplitudes do not correlate with estimated channel numbers obtained via TIRFM: ΔIS4A animals show 20% fewer channels in AZs (Figure 22), but similar transmission amplitudes (Figure 13) while ΔI-IIA animals exhibit control-like channel numbers in AZs (Figure 22), but ~40 % increase in transmission amplitude (Figure 12).

While single channel conductance could possibly be increased in IS4B isoforms, it is also possible that the remaining channels containing only IS4B cluster tighter to ensure proper synaptic transmission amplitudes. Recently, it has been shown that upon pharmacological perturbation of postsynaptic receptors, presynaptic cacophony channel density in AZs was increased in a time scale of minutes to ensure normal transmission amplitudes (Ghelani *et al.*, 2023). It has also been demonstrated that Ca_V1 channels can cooperate in functional clusters, which results in increased open probabilities and thus increased Ca^{2+} currents (Dixon *et al.*, 2015; Moreno *et al.*, 2016). Considering that fewer channels in ΔIS4A animals can still elicit a control-like transmission amplitude, I can envision a scenario in which the remaining IS4B isoforms cluster

in a more compact manner to cooperatively ensure sufficient transmission amplitudes as a compensatory mechanism. To test this, a tessellation analysis could be conducted on the existing TIRFM data, for which I would predict an increased channel density for ΔIS4A channels while mobility decreases to ensure constantly sufficient channel cooperation.

Testing single channel conductance could be achieved by transfecting different cacophony cDNA together with β and $\alpha_2\delta$ subunits in a heterologous expression system like sf9 (*Spodoptera frugiperda*) cells and patch-clamp these. Furthermore, one could try to patch-clamp presynaptic boutons, which has the advantage that data would be obtained on site and therefore in its native cellular environment. Unfortunately, bouton patches at NMJs have – to our knowledge - not been successful as of now. In addition, we would still be unable to assess specific channel properties to single isoforms since cacophony is spliced at more than the two sites that we have investigated. Accordingly, excising one or even two exons from these mutually exclusive exon pairs still enables a heterogeneous, albeit limited, population of cacophony channels.

Finally, the shift in activation voltage by 10 to 20 mV towards more hyperpolarized potentials (-50 to -60 mV) of IS4B channels in ΔIS4A animals (recorded from adult MNs) could provide an explanation (Ph.D. thesis, Lukas Kilo, 2021). Following this observation, small depolarizations may be sufficient to open these cacophony channels, thereby possibly facilitation vesicle release from presynaptic terminals.

4.3 Exon IS4A might be required upstream of NMJs for neuronal function

Removal of IS4A does not impact evoked synaptic transmission in a way that explains the observed behavioral defects (see above). Still, cacophony isoforms containing IS4A seem to be required for normal neuronal function since animals without it die much earlier (Figure 4). Previous whole-cell patch-clamp experiments of adult flight MNs in our lab have shown that removal of IS4A results in a shift in activation voltage of 10 to 20 mV towards more hyperpolarized potentials (-50 to -60 mV) in HVA currents (Ph.D. thesis, Lukas Kilo, 2021). This shift in activation voltage might result in hyperexcitability, which in turn would be a higher order defect in the somatodendritic region of motoneurons. This region is bypassed in TEVC since the nerves are cut and thus, stimulation is generated in the distal regions of the axon.

Consequently, a resulting impairment in behavior could be epilepsy, which has been described quite well in *Drosophila* (Ganetzky and Wu, 1982; Kuebler and Tanouye, 2000; Marley and Baines, 2011). Experiments on epilepsy have been conducted by collaborators in our lab (XXXXX, Bachelor's thesis), where flies were vortexed and been subjected to climb as

described in Kuebler and Tanouye, 2000. As expected, ΔIS4A animals showed a significantly longer latency time to start climbing after being vortexed as compared to controls (results not shown). In fact, results were comparable to epileptic fly lines like bang-sensitive 1 and 2, which carry a gain of function mutation in the voltage-gated sodium channel *para*. This provides evidence for the theory that the observed behavioral impairments in ΔIS4A animals are of consequence to hyperexcitability and not to defects at the NMJ. Additionally, XXXXX carried out an assay in which she recorded the DLMs extracellularly and observed that ΔIS4A animals exhibit trains of spontaneously occurring spikes when compared to Canton S (unpublished). This adds another hint that IS4A is needed to avoid hyperexcitable phenotypes. However, it needs to be considered that cacophony mediated current is not the main calcium current in larval crawling MNs (Worrell and Levine, 2008). Conversely, the same study revealed that both, a hypomorphic mutation (cac^{s}) or RNAi knockdown, affect firing properties and thus indicate that cacophony shapes firing properties of larval crawling MN to some extent.

In addition, it could be possible that IS4A is needed for normal input integration in dendrites, where calcium channels are known to boost synaptic input. Since IS4B isoforms activate towards more hyperpolarized potentials with respect to HVA currents, removal of IS4A could result in a hyperexcitability at dendrites, which in turn could lead to pathological responses to presynaptic input. Other experiments in our lab have shown that upon stimulation of pupal flight MNs, its soma, axons, and primary neurites without IS4A exhibit an increased calcium influx during calcium imaging (Lukas Kilo, Ph.D. thesis). Additionally, removal of I-IIA leads to a decreased calcium influx. Another experiment to gain more direct insight into the effects on dendritic input would be to puff nicotine as an agonist for the nicotinic acetylcholine receptors, which excite dendrites of adult flight MNs 1-5 and to conduct calcium imaging in exon-out variants and controls. Consequently, I would expect an increased calcium influx in ΔIS4A animals.

Considering the fact that IS4B is crucial for synaptic transmission and incorporated in most isoforms triggering neurotransmitter secretion into the synaptic cleft while IS4A is needed in the somatodendritic region, I conclude that IS4B is essential and sufficient for synaptic function and survival and IS4A is needed for less excitable channels and thus prevents hyperexcitability. Furthermore, an increase in calcium influx could also be detrimental to the cell as heightened Ca^{2+} levels can be toxic due to its involvement in regulating enzyme activity and transcription. This leads me to the hypothesis that IS4A isoforms function as a suitable ‘break’ to the more hyperpolarized excitable IS4B isoforms.

4.4 Alteration of synaptic transmission amplitude in I-II exon-out variants likely not due to missing interaction with $G_{\beta\gamma}$-subunits

As described previously, the interaction of the α_1-subunit with $G_{\beta\gamma}$ in the I-II loop is known to facilitate inactivation of VGCCs (Buraei and Yang, 2010b). Thus, the results of experiments considering $G_{\beta\gamma}$ knockdowns are in accordance with the theory first proposed by Bean in 1989, that the binding of $G_{\beta\gamma}$ converts VGCCs from a 'willing' to a 'reluctant' state concerning its opening probability (Bean, 1989). Additionally, G-protein coupled receptors like metabotropic glutamate receptors (mGluR) are known to regulate presynaptic channel activity in response to neurotransmitter release as form of autoregulation (Schulman, 2013; Huang and Thathiah, 2015).

Since the removal of I-IIB leads to reduced postsynaptic current amplitude and $G_{\beta\gamma}$ knockdown does not phenocopy this effect as we had actually predicted, this effect in ΔI-IIB animals is most probably not an acute effect of reduced $G_{\beta\gamma}$ binding. Considering the strongly reduced GFP-label in ΔI-IIB animals (Figure 6), it is probable that the decreased transmission amplitude is the result of fewer channels in the active zones. Unfortunately, until the time of the TIRFM experiments, I was not able to successfully employ CRISPR/Cas9 to excise I-IIB out of the mEOS4b-tagged cacophony channels. This has been done by my collaborators in this project and subsequent TIRFM revealed a cacophony channel number reduction of around 50% at the NMJ of ΔI-IIB animals (Bell *et al.*, 2024. This strengthens the hypothesis that the reduced evoked transmission amplitudes in TEVC experiments (Figure 12) is the result of reduced cacophony channel numbers. In addition, I-IIB excision leads to longer activation, but not inactivation time in evoked synaptic transmission. This is further evidence against the theory that the acute lack of interaction between I-IIB and $G_{\beta\gamma}$ is the cause of decreased synaptic transmission. I would expect a longer inactivation time upon I-IIB removal since $G_{\beta\gamma}$ subunits are known to promote channel inactivation.

The removal of exon I-IIA led to an increased synaptic transmission amplitude in my experiments and wild-type amplitude in XXXXX experiments. Still, the co-expression of a $G_{\beta\gamma}$ knockdown did not decrease the amplitude to match the one recorded in ΔI-IIB animals, further supporting the idea that the reduction in ΔI-IIB animals is likely not due to a lacking interaction with $G_{\beta\gamma}$ subunits.

There are three important facts that need to be noted regarding the α_1-subunit and $G_{\beta\gamma}$ subunit interaction. Firstly, only one of three G_β subunits was knocked down at a time. Consequently, we can only observe partial effects of this interaction. Secondly, the knockdown was achieved globally in motoneurons, thereby likely affecting other compartments and pathways, in which $G_{\beta\gamma}$ subunits are involved such as vesicle transport or protein synthesis (Zachariou, Duman

and Nestler, 2012). Thus, effects seen in the experiment with regards to $G_{\beta\gamma}$ subunit knockdown might not even be the primary result of interaction loss with the α_1-subunit. Lastly, it needs to be considered that the role of $G_{\beta\gamma}$ subunit and Ca_{β}-subunit interaction with one another is unclear and debated (Buraei and Yang, 2010a). While some studies have found evidence that suggests a competition of both regarding the AID domain in the I-II loop (Campbell *et al.*, 1995; Bourinet *et al.*, 1996), others have shown that β-subunits might be required for proper G-protein function in conjunction with VGCCs (Qin *et al.*, 1997; Meir *et al.*, 2000; Leroy *et al.*, 2005).

One indirect way to test whether cacophony isoforms with different I-II loops interact selectively with G-proteins would be to knockdown mGluR in the MNs presynaptic to the recorded muscles (via OK6-GAL4). This would circumvent the problems that arise with a knockdown of $G_{\beta\gamma}$ subunits, which are involved in many more processes as already described (Zachariou, Duman and Nestler, 2012). Compared to a $G_{\beta\gamma}$ knockdown, an mGluR knockdown could possibly narrow unintended effects and could provide information on autoregulation mediated via interaction of cacophony isoforms and $G_{\beta\gamma}$ subunits released from mGluR. Considering that ΔI-IIB cacophony channels lack the binding site for $G_{\beta\gamma}$ subunits, I would not expect an increased transmission amplitude in a concurrent knockdown of mGluR in MNs. The reason for this prediction is the inability to bind $G_{\beta\gamma}$ subunits of ΔI-IIB cacophony isoforms, thus already missing the target for mGluR as an autoregulatory element. Consistent with this, I would predict that a presynaptic mGluR knockdown in ΔI-IIA animals will increase transmission amplitudes beyond the elevated levels already recorded (Figure 12). This is due to the fact that all remaining I-IIB isoforms would usually bind $G_{\beta\gamma}$ subunits, which would not be available in usual numbers in mGluR knockdowns. Thus, inactivation via $G_{\beta\gamma}$ subunits would not occur or only at a reduced rate. However, one needs to keep in mind, that autoregulation could also be achieved via glutamate-gated chloride channels (GluClα), which have recently been shown to hyperpolarize the presynaptic membrane in an activity-dependent manner, thus decreasing transmitter release (Li *et al.*, 2021). However, both mechanisms do not have to be mutually exclusive and could be working in parallel.

4.5 sfGFP-tag influences voltage-gated calcium channels, especially upon perturbation

After endogenously tagging cacophony, (Gratz *et al.*, 2019) showed that their sfGFP-tag had no effect on evoked transmission and mEPSC amplitude as well as quantal content – an observation that is in accordance with the data I have shown multiple times in this study. Still, in my TEVC experiment, the sfGFP-tagged control shows distinctly slower inactivation kinetics. As stated earlier, the GFP-tag is located intracellularly at the N-terminus and could thereby

hinder $G_{\beta\gamma}$ subunit binding since these subunits are known to bind at the N-terminus among other sites in the α_1-subunit (Zamponi *et al.*, 1997; Cantí *et al.*, 1999; Zamponi and Currie, 2013). I envision that an intracellular protein of 238 amino acids (flybase.org) can block off closely located interaction sites considering how single amino acid sequence mutations in the I-II loop can severely reduce G-protein mediated inhibition (Tedford *et al.*, 2010). This site is proposed to interact with the N-terminus and thereby mediate G-protein function (Agler *et al.*, 2005; Tedford *et al.*, 2010). The conflicting point is that the exon-out variants were also tagged and didn't show this effect.

XXXXX discovered during her Bachelor's thesis that the knockdown of $G_{\beta\gamma}$ subunits in the background of untagged cacophony results in an increased synaptic transmission amplitude, which we concluded, is probably due to the lack of inactivation via these proteins. Surprisingly, knockdown of the same subunits in tagged cacophony channels negated this effect. This was somewhat counterintuitive since we would expect an effect of the tag in the presence, not in the absence of $G_{\beta\gamma}$ subunits. My most parsimonious explanation is that cac^{sfGFP} is able to elicit wild-type responses at least in amplitude while nothing else is altered. Though, upon perturbation, cac^{sfGFP} doesn't phenocopy wild-type cacophony. This hypothesis is supported by data from a colleague in my lab (XXXXX), who has found that the pharmacological block (quinidine) of Shab, a delayed rectifier voltage gated potassium channel, in stage P9 of pupal MN5 does not result in altered excitability during current clamp patch-clamp experiments. However, when Shab is blocked in the presence of tagged cacophony, cells enter a depolarization block more quickly and show double spikes (XXXXX, personal communication). If the sfGFP-tag indeed hinders interaction between the α1-subunit and G-protein subunits, this could possibly reduce G_{β}-mediated channel inhibition, resulting in a greater calcium influx. Ca^{2+} influx contributes to action potential shapes in pupal flight motoneurons (Heinrich and Ryglewski, 2020). The increased calcium influx in the presence of a pharmacological block of shab could then cause a quicker depolarization block since shab is responsible for repolarizing the cell after a cation influx during an action potential (Peng and Wu, 2007). A higher Ca^{2+} influx might then require fully functional potassium channels such as shab to rapidly terminate action potentials. The pharmacological perturbation of shab might be possible to overcome in wild-type animals with completely functional cacophony, but not in the presence of an sfGFP-tag, which is blocking the binding site for G_{β}-subunits.

Therefore, our previous conception that cac^{sfGFP} is a valid control for our exon-out variants has to be reconsidered and it has to be taken into account, that this GFP-tag is a potential confounder in electrophysiological experiments. Ideally, my TEVC experiments would be reconducted with untagged exon-out variants to clearly distinguish effects of exon excision and the GFP-tag.

4.6 Division of labor between IS4 exons considering fast and graded synapses

While synapses from MNs onto muscle fibers follow the 'all-or-none' principle, many synapses in the visual system of *Drosophila* mediate graded potentials, whose amplitudes are dependent on the input strength (Juusola *et al.*, 1996; Kurt, Warzecha and Egelhaaf, 2001; Astorga *et al.*, 2012). Both synapse types require VGCCs. In the visual and auditory systems of vertebrates, graded synapses (so-called ribbon synapses) use Ca_V1 channels for triggering vesicle release (Pangrsic, Singer and Koschak, 2018). In 2012, Astorga *et al.* published evidence of cacophony's presence (Ca_V2 homolog) in photoreceptor cells and contributions to depolarization and synaptic vesicle exocytosis (Astorga *et al.*, 2012). However, the antibodies used in this study were confirmed in our lab to be specific for DmCa1D, the homolog to Ca_V1 channels in vertebrates, and not cacophony (Kadas *et al.*, 2017). Considering this information, to our knowledge, the localization data by Astorga *et al.*, 2012 have to be accounted for with caution. Still, the results of the electrophysiological experiments, that cacophony mediated Ca^{2+} influx triggers synaptic vesicle release in photoreceptor terminals, remain unaffected by this point. That being stated, the experiments conducted in this study provide useful information on how different synapse types are subject to alternatively spliced VGCCs. Both TEVC experiments with different exon-out variants clearly show that only exons IS4B and I-IIB are required for a non-reduced transmission amplitude, with IS4B being essential and sufficient while the removal of I-IIB reduces amplitude by roughly 50%, but the remainng I-IIA isoforms are still sufficient. This is in accordance with data obtained by immunocytochemistry staining of NMJs where a reduction in GFP-label can be observed in ΔI-IIB and almost no GFP-label is visible in ΔIS4B animals.

In contrast, removal of either exons IS4A or I-IIA severely reduces photoreceptor potential and the lamina on and off responses are either strongly reduced (ΔI-IIA) or abolished (ΔIS4A). The general state of scientific knowledge has been that TRP and TRP-like channels, which are permeable for cations, mediate depolarization of photoreceptors upon photo-conversion (Montell, 2012). The reduced sustained photoreceptor responses upon removal of specific alternative cacophony exons (removal of IS4A and I-IIA) support the idea of cacophony involvement in photoreceptor depolarization. Photoreceptor cells use graded synapses onto lamina cells to transmit information: generally, the more photons are received, the more transmitter will be released into the synaptic cleft. Thus, lamina responses could possibly scale to transmission amplitude. The ERG experiments in this study clearly show that this process is dependent on cacophony since removal of exons lead to reduced photoreceptor potential amplitude, as stated above. Likewise, the immunocytochemistry data obtained by Lukas Kilo support the electrophysiological effects of these exon out variants in the visual system (Ph.D. thesis, Lukas

Kilo, 2021). All these data taken together suggest that there is a division of labor between IS4B and I-IIB being responsible for fast all-or-none synapses and IS4A and I-IIA being responsible for graded synapses. This is a theory that will be further tested by my collaborators XXXXX and XXXXX in the future.

Additionally, it would provide more information on which cells exactly are affected by alternative splicing if the effects on photoreceptor potential and the transient lamina responses could be separated clearly. I explored this very briefly in an explorative manner by reducing the light intensity onto the eye in Canton S animals. This was done to gain insight on whether the reduction in photoreceptor activity is the reason why postsynaptic potentials in the lamina cells are reduced or abolished. Due to the reduced light intensity, Canton S animals showed a reduced photoreceptor potential amplitude, but the postsynaptically induced lamina responses were still elicited, which provides evidence for the presence of cacophony in photoreceptor and lamina cells (results not shown). This is supported by data from XXXXX, who has tested the effects of various light intensities on PR and lamina responses. Consequently, this further confirms that the effects of cacophony exon excision on PR and lamina cells are separate. Therefore, cacophony likely serves functions in both retina and lamina. Beyond that, these data also support the idea that there is a division of labor between IS4A and I-IIA in PR and lamina neurons: While IS4A is supposedly needed for a full tonic PR depolarization, it seems essential for transient lamina responses in ERGs, suggesting IS4A function in both cell layers. In contrast, I-IIA is also seemingly needed for a full tonic PR depolarization, yet not essential for transient lamina responses. Still, I-IIA likely contributes to full lamina transients.

References

Adams, P.J. *et al.* (2009) 'CaV2.1 P/Q-type calcium channel alternative splicing affects the functional impact of familial hemiplegic migraine mutations: Implications for calcium channelopathies', *Channels*, 3(2), pp. 110–121. Available at: https://doi.org/10.4161/chan.3.2.7932.

Agler, H.L. *et al.* (2005) 'G protein-gated inhibitory module of N-type (CaV2.2) Ca 2+ channels', *Neuron*, 46(6), pp. 891–904. Available at: https://doi.org/10.1016/j.neuron.2005.05.011.

Allbritton, N.L., Meyer, T. and Stryer, L. (1992) 'Range of messenger action of calcium ion and inositol 1,4,5-trisphosphate', *Science*, 258(5089), pp. 1812–1815. Available at: https://doi.org/10.1126/science.1465619.

Astorga, G. *et al.* (2012) 'TRP, TRPL and Cacophony Channels Mediate Ca2+ Influx and Exocytosis in Photoreceptors Axons in Drosophila', *PLoS ONE*, 7(8). Available at: https://doi.org/10.1371/journal.pone.0044182.

Bagur, R. and Hajnóczky, G. (2017) 'Intracellular Ca2+ Sensing: Its Role in Calcium Homeostasis and Signaling', *Molecular Cell*, 66(6), pp. 780–788. Available at: https://doi.org/10.1016/j.molcel.2017.05.028.

Bean, B.P. (1989) 'Neurotransmitter inhibition of neuronal calcium currents by changes in channel voltage dependence', *Nature*, 340, pp. 153–156.

Bell, C. *et al.* (2024) 'Specific presynaptic functions require distinct Drosophila Cav2 splice isoforms', *eLife* [Preprint]. Available at: https://doi.org/10.7554/eLife.100394.1.

Berridge, M.J., Lipp, P. and Bootman, M.D. (2000) '2000-Review-Calcium Signalling', *Nature Reviews*, 1(October), pp. 11–21.

Borst JGG and Sakmann B (1996) 'Calcium influx and transmitter release in a fast CNS synapse', *Nature*, 2, pp. 431–434.

Borycz, J. *et al.* (2008) 'Drosophila ABC transporter mutants white, brown and scarlet have altered contents and distribution of biogenic amines in the brain', *Journal of Experimental Biology*, 211(21), pp. 3454–3466. Available at: https://doi.org/10.1242/jeb.021162.

Bourinet, E. *et al.* (1996) 'Determinants of the G protein-dependent opioid modulation of neuronal calcium channels', *Proceedings of the National Academy of Sciences of the United States of America*, 93(4), pp. 1486–1491. Available at: https://doi.org/10.1073/pnas.93.4.1486.

Brini, M. and Carafoli, E. (2009) 'Calcium pumps in health and disease', *Physiological Reviews*, 89(4), pp. 1341–1378. Available at: https://doi.org/10.1152/physrev.00032.2008.

Buraei, Z. and Yang, J. (2010a) 'The β subunit of voltage-gated Ca2+ channels', *Physiological Reviews*, pp. 1461–1506. Available at: https://doi.org/10.1152/physrev.00057.2009.

Buraei, Z. and Yang, J. (2010b) 'The β subunit of voltage-gated Ca2+ channels', *Physiological Reviews*, pp. 1461–1506. Available at: https://doi.org/10.1152/physrev.00057.2009.

Cain, S.M. and Snutch, T.P. (2011) 'Voltage-gated calcium channels and disease', *BioFactors*, pp. 197–205. Available at: https://doi.org/10.1002/biof.158.

Campbell, V. *et al.* (1995) 'Inhibition of the interaction of G protein G(o) with calcium channels by the calcium channel beta-subunit in rat neurones.', *The Journal of Physiology*, 485(2), pp. 365–372. Available at: https://doi.org/10.1113/jphysiol.1995.sp020735.

Cantí, C. *et al.* (1999) 'Identification of residues in the N terminus of α1B critical for inhibition of the voltage-dependent calcium channel by Gβγ', *Journal of Neuroscience*, 19(16), pp. 6855–6864. Available at: https://doi.org/10.1523/jneurosci.19-16-06855.1999.

Catterall, W. a (2000) 'S Tructure and R Egulation of', *Annual Reviews of Cell and Developmental Biology*, 16(521), p. 555.

Catterall, W.A. (2011) 'Voltage-gated calcium channels', *xPharm: The Comprehensive Pharmacology Reference*, pp. 1–4. Available at: https://doi.org/10.1016/B978-008055232-3.60392-7.

Clapham, D.E. (1995) 'Calcium signaling', *Cell*, 80(2), pp. 259–268. Available at: https://doi.org/10.1016/0092-8674(95)90408-5.

Clapham, D.E. (2007) 'Calcium Signaling', *Cell*, 131(6), pp. 1047–1058. Available at: https://doi.org/10.1016/j.cell.2007.11.028.

Coombe, P.E. (1986) 'The large monopolar cells L1 and L2 are responsible for ERG transients in Drosophila', *Journal of Comparative Physiology A*, 159(5), pp. 655–665. Available at: https://doi.org/10.1007/BF00612038.

Curtis, D. *et al.* (2011) 'Case-case genome-wide association analysis shows markers differentially associated with schizophrenia and bipolar disorder and implicates calcium channel genes', *Psychiatric Genetics*, 21(1), pp. 1–4. Available at: https://doi.org/10.1097/YPG.0b013e3283413382.

Dixon, R.E. *et al.* (2015) 'Graded Ca2+/calmodulin-dependent coupling of voltage-gated CaV1.2 channels', *eLife*, 2015(4), pp. 1–21. Available at: https://doi.org/10.7554/eLife.05608.

Dolphin, A.C. (2013) 'The α2δ subunits of voltage-gated calcium channels', *Biochimica et Biophysica Acta - Biomembranes*, pp. 1541–1549. Available at: https://doi.org/10.1016/j.bbamem.2012.11.019.

Dolphin, A.C. (2016) 'Voltage-gated calcium channels and their auxiliary subunits: physiology and pathophysiology and pharmacology', *Journal of Physiology*, 594(19), pp. 5369–5390. Available at: https://doi.org/10.1113/JP272262.

Dolphin, A.C. (2018) 'Voltage-gated calcium channel α 2 δ subunits: An assessment of proposed novel roles [version 1; referees: 2 approved]', *F1000Research*. F1000 Research Ltd. Available at: https://doi.org/10.12688/f1000research.16104.1.

Dolphin, A.C. and Lee, A. (2020) 'Presynaptic calcium channels: specialized control of synaptic neurotransmitter release', *Nature Reviews Neuroscience*, 21(4), pp. 213–229. Available at: https://doi.org/10.1038/s41583-020-0278-2.

Doudna, J.A. and Charpentier, E. (2014) 'The new frontier of genome engineering with CRISPR-Cas9', *Science*, 346(6213). Available at: https://doi.org/10.1126/science.1258096.

Duch, C., Vonhoff, F. and Ryglewski, S. (2008) 'Dendrite Elongation and Dendritic Branching Are Affected Separately by Different Forms of Intrinsic Motoneuron Excitability', *Journal of Neurophysiology*, 100(5), pp. 2525–2536. Available at: https://doi.org/10.1152/jn.90758.2008.

Dunlap, K., Luebke, J.I. and Turner, T.J. (1995) 'Exocytotic Ca2+ channels in mammalian central neurons', *Trends in Neurosciences*, 18(2), pp. 89–98. Available at: https://doi.org/10.1016/0166-2236(95)80030-6.

Eggermann, E. *et al.* (2012) 'Nanodomain coupling between Ca 2+ channels and sensors of exocytosis at fast mammalian synapses', *Nature Reviews Neuroscience*, 13(1), pp. 7–21. Available at: https://doi.org/10.1038/nrn3125.

Fernández-Quintero, M.L. *et al.* (2021) 'Structural determinants of voltage-gating properties in calcium channels', *eLife*, 10, pp. 1–22. Available at: https://doi.org/10.7554/eLife.64087.

Ferreira, M.A.R. *et al.* (2008) 'Collaborative genome-wide association analysis supports a role for ANK3 and CACNA1C in bipolar disorder', *Nature Genetics*, 40(9), pp. 1056–1058. Available at: https://doi.org/10.1038/ng.209.

Fisher, Y.E. *et al.* (2017) 'FlpStop, a tool for conditional gene control in Drosophila', *eLife*, 6, pp. 1–33. Available at: https://doi.org/10.7554/eLife.22279.

Flaive, A. *et al.* (2020) 'Serotonergic Modulation of Locomotor Activity From Basal Vertebrates to Mammals', *Frontiers in Neural Circuits*, 14. Available at: https://doi.org/10.3389/fncir.2020.590299.

Fouquet, W. *et al.* (2009) 'Maturation of active zone assembly by Drosophila Bruchpilot', *Journal of Cell Biology*, 186(1), pp. 129–145. Available at: https://doi.org/10.1083/jcb.200812150.

Fröhlich, A. and Meinertzhagen, I.A. (1982) 'Synaptogenesis in the first optic neuropile of the fly's visual system', *Journal of Neurocytology*, 11(1), pp. 159–180. Available at: https://doi.org/10.1007/BF01258010.

Gaitanidis, A. *et al.* (2019) 'Longitudinal assessment of health-span and pre-death morbidity in wild type Drosophila', *Aging*, 11(6), pp. 1850–1873. Available at: https://doi.org/10.18632/aging.101880.

Ganetzky, B. and Wu, C.F. (1982) 'Drosophila mutants with opposing effects on nerve excitability: Genetic and spatial interactions in repetitive firing', *Journal of Neurophysiology*, 47(3), pp. 501–514. Available at: https://doi.org/10.1152/jn.1982.47.3.501.

von Gersdorff, H. and Borst, J.G.G. (2002) 'Short-term plasticity at the calyx of held', *Nature Reviews Neuroscience*, 3(1), pp. 53–64. Available at: https://doi.org/10.1038/nrn705.

Ghelani, T. *et al.* (2023) 'Interactive nanocluster compaction of the ELKS scaffold and Cacophony Ca2+ channels drives sustained active zone potentiation', *Science Advances*, 9(7), pp. 1–22. Available at: https://doi.org/10.1126/sciadv.ade7804.

Gratz, S.J. *et al.* (2019) 'Endogenous tagging reveals differential regulation of Ca2+ channels at single active zones during presynaptic homeostatic potentiation and depression', *Journal of Neuroscience*, 39(13), pp. 2416–2429. Available at: https://doi.org/10.1523/JNEUROSCI.3068-18.2019.

Hanes, A.L. *et al.* (2020) 'Divergent Synaptic Scaling of Miniature EPSCs following Activity Blockade in Dissociated Neuronal Cultures', *The Journal of Neuroscience*, 40(21), pp. 4090–4102. Available at: https://doi.org/10.1523/JNEUROSCI.1393-19.2020.

Heckman, C.J., Lee, R.H. and Brownstone, R.M. (2003) 'Hyperexcitable dendrites in motoneurons and their neuromodulatory control during motor behavior', *Trends in Neurosciences*, 26(12), pp. 688–695. Available at: https://doi.org/10.1016/j.tins.2003.10.002.

Heinrich, L. and Ryglewski, S. (2020) 'Different functions of two putative Drosophila α2δ subunits in the same identified motoneurons', *Scientific Reports*, 10(1). Available at: https://doi.org/10.1038/s41598-020-69748-8.

Held, R.G. *et al.* (2020) 'Synapse and Active Zone Assembly in the Absence of Presynaptic Ca2+ Channels and Ca2+ Entry', *Neuron*, 107(4), pp. 667-683.e9. Available at: https://doi.org/10.1016/j.neuron.2020.05.032.

Hering, S. *et al.* (2008) 'Pore stability and gating in voltage-activated calcium channels', *Channels*, 2(2), pp. 61–69. Available at: https://doi.org/10.4161/chan.2.2.5999.

Hering, S. *et al.* (2018) 'Calcium channel gating', *Pflugers Archiv European Journal of Physiology*, 470(9), pp. 1291–1309. Available at: https://doi.org/10.1007/s00424-018-2163-7.

Higley, M.J. and Sabatini, B.L. (2012) 'Calcium signaling in dendritic spines', *Cold Spring Harbor Perspectives in Biology*, 4(4), pp. 1–18. Available at: https://doi.org/10.1101/cshperspect.a005686.

Howlader, G. and Sharma, V.K. (2006) 'Circadian regulation of egg-laying behavior in fruit flies Drosophila melanogaster', *Journal of Insect Physiology*, 52(8), pp. 779–785. Available at: https://doi.org/10.1016/j.jinsphys.2006.05.001.

Huang, Y. and Thathiah, A. (2015) 'Regulation of neuronal communication by G protein-coupled receptors', *FEBS Letters*, 589(14), pp. 1607–1619. Available at: https://doi.org/10.1016/j.febslet.2015.05.007.

Hutchins, B.I. and Kalil, K. (2008) 'Differential Outgrowth of Axons and their Branches Is Regulated by Localized Calcium Transients', *The Journal of Neuroscience*, 28(1), pp. 143–153. Available at: https://doi.org/10.1523/JNEUROSCI.4548-07.2008.

Imlach, W. and McCabe, B.D. (2009) 'Electrophysiological Methods for Recording Synaptic Potentials from the NMJ of Drosophila Larvae', *Journal of Visualized Experiments* [Preprint], (24). Available at: https://doi.org/10.3791/1109.

Jackman, S.L. and Regehr, W.G. (2017) 'The Mechanisms and Functions of Synaptic Facilitation', *Neuron*, 94(3), pp. 447–464. Available at: https://doi.org/10.1016/j.neuron.2017.02.047.

Jalkanen, R. *et al.* (2006) 'X linked cone-rod dystrophy, CORDX3, is caused by a mutation in the CACNA1F gene', *Journal of Medical Genetics*, 43(8), pp. 699–704. Available at: https://doi.org/10.1136/jmg.2006.040741.

James, T.D., Zwiefelhofer, D.J. and Frank, C.A. (2019) 'Maintenance of homeostatic plasticity at the Drosophila neuromuscular synapse requires continuous IP3-directed signaling', *eLife*, 8. Available at: https://doi.org/10.7554/eLife.39643.

Jurkovicova-Tarabova, B. *et al.* (2018) 'Role of individual s4 segments in gating of cav3.1 t-type calcium channel by voltage', *Channels*, 12(1), pp. 378–387. Available at: https://doi.org/10.1080/19336950.2018.1543520.

Juusola, M., *et al.* (1996) 'The presynaptic signal: photoreceptor encoding', *Trends Neurosci.* , 19(96), pp. 292–297.

Kadas, D. *et al.* (2017) 'Dendritic and axonal L-type calcium channels cooperate to enhance motoneuron firing output during Drosophila larval locomotion', *Journal of Neuroscience*, 37(45), pp. 10971–10982. Available at: https://doi.org/10.1523/JNEUROSCI.1064-17.2017.

Kater, S.B. and Mills, L.R. (1991) 'Regulation of growth cone behavior by calcium', *Journal of Neuroscience*, 11(4), pp. 891–899. Available at: https://doi.org/10.1523/jneurosci.11-04-00891.1991.

Katz, B. and Miledi, R. (1967) 'Ionic requirements of synaptic transmitter release [42]', *Nature*, 215(5101), p. 651. Available at: https://doi.org/10.1038/215651a0.

Kawasaki, F. *et al.* (2004) 'Active Zone Localization of Presynaptic Calcium Channels Encoded by the cacophony Locus of Drosophila', *Journal of Neuroscience*, 24(1), pp. 282–285. Available at: https://doi.org/10.1523/JNEUROSCI.3553-03.2004.

Kawasaki, F., Collins, S.C. and Ordway, R.W. (2002) 'Synaptic calcium-channel function in Drosophila: Analysis and transformation rescue of temperature-sensitive paralytic and lethal mutations of Cacophony', *Journal of Neuroscience*, 22(14), pp. 5856–5864. Available at: https://doi.org/10.1523/jneurosci.22-14-05856.2002.

Kawasaki, F., Felling, R. and Ordway, R.W. (2000) *A Temperature-Sensitive Paralytic Mutant Defines a Primary Synaptic Calcium Channel in Drosophila*.

Kilo, L. (2021) *Redundant, exclusive, and cooperative functions of alternative exons in Drosophila Cav2 channels*. Johannes Gutenberg-Universität.

King, D.G. and Wyman, R.J. (1980) 'Anatomy of the giant fibre pathway in Drosophila. I. Three thoracic components of the pathway', *Journal of Neurocytology*, 9(6), pp. 753–770. Available at: https://doi.org/10.1007/BF01205017.

Kisilevsky, A.E. *et al.* (2008) 'D1 Receptors Physically Interact with N-Type Calcium Channels to Regulate Channel Distribution and Dendritic Calcium Entry', *Neuron*, 58(4), pp. 557–570. Available at: https://doi.org/10.1016/j.neuron.2008.03.002.

Kittel, R. J. *et al.* (2006) 'Active zone assembly and synaptic release', *Biochemical Society Transactions*, 34(5), pp. 939–941. Available at: https://doi.org/10.1042/BST0340939.

Kittel, Robert J *et al.* (2006) 'Bruchpilot Promotes Active Zone Assembly, Ca2þ Channel Clustering, and Vesicle Release', *Science*, 312(May), pp. 1051–1054.

Krebs, J. (2022) 'Structure, Function and Regulation of the Plasma Membrane Calcium Pump in Health and Disease', *International Journal of Molecular Sciences*, 23(3). Available at: https://doi.org/10.3390/ijms23031027.

Kuebler, D. and Tanouye, M.A. (2000) 'Modifications of seizure susceptibility in Drosophila', *Journal of Neurophysiology*, 83(2), pp. 998–1009. Available at: https://doi.org/10.1152/jn.2000.83.2.998.

Kurt, R., Warzecha, A.K. and Egelhaaf, M. (2001) 'Transfer of visual motion information via graded synapses operates linearly in the natural activity range', *Journal of Neuroscience*, 21(17), pp. 6957–6966. Available at: https://doi.org/10.1523/jneurosci.21-17-06957.2001.

Lander, E.S. *et al.* (2001) 'Erratum: Initial sequencing and analysis of the human genome: International Human Genome Sequencing Consortium (Nature (2001) 409 (860-921))', *Nature*, 412(6846), pp. 565–566. Available at: https://doi.org/10.1038/35087627.

Lazarevic, V. *et al.* (2013) 'Molecular mechanisms driving homeostatic plasticity of neurotransmitter release', *Frontiers in Cellular Neuroscience*, 7. Available at: https://doi.org/10.3389/fncel.2013.00244.

De Leon, M. *et al.* (1995) 'Inactivation of L-Type Ca 2 + Channels', 270(December).

Leroy, J. *et al.* (2005) 'Interaction via a key tryptophan in the I-II linker of N-type calcium channels is required for β1 but not for palmitoylated β2, implicating an additional binding site in the regulation of channel voltage-dependent properties', *Journal of Neuroscience*, 25(30), pp. 6984–6996. Available at: https://doi.org/10.1523/JNEUROSCI.1137-05.2005.

Li, X. *et al.* (2021) 'Autocrine inhibition by a glutamate-gated chloride channel mediates presynaptic homeostatic depression', *Science Advances*, 7(49). Available at: https://doi.org/10.1126/sciadv.abj1215.

Marley, R. and Baines, R.A. (2011) 'Increased persistent Na+ current contributes to seizure in the slamdance bang-sensitive Drosophila mutant', *Journal of Neurophysiology*, 106(1), pp. 18–29. Available at: https://doi.org/10.1152/jn.00808.2010.

McCudden, C.R. *et al.* (2005) 'G-protein signaling: back to the future', *Cellular and Molecular Life Sciences*, 62(5), pp. 551–577. Available at: https://doi.org/10.1007/s00018-004-4462-3.

Meir, A. *et al.* (2000) 'Calcium channel β subunit promotes voltage-dependent modulation of α1B by Gβγ', *Biophysical Journal*, 79(2), pp. 731–746. Available at: https://doi.org/10.1016/S0006-3495(00)76331-4.

Montell, C. (2012) 'Drosophila visual transduction', *Trends in Neurosciences*, 35(6), pp. 356–363. Available at: https://doi.org/10.1016/j.tins.2012.03.004.

Moreno, C.M. *et al.* (2016) 'Ca2+ entry into neurons is facilitated by cooperative gating of clustered Cav1.3 channels', *eLife*, 5(MAY2016), pp. 1–26. Available at: https://doi.org/10.7554/eLife.15744.

Mueller, B.D. *et al.* (2023) 'CaV1 and CaV2 calcium channels mediate the release of distinct pools of synaptic vesicles', *eLife*, 12, pp. 1–35. Available at: https://doi.org/10.7554/eLife.81407.

Müllner, C. *et al.* (2004) 'Familial hemiplegic migraine type 1 mutations K1336E, W1684R, and V1696I alter Cav2.1 Ca2+ channel gating: Evidence for β-subunit isoform-specific effects', *Journal of Biological Chemistry*, 279(50), pp. 51844–51850. Available at: https://doi.org/10.1074/jbc.M408756200.

Myers, J.L. *et al.* (2021) 'Mutants of the white ABCG Transporter in Drosophila melanogaster Have Deficient Olfactory Learning and Cholesterol Homeostasis', *International Journal of Molecular Sciences*, 22(23), p. 12967. Available at: https://doi.org/10.3390/ijms222312967.

Niemeyer, B.A. *et al.* (1996) 'The Drosophila light-activated conductance is composed of the two channels TRP and TRPL', *Cell*, 85(5), pp. 651–659. Available at: https://doi.org/10.1016/S0092-8674(00)81232-5.

Paez-Segala, M.G. *et al.* (2015) 'Fixation-resistant photoactivatable fluorescent proteins for CLEM', *Nature Methods*, 12(3), pp. 215–218. Available at: https://doi.org/10.1038/nmeth.3225.

Pan, Q. *et al.* (2008) 'Deep surveying of alternative splicing complexity in the human transcriptome by high-throughput sequencing', *Nature Genetics*, 40(12), pp. 1413–1415. Available at: https://doi.org/10.1038/ng.259.

Pangrsic, T., Singer, J.H. and Koschak, A. (2018) 'Voltage-Gated Calcium Channels: Key Players in Sensory Coding in the Retina and the Inner Ear', *Physiological Reviews*, 98(4), pp. 2063–2096. Available at: https://doi.org/10.1152/physrev.00030.2017.

Peng, I.-F. and Wu, C.-F. (2007) 'Differential Contributions of Shaker and Shab K+ Currents to Neuronal Firing Patterns inDrosophila', *Journal of Neurophysiology*, 97(1), pp. 780–794. Available at: https://doi.org/10.1152/jn.01012.2006.

Perrimon, N., Engstrom, L. and Mahowald, A.P. (1989) 'Zygotic lethals with specific maternal effect phenotypes in Drosophila melanogaster. I. Loci on the X chromosome.', *Genetics*, 121(2), pp. 333–352. Available at: https://doi.org/10.1093/genetics/121.2.333.

Peterson, B.Z. *et al.* (2000) 'Critical determinants of Ca2+-dependent inactivation within an EF-hand motif of L-type Ca2+ channels', *Biophysical Journal*, 78(4), pp. 1906–1920. Available at: https://doi.org/10.1016/S0006-3495(00)76739-7.

Peterson, B.Z., DeMaria, C.D. and Yue, D.T. (1999) 'Calmodulin is the Ca2+ sensor for Ca2+-dependent inactivation of L- type calcium channels', *Neuron*, 22(3), pp. 549–558. Available at: https://doi.org/10.1016/S0896-6273(00)80709-6.

Platzer, J. *et al.* (2000) 'Congenital deafness and sinoatrial node dysfunction in mice lacking class D L-type Ca2+ channels', *Cell*, 102(1), pp. 89–97. Available at: https://doi.org/10.1016/S0092-8674(00)00013-1.

Pragnell, M. *et al.* (1994) 'Calcium channel p-subunit binds to a conserved motif in the 1-11 cytoplasmic linker of the a1·subunit', *Nature*, 368(March), pp. 67–70.

Qin, N. *et al.* (1997) 'Direct interaction of Gβγ with a C-terminal Gβγ-binding domain of the Ca2+ channel α1 subunit is responsible for channel inhibition by G protein-coupled receptors', *Proceedings of the National Academy of Sciences of the United States of America*, 94(16), pp. 8866–8871. Available at: https://doi.org/10.1073/pnas.94.16.8866.

Ranganathan, R., Harris, W.A. and Zuker, C.S. (1991) 'The molecular genetics of invertebrate phototransduction', *Trends in Neurosciences*, 14(11), pp. 486–493. Available at: https://doi.org/10.1016/0166-2236(91)90060-8.

Rosenberg, S.S. and Spitzer, N.C. (2011) 'Calcium Signaling in Neuronal Development', *Cold Spring Harbor Perspectives in Biology*, 3(10), pp. a004259–a004259. Available at: https://doi.org/10.1101/cshperspect.a004259.

Rozenfeld, E. *et al.* (2023) 'Homeostatic synaptic plasticity rescues neural coding reliability', *Nature Communications*, 14(1), p. 2993. Available at: https://doi.org/10.1038/s41467-023-38575-6.

Ryglewski, S. *et al.* (2012) 'Ca v2 channels mediate low and high voltage-activated calcium currents in Drosophila motoneurons', *Journal of Physiology*, 590(4), pp. 809–825. Available at: https://doi.org/10.1113/jphysiol.2011.222836.

Saito, H. *et al.* (2009) 'Knockdown of Cav2.1 calcium channels is sufficient to induce neurological disorders observed in natural occurring Cacna1a mutants in mice', *Biochemical and Biophysical Research Communications*, 390(3), pp. 1029–1033. Available at: https://doi.org/10.1016/j.bbrc.2009.10.102.

Sanchez-Sandoval, A.L. *et al.* (2018) 'Contribution of S4 segments and S4-S5 linkers to the low-voltage activation properties of T-type CaV3.3 channels', *PLoS ONE*, 13(2). Available at: https://doi.org/10.1371/journal.pone.0193490.

Sato, M., Suzuki, T. and Nakai, Y. (2013) 'Waves of differentiation in the fly visual system', *Developmental Biology*, 380(1), pp. 1–11. Available at: https://doi.org/10.1016/j.ydbio.2013.04.007.

Von Schilcher, F. (1976) 'The behavior of cacophony, a courtship song mutant in Drosophila melanogaster', *Behavioral Biology*, 17(2), pp. 187–196. Available at: https://doi.org/10.1016/S0091-6773(76)90444-2.

Schulman, H. (2013) 'Intracellular Signaling', *Fundamental Neuroscience: Fourth Edition*, pp. 189–209. Available at: https://doi.org/10.1016/B978-0-12-385870-2.00009-3.

Shah, V.N., Chagot, B. and Chazin, W.J. (2006) 'Calcium-Dependent Regulation of Ion Channels', *Calcium Bind Proteins*, 1(4), pp. 203–212.

Simms, B.A. and Zamponi, G.W. (2014) 'Neuronal Voltage-Gated Calcium Channels: Structure, Function, and Dysfunction', *Neuron*, 82(1), pp. 24–45. Available at: https://doi.org/10.1016/j.neuron.2014.03.016.

Simons, T.J.B. (1988) 'Calcium and neuronal function', *Neurosurgical Review*, 11(2), pp. 119–129. Available at: https://doi.org/10.1007/BF01794675.

Singh, B. *et al.* (2007) 'Mutational analysis of CACNA1G in idiopathic generalized epilepsy. Mutation in brief #962. Online.', *Human mutation*, 28(5), pp. 524–525. Available at: https://doi.org/10.1002/humu.9491.

Smith, L.A. *et al.* (1996) 'A Drosophila calcium channel α1 subunit gene maps to a genetic locus associated with behavioral and visual defects', *Journal of Neuroscience*, 16(24), pp. 7868–7879. Available at: https://doi.org/10.1523/jneurosci.16-24-07868.1996.

Smith, L.A. *et al.* (1998a) *Courtship and Visual Defects of cacophony Mutants Reveal Functional Complexity of a Calcium-Channel 1 Subunit in Drosophila*.

Smith, L.A. *et al.* (1998b) *Courtship and Visual Defects of cacophony Mutants Reveal Functional Complexity of a Calcium-Channel 1 Subunit in Drosophila*.

Splawski, I. *et al.* (2005) 'Severe arrhythmia disorder caused by cardiac L-type calcium channel mutations', *Proceedings of the National Academy of Sciences of the United States of America*, 102(23), pp. 8089–8096. Available at: https://doi.org/10.1073/pnas.0502506102.

Splawski, I. *et al.* (2006) 'CACNA1H mutations in autism spectrum disorders', *Journal of Biological Chemistry*, 281(31), pp. 22085–22091. Available at: https://doi.org/10.1074/jbc.M603316200.

Strehler, E.E. *et al.* (2008) 'Plasma membrane Ca 2+-pumps: structural diversity as basis for functional versatility PMCAs are important parts of the toolkit for cellular Ca 2+ regulation', 35(Pt 5), pp. 919–922.

Strom, S.P. *et al.* (2010) 'High-density SNP association study of the 17q21 chromosomal region linked to autism identifies CACNA1G as a novel candidate gene', *Molecular Psychiatry*, 15(10), pp. 996–1005. Available at: https://doi.org/10.1038/mp.2009.41.

Stuart, G.J. and Spruston, N. (2015) 'Dendritic integration: 60 years of progress', *Nature Neuroscience*, 18(12), pp. 1713–1721. Available at: https://doi.org/10.1038/nn.4157.

Südhof, T.C. (2012a) 'Calcium control of neurotransmitter release', *Cold Spring Harbor Perspectives in Biology*, 4(1). Available at: https://doi.org/10.1101/cshperspect.a011353.

Südhof, T.C. (2012b) 'The presynaptic active zone', *Neuron*, 75(1), pp. 11–25. Available at: https://doi.org/10.1016/j.neuron.2012.06.012.

Takagi, H. (2000) 'Roles of ion channels in EPSP integration at neuronal dendrites', *Neuroscience Research*, 37(3), pp. 167–171. Available at: https://doi.org/10.1016/S0168-0102(00)00120-6.

Takahashi, M. *et al.* (1987) 'Subunit structure of dihydropyridine-sensitive calcium channels from skeletal muscle', *Proceedings of the National Academy of Sciences of the United States of America*, 84(15), pp. 5478–5482. Available at: https://doi.org/10.1073/pnas.84.15.5478.

Tedford, H.W. *et al.* (2010) 'Scanning mutagenesis of the I-II loop of the Cav2.2 calcium channel identifies residues Arginine 376 and Valine 416 as molecular determinants of voltage dependent G protein inhibition', *Molecular Brain*, 3(1), pp. 1–7. Available at: https://doi.org/10.1186/1756-6606-3-6.

Tsien, R.W. *et al.* (1988a) 'Multiple types of neuronal caldum channels and their selective modulation', *Trends in Neurosciences*, 11(10), pp. 431–438. Available at: https://doi.org/10.1109/IIH-MSP.2014.175.

Tsien, R.W. *et al.* (1988b) 'Multiple types of neuronal caldum channels and their selective modulation', *Trends in Neurosciences*, 11(10), pp. 431–438. Available at: https://doi.org/10.1109/IIH-MSP.2014.175.

Verkhratsky, A.J. and Petersen, O.H. (1998) 'Neuronal calcium stores', 24, pp. 333–343.

Vonhoff, F. and Duch, C. (2010) 'Tiling among stereotyped dendritic branches in an identified Drosophila motoneuron', *Journal of Comparative Neurology*, 518(12), pp. 2169–2185. Available at: https://doi.org/10.1002/cne.22380.

Wadel, K., Neher, E. and Sakaba, T. (2007) 'The Coupling between Synaptic Vesicles and Ca2+ Channels Determines Fast Neurotransmitter Release', *Neuron*, 53(4), pp. 563–575. Available at: https://doi.org/10.1016/j.neuron.2007.01.021.

Wagh, D.A. *et al.* (2006) 'Bruchpilot, a protein with homology to ELKS/CAST, is required for structural integrity and function of synaptic active zones in Drosophila', *Neuron*, 49(6), pp. 833–844. Available at: https://doi.org/10.1016/j.neuron.2006.02.008.

Wang, E.T. *et al.* (2008) 'Alternative isoform regulation in human tissue transcriptomes', *Nature*, 456(7221), pp. 470–476. Available at: https://doi.org/10.1038/nature07509.

West, A.E. *et al.* (2001) 'Calcium regulation of neuronal gene expression', *Proceedings of the National Academy of Sciences of the United States of America*, 98(20), pp. 11024–11031. Available at: https://doi.org/10.1073/pnas.191352298.

Wierenga, C.J., Ibata, K. and Turrigiano, G.G. (2005) 'Postsynaptic Expression of Homeostatic Plasticity at Neocortical Synapses', *The Journal of Neuroscience*, 25(11), pp. 2895–2905. Available at: https://doi.org/10.1523/JNEUROSCI.5217-04.2005.

Worrell, J.W. and Levine, R.B. (2008) 'Characterization of Voltage-Dependent Ca 2+ Currents in Identified Drosophila Motoneurons In Situ', *Journal of Neurophysiology*, 100(2), pp. 868–878. Available at: https://doi.org/10.1152/jn.90464.2008.

Wu, C.F. and Wong, F. (1977) 'Frequency characteristics in the visual system of Drosophila: genetic dissection of electroretinogram components.', *The Journal of general physiology*, 69(6), pp. 705–724. Available at: https://doi.org/10.1085/jgp.69.6.705.

Wu, K.D. *et al.* (1995) 'Localization and quantification of endoplasmic reticulum Ca2+-ATPase isoform transcripts', *American Journal of Physiology - Cell Physiology*, 269(3 38-3). Available at: https://doi.org/10.1152/ajpcell.1995.269.3.c775.

Yamamoto, S. and Seto, E.S. (2014) 'Dopamine dynamics and signaling in Drosophila: an overview of genes, drugs and behavioral paradigms', *Experimental Animals*, 63(2), pp. 107–119. Available at: https://doi.org/10.1538/expanim.63.107.

Yarali, A. *et al.* (2009) 'Genetic Distortion of the Balance between Punishment and Relief Learning in Drosophila', *Journal of Neurogenetics*, 23(1–2), pp. 235–247. Available at: https://doi.org/10.1080/01677060802441372.

Zachariou, V., Duman, R.S. and Nestler, E.J. (2012) 'G Proteins', in *Basic Neurochemistry*. Elsevier, pp. 411–422. Available at: https://doi.org/10.1016/B978-0-12-374947-5.00021-3.

Zamponi, G.W. *et al.* (1997) 'Crosstalk between G proteins and protein kinase C mediated by the calcium channel α1 subunit', *Nature*, 385(6615), pp. 442–446. Available at: https://doi.org/10.1038/385442a0.

Zamponi, G.W. and Currie, K.P.M. (2013) 'Regulation of CaV2 calcium channels by G protein coupled receptors', *Biochimica et Biophysica Acta - Biomembranes*, pp. 1629–1643. Available at: https://doi.org/10.1016/j.bbamem.2012.10.004.

5. Appendix

5.1 Salines & buffers

Saline/Buffer (methods)	**Chemicals/Reagents**
Ringer Saline (dissection of larvae for immunohistochemistry)	128 mM NaCl 2 mM KCl 1.8 mM $CaCl_2$ 4 mM $MgCl_2$ 5 MM HEPES D-Saccharose 7.24 – 7.25 pH
HL 3.1 Saline (TEVC, TIRFM)	70 mM NaCl 5 mM KCl 0.5 mM $CaCl_2$ 4 mM $MgCl_2$ 10 mM $NaHCO_3$ 5mM D-Trehalose 115 mM D-Saccharose 5mM HEPES
5X TAE (gel electrophoresis)	54 g Trizma-Base 27.5g boric acid 20 mL 0.5 mM EDTA Adjust volume to 1L by adding H_2O
Squishing buffer (DNA isolation)	10 mM Tris-Cl 1 mM EDTA 25 mM NaCl

5.2 Chemicals

Chemical	Supplier	Art.-No.
$CaCl_2$	Sigma Life Sciences	M8266-100G
KCl	Roth	HNO2.1
$MgCl_2$	Sigma Life Sciences	C5670-100G
NaCl	Roth	0962.1
D-Saccharose	Roth	4621.2
D-Trehalose	Roth	5151.4
$NaHCO_3$	Sigma Aldrich	40167-2.5Kg
HEPES	Roth	9105.2
Triton-X	Roth	3051.3
Glycerol	Roth	6962.5
PBS	Calbiochem	524650
Trizma Base	Sigma Aldrich	T6066
EDTA	Roth	8040.3
Tris-Cl	Roth	9090.2
Boric acid	Roth	6943.2
Agarose	Roth	3810.3
Gel Red (Roti-GelStain)	Roth	0984.1
Ethanol 99.8%	Roth	9065.4
***Taq* DNA-Polymerase** **dNTPs** **10x ThermoPol Reaction Buffer**	New England Biolabs	M0267S
H_2O	Sigma Aldrich	W4502-50ML
Methylsalycylate	Sigma Aldrich	M6752-250ML
Vectashield	Vector Laboratories	H-1000
DNA Ladder 1kb	New England Biolabs	N3232S
DNA Ladder 1kb plus	New England Biolabs	N0550S

5.3 Softwares used

Software	Purpose
Axoscope	TEVC/Current clamp data acquisition

Software	Purpose
Clampfit	TEVC/Current clamp data analysis
GraphPad Prism	Statistical Analysis of all acquired data
CorelDraw	Image processing
FIJI including plugin NanoCore	Data pre-processing of TIRFM data, drift correction
FIMtrack	Tracking of larval crawling
Microsoft Excel	Data processing and analysis
NIS-Elements	Imaging of samples during TIRFM
Python (Anaconda)	Script used for ROI detection in maximum projection views and subsequent data selection by quality parameters

5.4 Antibody application and concentration

Methods	Primary antibody Supplier, Art.-No.	Secondary antibody Supplier, Art.-No.
Immunohistochemistry of larval muscles/NMJs – Confocal microscopy	Mouse α-brp (1:300) *DSHB, #nc82* Rabbit α-HRP (1:600) *Jackson-ImmunoResearch, #323-005-021*	Goat α-mouse (1:400) *Jackson ImmunoResearch, #115-605-0003* Donkey α-rabbit (1:400) *Jackson ImmunoResearch, #711-545-152*
TIRFM	Alexa 488 Goat α-HRP (1:300)	-

5.5 Fly lines used for experiments

TEVC M6

Fly line
Canton S ($\frac{+}{+}$; $\frac{+}{+}$; $\frac{+}{+}$)
w+ cac^{sfGFP}
w- cac$^{sfGFP\Delta IS4A}$
w+ cac$^{sfGFP\Delta I\text{-}IIA}$
w- cac$^{sfGFP\Delta I\text{-}IIB}$
$\frac{w-\ cacsfGFP\Delta IS4B}{w+RFP\Delta IS4A}$

TEVC M12

Fly line
$\frac{w+\ cacsfGFP}{\mathrm{w}-\ \mathrm{cacsfGFP\Delta IS4A}}$
w- cacsfGFPΔIS4A
$\frac{w-\ cacsfGFP\Delta IS4B}{w+RFP\Delta IS4A}$
$\frac{w-\ cacsfGFP\Delta IS4B}{w-cacFlpStop}$; $\frac{OK6-GAL4}{UAS-Flp}$
$\frac{w-\ cacsfGFP\Delta IS4B}{w-cacFlpStop}$; $\frac{+}{UAS-Flp}$
$\frac{w+\ cacsfGFP}{\mathrm{w}-\ \mathrm{cacFlpStop}}$; $\frac{OK6-GAL4}{UAS-Flp}$

Electroretinograms

Fly line
Canton S
w+ cac^{sfGFP}
‘Cac1‘ [P{GawB}Elav155-GAL4 cacH129 sd1, f1 ; + ; P{w^{+mc} UAS-cac1-EGFP}786C]
cac^{H18}
w+ cac$^{sfGFP\Delta IS4A}$
w+ cac$^{sfGFP\Delta I\text{-}IIA}$

Adult DLM recordings

Fly line
Canton S
$\frac{cacFlpStop}{Y}$; $\frac{UAS-Flp}{+}$; $\frac{23H06-GAL4}{+}$
$\frac{cacFlpStop}{cacsfGFP\Delta IS4B}$; $\frac{UAS-Flp}{+}$; $\frac{23H06-GAL4}{+}$
$\frac{cacFlpStop}{Y}$; + ; +

TIRFM

Fly line
w- $cacm^{EOS4b}$
w- $cacm^{EOS4b\ \Delta IS4A}$
w- $cacm^{EOS4b\ \Delta I\text{-}IIA}$

Larval crawling

Fly line
Canton S
w+ cac^{sfGFP}
w- $cac^{sfGFP\Delta IS4A}$
w+ $cac^{sfGFP\Delta I\text{-}IIA}$
w- $cac^{sfGFP\Delta I\text{-}IIB}$
w- $cac^{sfGFP\Delta IS4A,\ \Delta I\text{-}IIA}$
$\frac{w-\ cacsfGFP\Delta IS4B}{w+RFP\Delta IS4A}$
$\frac{w-\ cacsfGFP\Delta I-IIB}{w+cacsfGFP\Delta I-IIA}$

Acknowledgements:

Since this thesis could not have been possible without the various types of support from many people, I would like to dedicate the next few lines to them.

First and foremost, my deepest gratitude goes out to my supervisor Dr. Stefanie Ryglewski for believing in me and giving me this opportunity to start, develop and finish this work with unceasing guidance and support. I am incredibly thankful for having had the right amount of experimental freedom as well as guidance and mentorship during my time in this lab, which helped me grow as a scientist as well as a person.

Moreover, I would like to thank Prof. Dr. Carsten Duch for his constant support since the beginning of my bachelor's thesis. I very much appreciate the tremendously helpful input and feedback, which was fundamental to this thesis. Additionally, I thank Prof. Dr. Martin Heine for the opportunity to acquire and analyze data on channel number estimation for this thesis, which to me are a substantial addition to this project. I especially appreciate the effort of helping me to adjust the experiment numerous times and intellectually integrating the results into my project. In addition, I would like to thank Prof. Dr. Marion Silies for providing me with the tracking apparatus for the larval crawling experiment and for her input on the *Drosophila* visual system.

Additionally, I would like to thank my partners in this endeavor, Dr. Lukas Kilo, XXXXX and XXXXX. I am extraordinarily grateful to Lukas for his mentorship during our time together in the lab and to XXXXX and XXXXX for all the fruitful intellectual exchanges we had when discussing and integrating the ideas on our projects. You also always kept me motivated during times when experiments or ideas failed, for which I'm incredibly thankful. My gratitude also goes out to XXXXX, who provided me with the channel counting Python script, which was exceptionally helpful and time saving during data analysis. Thanks a lot to all the students who contributed to this work, especially XXXXX for her immense contributions on G-protein subunits. My thanks go out to all the members of the Duch and Ryglewski labs, with whom I had a blast during the last several years!

Last, but not least, I would like to thank my friends, family and sports teammates for supporting and motivating me all the way. Most importantly, I would like to thank my grandmother, who passed away this spring and unfortunately cannot witness this milestone in my life. Thank you so much for everything you have done for me.

Lebenslauf